DEVELOPMENT OF CLIMATE-BASED INDICES FOR ASSESSING THE HYGROTHERMAL PERFORMANCE OF WOOD-FRAME WALLS UNDER HISTORICAL AND FUTURE CLIMATES

Chetan Aggarwal

A Thesis
In the Department
of
Building, Civil and Environmental Engineering

Presented in Partial Fulfillment of the
Requirements For the Degree of
Doctor of Philosophy (Building, Civil and Environmental Engineering)
at Concordia University
Montreal, Quebec, Canada

January 2023

DÉVELOPPEMENT D'INDICES CLIMATIQUES POUR L'ÉVALUATION DES PERFORMANCES HYGROTHERMIQUES DES MURS À OSSATURE EN BOIS SOUS LES CLIMATS HISTORIQUE ET FUTUR

Chetan Aggarwal

Thèse
présentée
au
Département de Génie du bâtiment, civil et environnemental

comme exigence partielle au grade de
philosophae doctor (génie du bâtiment, civil et environnemental)
Université Concordia
Montréal, Québec, Canada

Janvier 2023

CONCORDIA UNIVERSITY

SCHOOL OF GRADUATE STUDIES

This is to certify that the thesis prepared

By: Chetan Aggarwal

Entitled: Development of climate-based indices for assessing the hygrothermal performance of wood-frame walls under historical and future climates

and submitted in partial fulfillment of the requirements for the degree of

Doctor of Philosophy (Building Engineering)

complies with the regulations of the University and meets the accepted standards with respect to originality and quality.

Signed by the final examining committee:

______________________________ Chair

Dr. Sivakumar Narayanswamy

______________________________ External Examiner

Dr. Juha Vinha

______________________________ Examiner

Dr. Liangzhu Wang

______________________________ Examiner

Dr. Ted Stathopoulos

______________________________ Examiner

Dr. Hoi Dick Ng

______________________________ Thesis Supervisor

Dr. Hua Ge

______________________________ Thesis Supervisor

Dr. Maurice Defo

Approved by ______________________________ Graduate Program Director

Dr. Mazdak Nik-Bakht

March/09/2023 ______________________________ Dean of faculty

Dr. Mourad Debbabi

ABSTRACT

Development of climate-based indices for assessing the hygrothermal performance of wood-frame walls under historical and future climates

Chetan Aggarwal, Ph.D.

Concordia University, 2023

It is generally understood that the average temperature of the earth is increasing, resulting in an increased number of extreme events. To assess the impact of climate change on the durability of the building envelope, a commonly used method is to use hygrothermal modeling tools to perform simulations. The hygrothermal response varies depending on the location, material properties, type of wall assemblies, etc., and hence proper inputs are required. In general, indicator based on simulation results indicates the moisture risk. However, to obtain this indicator and considering different situations, a large number of simulations are required. This research thus focused on developing a climate-based index that can give a range of expected performance of the wall without performing the simulations.

Firstly, different existing climate-based indices were computed and correlated with the performance indicator to quantify the risk. The purpose is to see if any existing climate-based indices can lead to accurate risk assessment and the analysis showed that none of these indices lead to reliable risk assessment. Thus, a machine learning algorithm, Partial Least Squares (PLS) regression was used to develop a new climate-based index. Three cities from different climate zones across Canada and two wall claddings were considered for model development. For each city and future projected climate, the index was calculated, and correlated with the performance indicator to quantify the risk.—PLS modeling technique proves to be an effective way in predicting the hygrothermal response and to improve computational efficiency. A PLS model was developed for a brick cladding wall and the model was applied to other wall types and a larger climate range (15 runs of data with each run having 31 years of historical and future climate data). The results showed that the moisture risk increases in the future periods for all three cities and wall claddings and a similar performance was noted for different climate runs. The predicted results from the

meta-model can be used as a screening measure to limit the number of simulations to cases where the predicted hygrothermal performance is above a certain threshold set by the user.

Acknowledgement

I would like to thank my supervisors Dr. Hua Ge and Dr. Maurice Defo for their constant support and guidance throughout my PhD journey. My sincere gratitude to them for sharing their expertise and knowledge and without whom the completion of my thesis would have been virtually impossible. Besides my supervisors, I would like to thank the members of my thesis committee for their insightful comments and encouragement.

My sincere thanks to Dr. Michael Lacasse who provided me an opportunity to join the NRC Construction research center as an intern and gave me access to the research facilities. Without his precious support, it would not be possible to conduct this research. I am extremely grateful to the entire team of NRC Construction research center and CZEBS Concordia University who have helped me in various aspects for completing the thesis on time. I thank my fellow lab mate Sahar Sahyoun, Naman Bansal, Dr. Lin Wang, and Dr. Abhishek Gaur for the encouraging discussions and for all the fun we have had during the PhD journey.

My appreciation also goes out to my father, Mr. Rakesh Aggarwal, my mother, Mrs. Pinki Aggarwal, my sister, Ms. Heena Aggarwal and my wife, Mrs. Shikha Garg for their encouragement and support all through my studies and for everything they have done for me.

Special thanks to Max Junginger for his support and motivation.

Table of contents

List of Figures

List of Tables

Nomenclature

Symbol	Parameter	Unit
A	Conductive heat flux to porous material	W/m^2
c	Specific heat capacity of dry material	J/kg·K
Cloud	Cloud index	-
e	Vapor pressure of air	Pa
e_a	Saturated vapor pressure of air	Pa
F_D	Rain deposition factor	-
F_E	Rain exposure factor	-
f_{sky}	Sky radiation factor	-
f_{grd}	Ground radiation factor	-
F_L	Empirical constant	kg.s/(m^3·m)
h_m	Convective vapor transfer coefficient	s.m^{-1}
I	Latent heat of vaporization	J/kg
I_{min}	Lowest value of index	-
I_{max}	Highest value of index	-
J_{vc}	Convective vapor flux	kg/m·s
J_{vd}	Diffusive vapor flux	kg/m·s
J_l	Moisture flux	kg/m·s
$j^Q_{dir,n}$	Direct radiation flux normal to the surface	W/m^2
$j^Q_{dir,h}$	Direct radiation flux on a horizontal surface	W/m^2
$j^Q_{diff,n}$	Diffuse radiation flux normal to the surface	W/m^2
$j^Q_{diff,h}$	Diffuse radiation flux on a horizontal surface	W/m^2
$j^Q_{glob,h}$	Global radiation flux on a horizontal surface	W/m^2
k	Number of hours	-
K	Net short-wave radiation	W/m^2
L	Net longwave radiation	W/m^2
l_{geo}	Geographic latitude	^{o}
h_v	Enthalpy of water vapor	J/kg

h_l	Enthalpy of liquid water	J/kg
k_l	Liquid water conductivity	kg/m.s.Pa
p_c	Capillary pressure	Pa
P_v	Partial vapor pressure	Pa
p	Vapor pressure	Pa
Q_m	Moisture source	kg/m^3
q_{cond}	Conductive heat flux	W/m^2
Rad	Solar radiation	W/m^2
Rain	Wind-driven rain	mm
r_{albedo}	ground reflection coefficient	-
R_h	Horizontal rainfall amount	mm
RH_{crit}	Critical relative humidity	%
RH_L	Limiting relative humidity	%
s_d	External coating factor	-
T	Temperature	K or °C
T_L	Limiting temperature	°C
V_{10}	Hourly average wind speed at 10 m	m/s
v	Air velocity	m/s
w	Moisture content	kg/m^3
w_{sat}	Humidity ratio at saturation	-
w_l	Liquid water content	kg/m^3
w_v	Water vapor content	kg/m^3

Greek symbols

α_{wall}	Wall orientation	radian
α_{wind}	Wind direction	radian
β_v	Water vapor exchange coefficient	s/m
$\varepsilon_{lw,grd}$	Long wave emission coefficient of ground	-
θ	Angle between wind direction and façade normal	°
$\theta_{s,min}$	Minimum indoor surface temperature	°C

θ_i	Inside temperature	°C
θ_e	Outside temperature	°C
λ	Thermal conductivity	W/m.K
Δ	Slope between saturation vapor pressure and air temperature	-
σ	Stefan Boltzmann constant	$W/m^2.K^4$
μ	degree of saturation	-
ρ	Bulk density of material	kg/m^3
γ	Psychometric constant	$Pa.K^{-1}$

Abbreviations

ACH	Air change per hour
CFSR	Climate Forecast System Reanalysis
CBI	Climate based index
CI	Climatic Index
CNN	Convolutional neural network
CZ	Climate Zone
DI	Drying index
ECCC	Environment and Climate Change Canada
GCM	General Circulation Models
HAM	Heat, air and moisture
HDD	Heating Degree Days
I_{sev}	Severity index
MAE	Mean absolute error
MC	Moisture content
MI	Moisture index
MRY	Moisture reference year
OSB	Oriented strand board
MLR	Multiple linear regression
MLP	Multilayer perceptron
MoI	Mould Index
PLS	Partial Least Squares

R^2	Coefficient of determination
RBI	Response based index
RCP	Representative Concentration Pathway
RH	Relative humidity
RNN	Recurrent neural networks
RMSE	Root mean square error
RMSECV	Root mean square error of cross-validation
SVR	Support Vector Regression
TZO	Time Zone
WDR	Wind-driven rain
WI	Wetting index

Preface

This is a manuscript-based thesis, a collection of two published journal papers, one submitted paper (under review) and one paper under preparation. The three papers compose Chapter 4 ~ Chapter 6, with Chapter 6 also including some content from the paper under preparation.

For easy reading, the four manuscripts are modified from the original ones. The numbering of equations, tables, and figures includes the numbers of the chapters, and the references of different chapters are combined at the end of the thesis.

Chapter 1 Introduction

1.1. Background

The global climate is constantly changing, and the effects of climate change are being observed across the world. For instance, it has been observed that the global mean temperature has increased by 0.85°C over the last 130 years, and for arctic latitudes, it has been even worse with temperature rise as high as three times the global mean temperature rise (IPCC, 2021). For Canada, there is an increase of 20-25% in precipitation and approximately a 2-3°C rise in temperature (Environment and natural resources, 2020). Given this alarming situation, Canada has committed to reducing its greenhouse gas emissions by 30% (in comparison to the level in 2005) before 2030 (Environment and Climate Change Canada, 2016), and to achieve carbon neutrality by 2050 (Government of Canada, 2020). According to the Canada greenhouse emissions data report, there is an 8.5% decline in national greenhouse emissions per capita from 2005 to 2019 (Environmental and Indicators Canada, 2022). With higher projected rainfall and more extreme wind-driven rain events in the future, the building will be subjected to more intense climate loads, and will potentially lead to an increased risk of premature degradation of building elements (Lacasse et al., 2020).

Nik et al., (2012) analyzed the impact of climate change on the hygrothermal performance and mould growth risk in attic space for buildings located in Sweden. They found that with more severe climate conditions, mould growth risk would increase in the future. Another study by (Nik et al., 2015) found that a higher quantity of moisture would be present in the walls for the future climate. Hao et al., (2020) reviewed the impact of climate change on retrofitted historical buildings across Europe. They reported that for historic buildings, with more extreme rain events in the future, the risk of water runoff along masonries would increase and consequently increase the relative humidity in the construction and risk for mould growth and decay of wooden beams.

Hygrothermal simulations are commonly used for moisture performance evaluation of the wall assembly (Straube et al., 2003; Glass et al., 2013). The climate variables that affect the response of the wall include temperature, relative humidity, solar radiation, cloud cover, wind speed and direction, and rainfall intensity and frequency. Given the number of climatic variables, the number of years, and the climate change scenarios required to take into account the uncertainty in the projected future climate, the cost of computation can be considerably high. One approach that could help in reducing the computational efforts is to select the representative year(s) referred to as Moisture Reference Year (MRY) from a long-term (e.g., at least > 10 years) series of climate data (Zhou et al., 2016). The selection of representative climate data is necessary to provide an accurate assessment (Delgado et al., 2012).

The purpose of selecting MRY is to reduce computing time and effort. However, how reliable and consistent the existing MRY selection methods are, or in other words, for example, will the worst moisture reference year result in the worst moisture risk, is the question that needs to be answered. Aggarwal et al., (2020) evaluated three indices in terms of their capability in selecting the worst year based on the number of hours when the mould index is greater than 3 from a series of weather data. For this purpose, they performed the simulations for a wood-framed wall with brick veneer cladding for three cities in Canada under historical and future climates. It was observed that none of the methods identified the worst year with 100% accuracy. Sahyoun et al., (2020) performed the hygrothermal analysis of wood-frame wall assembly in Canada to determine the effect of selected MRY on durability assessment. They compared MRY selected using two climate-based indices with MRY selected based on long-term simulation results. It was found that different MRY selection methods resulted in a different selection of MRY and the MRY selected based on long-term simulation results had a higher mould index. Vandemeulebroucke et al., (2020) investigated the potential of various methods to rank the climate years and climate ensembles. They found that different rankings were obtained with different methods and the correlation between the climate-based indices and the actual performance remained poor. Vandemeulebroucke et al., (2022) evaluated 21 existing moisture reference year (MRY) selection methods and developed a decision framework to select appropriate climate data for hygrothermal simulations. They compared the results with long-term simulations and simulations using MRYs for solid masonry walls in Brussels. They recommend using perform long-term simulations for the best results. As second-best case, they suggested to select the MRY with respect to a long-term simulation for a reference case and finally they proposed the use of a climate-based MRY to obtain a first estimate of the results. From these studies, it was observed that existing climate-based indices do not show reliability and consistency in ranking the severity of weather years when compared to the actual hygrothermal responses and moisture risks obtained from simulation results. In other words, the most severe weather year indicated by the climate-based indices does not necessarily represent the actual worst hygrothermal performance of wall assemblies. Climate-based indices taking into account more climatic parameters perform better and their performance is influenced by the type of wall constructions, type of moisture loads, and climatic characteristics of the locations (Zhou et al., 2016). Therefore, to assess the moisture risks of building envelope assemblies under projected future climates, given the uncertainty in the future climate projection, a more reliable climate-based index is needed to better correlate response-based indices with climate-based indices for typical Canadian climates. Thus there is a need to develop a climate-based index specific to Canadian climates and wall constructions.

1.2. Objectives and scope

The objective of this thesis is to develop a climate-based index and a framework for the reliable assessment of moisture risks in wood frame walls under projected future climates taking into account the uncertainty associated with the future climates. To achieve the proposed objective, the methodology employed involves (1) Reviewing current approaches to the selection of MRYs and reviewing the response-based indices for moisture performance assessment; (2) Evaluating the reliability of existing climate-based indices in assessing moisture risks using direct correlation with the response-based indices and a ranking analysis; (3) Developing new climate-based index if none of the existing indices prove to be reliable; and (4) Applying the new climate-based index to assess moisture risks under projected future climates for representative Canadian cities.

The research is of great importance as it fills the existing knowledge gaps pertaining to analyzing the hygrothermal performance of wood frame wall assemblies under the impact of climate change. The study will help in developing a deep insight into the problem and aid to identify the possible solutions to mitigate the impact of extreme climate change events on buildings. Based on the proposed climate-based index, one will be able to establish an impact assessment of the wall performance when subjected to the expected climate change without needing to perform a tremendous number of simulations. It will further help in mapping the moisture risk of buildings in Canada and identify hazardous situations. Moreover, the results from the hygrothermal response will foster the process of monitoring infrastructure performance and adaptation actions. Finally, the proposed index will help in the ranking of years based on their moisture severity and thereby assist in the selection of MRY. Having an MRY will further help in reducing computational time and effort.

1.3. Outline of the thesis

Chapter 2 reports a comprehensive literature review, which includes an overview of hygrothermal models, a review of the response-based indices for moisture performance assessment, moisture reference year (MRY) selection methods and existing regression methods, and Partial Least Squares (PLS) regression for developing a machine learning prediction model. Based on the comprehensive literature review, this chapter identifies the detailed knowledge gaps and illustrates the research questions.

Chapter 3 reports the hygrothermal simulations methodology. It includes a description of the wall assembly used, various simulation parameters such as wall orientation, moisture sources, critical location for moisture performance assessment, simulation solver setting, etc.

Chapter 4 evaluates the reliability of existing climate-based indices in assessing the moisture performance of the wall assemblies. The evaluation is based on different correlation methods and ranking analysis methods. This chapter also illustrates the results using existing climate-based indices and compares them with the simulation results.

Chapter 5 presents the development of a new climate-based index for moisture performance assessment using the Partial Least Squares (PLS) regression model. This chapter details the parameters used for model development along with the selection of different training and test datasets. It further depicts the prediction results based on the newly developed index and compares them with the simulation results to assess the reliability of the model.

Chapter 6 reports the application of the PLS model on different wall claddings, considering climate uncertainties and different global warming scenarios. The chapter illustrates the results showing the applicability of the model in different scenarios.

Chapter 7 summarizes the contributions and conclusions of this thesis. This chapter provides a summary related to each chapter and discusses future work.

Chapter 2 Literature review

2.1. Overview of hygrothermal models

The hygrothermal models are based on the heat, air, and moisture (HAM) transfer through the porous building materials. These tools are widely used to simulate the hygrothermal response of wall assemblies. The hygrothermal simulations can help in analyzing the temperature and moisture content across different wall components and further assist in evaluating its hygrothermal performance. There is a significant variation among different hygrothermal models depending on their mathematical complexity. Straube and Burnett, (2001) showed that the complexity of the model depends on the extent to which the model considers different parameters such as weather parameters, material properties, moisture transfer, and type of flow (transient or steady state). A comprehensive review of different HAM models can be found in the literature (Hens, 1996). HAM models can be classified as steady or transient-state and one or two-dimensional. This thesis focuses on the one-dimensional transient HAM model. The governing equations for the moisture transport processes and heat transfer implemented in the model are discussed in detail in the next section.

2.1.1. Moisture transfer

Moisture transfer occurs through porous materials, and it can be categorized into three regions namely, the hygroscopic region, capillary region, and over-capillary region. In the hygroscopic region, moisture transfer takes place by vapor diffusion. The increase in relative humidity results in the vapor molecules bonded to the surface of porous material which in turn increases the moisture content. With increasing moisture content and the inability of surface tension to hold the moisture molecules, the moisture moves into the pores and moisture transfer takes place. In the capillary region, a proportion of the pores are filled with liquid water and the transfer of moisture occurs due to vapor diffusion and liquid conduction. In the over-capillary region, the relative humidity reaches 100% as all the pores are filled with water, and the moisture transfer mainly because of liquid conduction.

Vapor Transport

Vapor transport in porous material can be categorized into vapor diffusion and vapor convection. Water vapor diffuses through a porous material from places with higher partial vapor pressure to places with lower partial vapor pressure. Vapor transport occurs due to the gradient of partial vapor pressure according to the equation (2-1) (ASHRAE Fundamentals Handbook, 2017):

$$J_{vd} = -\delta . \nabla p \tag{2-1}$$

where J_{vd} is diffusive vapor flow (kg/m·s), δ is the water vapor permeability (kg/m·s·pa) and p is vapor pressure (Pa).

Vapor convection occurs due to air movement, which can be led by buoyancy force, wind-induced pressure, and mechanical force. The vapor convection is only taken into account when the airflow, such as infiltration or exfiltration, is considered in the HAM model (Li, 2008). The vapor convection takes place according to the equation (2-2):

$$J_{vc} = v . p \tag{2-2}$$

where v is the air velocity (m/s) and p is vapor pressure (Pa)

Liquid transport

The transport of liquid through the porous material can be described by either the moisture diffusivity method or the liquid conductivity method depending on the parameter used as the driving potential for liquid transport. The moisture diffusivity method uses moisture content while the liquid conductivity method uses capillary pressure as the driving potential. Equations (2-3) and (2-4) describe the moisture diffusivity and liquid conductivity methods respectively (ASHRAE Fundamentals Handbook, 2017).

$$J_l = k_l . \nabla p_c \tag{2-3}$$

where, k_l is liquid water conductivity (kg/m·s·pa) and p_c is capillary pressure (Pa).

$$J_l = -D_w . \nabla w \tag{2-4}$$

where, D_w is moisture diffusivity (m^2/s) and w is moisture content (kg/m^3).

2.1.2. Heat and moisture balance equations

Moisture Balance Equation

The principle of conservation of mass states that mass is conserved for a system. The rate of moisture change in time at a given control volume should be equal to the sum of all the incoming and outgoing fluxes together with the source production rate. Combining the vapor transfer and liquid transfer, the moisture balance equation can be written as follows: (ASHRAE Fundamentals Handbook, 2017)

$$\frac{\partial w}{\partial t} = -\nabla(J_v + J_l) + Q_m \tag{2-5}$$

Where, Q_m is the moisture source (kg/m^3).

Heat Balance Equation (ASHRAE Fundamentals Handbook, 2017)

The heat transfer through the building envelope takes place via conductive and convective heat transfer. Heat conduction can be described using Fourier's law of conduction (equation (2-6)):

$$q_{cond} = -\lambda . \nabla T \tag{2-6}$$

Where, λ is thermal conductivity (W/m·K) and T is the temperature (K)

On the other hand, convective heat comprises latent heat and sensible heat. The convective heat is carried by the moisture that passes through the building envelope and it is described by the following equation:

$$q_{conv} = J_v . h_v + J_l . h_l \tag{2-7}$$

Where, h_v is the enthalpy of water vapor (J/kg) and h_l is the enthalpy of liquid water (J/kg).

The building component can hold a certain amount of heat depending on the temperature and moisture content and it can be written as follows:

$$H = \rho c T + h_v . w_v + h_l . w_l \tag{2-8}$$

Where, ρ is the bulk density (kg/m^3), c is the specific heat capacity of dry material (J/kg·K), w_v is water vapor content (kg/m^3) and w_l is liquid water content (kg/m^3).

Finally, the heat balance equation can be written as follows based on the law of energy conservation:

$$\frac{\partial H}{\partial T} = -\nabla(q_{cond} + q_{conv}) \tag{2-9}$$

2.1.3. Hygrothermal simulation tools

Based on the hygrothermal models and governing equations of heat and moisture transfer, various hygrothermal simulation tools are developed (Rode, 1990; Kunzel, 1995; Hens, 1996; Burch, 1997; Kalagasidis, 2004; Salonvaara, 2004; Janssen et al., 2007). The application of these simulation tools along with a comparison among different tools can be found in the literature (Kunzel, 1998; Beaulieu et al., 2001; Delgado, 2013).

Hygrothermal simulation tools usually require four inputs: material properties, climate data, boundary conditions, and geometry. The material properties include properties such as thermal conductivity, vapor permeability, density, specific heat capacity, sorption isotherm, suction pressure, liquid diffusivity, specific moisture capacity, etc. These properties govern the characteristics of the material and dictate how one material component interacts with the other. Climate data describe the conditions to which the wall is being exposed. It includes different climate parameters such as temperature, relative humidity, wind speed, rain, solar radiation, etc. The boundary conditions illustrate conditions at the boundaries, model selections, parameters, and assigned climate conditions. The indoor conditions include the temperature and relative humidity on the interior side of the building. Finally, the geometry of the wall assembly signifies how different wall components are arranged and it defines the space where the hygrothermal simulation takes place.

Hygrothermal simulations are widely used as an alternative to traditional lab testing because of their ability to maintain reasonable accuracy along with reduced time and cost. They help researchers to identify the building envelope system based on the desired performance matrix such as durability, affordability, etc. Various studies (Maref et al., 2002; Kalamees and Vinha, 2003) reported the comparison among various hygrothermal models and with the experimental data. Despite some differences in the results among different models, they were found to be in good agreement with each other. Mundt-Petersen, (2013) performed the hygrothermal simulations for five wood-frame houses using WUFI and compared them with the experimental results. The simulated relative humidity and temperature of the walls were compared with the measurement results, and the simulation results generally showed a good agreement with the measurements.

2.2. Review of the response-based indices for moisture performance assessment

Moisture-related problems are common in buildings. The moisture once penetrated into the exterior surface of the wall and if it does not get enough opportunity to dry, it will start accumulating and will lead to moisture risk and affect the performance of buildings. The hygrothermal response of an exterior wall is a function of several parameters including the wall configuration, the materials selection, and the outdoor climate (Kočí et al., 2017). However, to assess the hygrothermal response of the wall, performance indicators or damage functions, which are defined as response-based indices are required. These indices will give a quantitative measure for assessing the level of risks. The choice of the index depends on the wall type and the damage that a specific wall type is more prone to. In this section, the most commonly used response-based indices are discussed.

2.2.1. Mould Growth

The word mould is a common term referring to fungi that can grow on building materials in homes or other buildings. Damp conditions and mould growth in homes increase the risk of respiratory allergy symptoms and exacerbate asthma in mould-sensitive individuals (Health Canada, 2011). More than 1000 species of mould are found in the United States with more than 100,000 recognized species worldwide (Occupational Safety and Health Administration (OSHA, 2011)). Mould can grow with an acceptable level of moisture, temperature, and air (Chen and Garcia, 2004). Mould can also cause material stain or discoloration, and over time can cause wood decay and structural damage and sometimes can be detected by a musty odor (Wahab et al., 2014).

The mould growth in the building structure is mainly affected by the level of humidity and the surface temperature (Viitanen and Ritschkoff, 1991; Hukka and Viitanen, 1999; Viitanen and Ojanen, 2007). Due to a large number of mould species, there are different criteria for the critical level of temperature and relative humidity above which mould starts to grow. In general, it has been seen that mould growth rapidly in regions with higher relative humidity (above 80%) and higher temperature (above 0ºC). The critical level of humidity and temperature could vary according to mould species and as concluded by Nielsen (2012) that Cladosporium and Penicillium can develop on wood surfaces even at a temperature as low as -5 °C. Moreover, the critical humidity level is also dependent on temperature and exposure time (Viitanen and Ritschkoff, 1991; Viitanen and Ojanen, 2007). Moreover, the extent of mould growth that is going to occur depends largely on the material properties of the surface. It has been found that the mould growth on other building materials may not be equal to that on wooden materials (Ritschkoff et al., 2000). The following section will detail the available mathematical models to quantify mould growth.

Mould Growth models:

Understanding the adverse impact that mould can impose on the health of occupants, it has become a subject of utmost importance to quantify mould growth so that preventive measures can be taken. There are many mould models available in the literature to evaluate mould growth on wood-based materials as a function of humidity, temperature, and exposure time. International Energy Agency (IEA) proposed a surface relative humidity (RH) threshold dependent on the elapsed time (IEA, 1991). Different thresholds have been set for RH depending on the exposure time i.e. 80%, 89%, or 100% for 1 month, 1 week, and 1 day, respectively. For temperature, a ratio including the surface temperature, indoor and outdoor temperature has been computed and a value of 0.7 is proposed (experimental results), related to an acceptable mould risk of 5% (Vereecken et al., (2012)).

$$\tau = \frac{\theta_{s,min} - \theta_e}{\theta_i - \theta_e} \geq 0.7 \tag{2-10}$$

Where, $\theta_{s,min}$ (°C) is the minimum indoor surface temperature and θ_i and θ_e are the inside and outside temperatures (°C) respectively.

Mould growth models are classified into two categories depending on the growth stage of the mould. In the first category, the study is made when mould is in the beginning phase and just starts to develop and in the second category, the process of mould development is studied along with its declination when the conditions become unfavorable for mould growth. This has been a part of various studies (Vereecken and Roels, 2012; Gradeci et al., 2017) where they analyzed the two categories of mould growth. A numerical mould growth model, the VTT model was developed based on laboratory testing with Northern wood species (Viitanen and Ritschkoff 1991; Viitanen 1997; Hukka and Viitanen, 1999; Viitanen et al., 2000). However, the model has been applied in mould growth risk analysis for pine and spruce sapwood only and could not account well for the impact of seasonal variation of weather on mould. To overcome these deficiencies in the model, the mould growth model was modified to incorporate seasonal cycles and building materials, in addition to timber (Viitanen et al., 2011; Ojanen et al., 2010; Vereecken and Roels, 2012). As suggested in the model (Viitanen et al., 2011), the mould index can vary between zero and six, where an index of 0 means no mould growth and 6 means the surface is fully covered with mould. Moreover, as mould index is based on visual inspection, so the index has been classified as follows (Viitanen et al., 2011):

- 0 - no growth
- 1 - some growth detected only with microscopy
- 2 - moderate growth detected with microscopy
- 3 - visually detected coverage of less than 10%
- 4 - visually detected coverage of more than 10%
- 5 - visually detected coverage of more than 50%
- 6 - visually detected coverage 100%

As shown in Figure 2.1, below 0ºC and above 50ºC, the conditions for mould growth are unfavorable and hence mould can grow only between these two extremes of temperature. For temperatures below 20ºC, critical humidity is calculated using equation (2-11) (Hukka and Viitanen, 1999):

$$RH_{crit} = -0.00267T^3 + 0.160T^2 - 3.13T + 100 \tag{2-11}$$

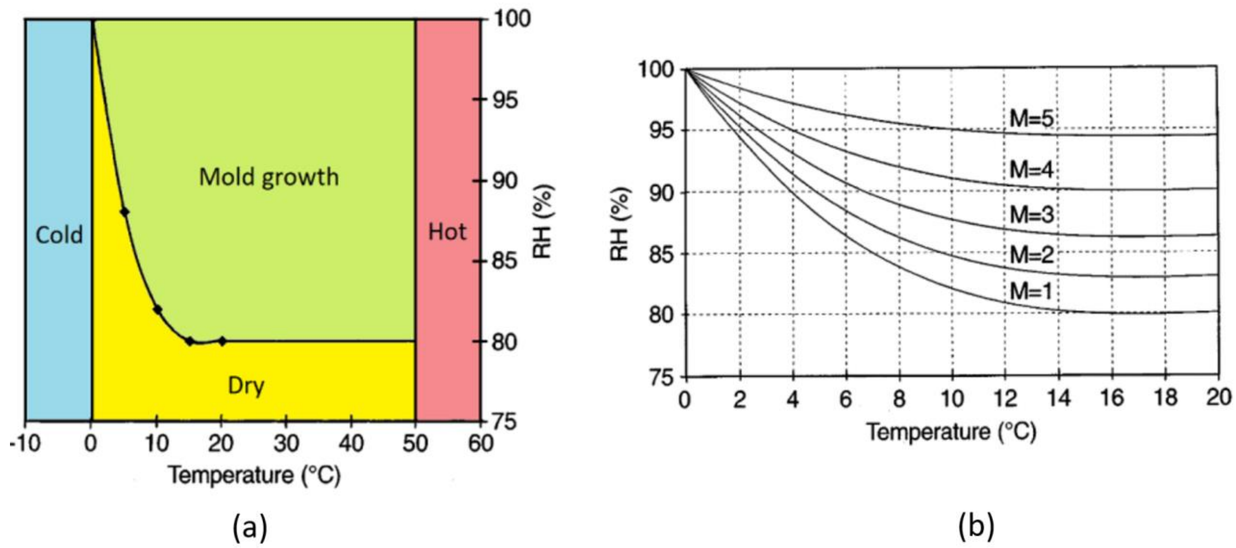

Figure 2.1: (a) Classification of regions based on temperature and RH for mould growth (b) Quantitative measure of mould index for a given temperature and RH (Hukka and Viitanen, 1999)

To incorporate different types of materials, they were divided into four sensitivity classes based on their properties and they are shown in Table 2.2 along with examples of the type of material in each class. The humidity threshold for medium and resistant materials is set at 85% for mould to start growing (Ojanen et al., 2010). Finally, four decline classes were also formed illustrating the fall in mould value during the unfavorable conditions.

Based on ASHRAE 160 (ASHRAE, 2010), the initial value of the mould index (M) shall be zero (M = 0 at time t = 0). The mould index is accumulated for each hour using the following equation:

$$\mathrm{M_t} = \mathrm{M_{t-1}} + \Delta\mathrm{M} \tag{2-12}$$

where

$\mathrm{M_t}$ = mould index for the current hour

$\mathrm{M_{t-1}}$ = mould index for the previous hour

$\Delta\mathrm{M}$ = change in mould index, calculated for each hour using equation (2-12)

If the surface temperature ($\mathrm{T_s}$) is greater than 0°C at the current hour, the critical surface relative humidity for mould initiation (RH_{crit}) (in %) is calculated using equation (2-13) or (2-14), according to the material sensitivity class.

Very sensitive class or sensitive class:

$$RH_{crit} = \begin{cases} -0.00267\mathrm{T_s^3} + 0.160\mathrm{T_s^2} - 3.13\mathrm{T_s} + 100 \text{ when } \mathrm{T_s} \leq 20°\mathrm{C} \\ 80 \text{ when } \mathrm{T_s} > 20°\mathrm{C} \end{cases} \tag{2-13}$$

Medium resistant class or resistant class:

$$RH_{crit} = \begin{cases} -0.00267\mathrm{T_s^3} + 0.160\mathrm{T_s^2} - 3.13\mathrm{T_s} + 100 \text{ when } \mathrm{T_s} \leq 7°\mathrm{C} \\ 85 \text{ when } \mathrm{T_s} > 7°\mathrm{C} \end{cases} \tag{2-14}$$

If the relative humidity at the material surface (RH_s) (in %) is greater than RH_{crit} at the current hour, then an increase in the mould index is calculated using equation (2-15).

$$\Delta\mathrm{M} = \frac{\mathrm{k_1 k_2}}{168\exp(-0.68\ln\mathrm{T_s} - 13.9\ln\mathrm{RH_s} + 0.14\mathrm{W} + 66.02)} \tag{2-15}$$

where

$\mathrm{k_1}$ = mould growth intensity factor selected from Table 2.1 according to material sensitivity class and current value of M

$\mathrm{k_2}$ = mould index attenuation factor calculated using equation (2-16)

W = parameter selected from Table 2.1 according to material sensitivity class

Table 2.1: Parameters for equation (2-15) (Source: ASHRAE 160, 2010)

Sensitivity class	K_1		W	A	B	C
	If (M<1)	If (M>1)				
Very sensitive	1	2	0	1	7	2
Sensitive	0.578	0.386	1	0.3	6	1
Medium resistant	0.072	0.097	1	0	5	1.5
Resistant	0.033	0.014	1	0	3	1

The mould index attenuation factor (k_2) is calculated using equation (2-16):

$$k_2 = max\{1 - exp[2.3(M - M_{max})], 0\} \tag{2-16}$$

where M_{max} is the maximum mould index corresponding to the surface temperature and relative humidity at the current hour, calculated using equation (2-17):

$$M_{max} = A + B\left(\frac{RH_{crit} - RH_s}{RH_{crit} - 100}\right) - C\left(\frac{RH_{crit} - RH_s}{RH_{crit} - 100}\right)^2 \tag{2-17}$$

where the coefficients A, B, and C are selected from Table 2.1 according to material sensitivity class.

If T_s < 0°C or $RH_s < RH_{crit}$ at the current hour, then a decline in the mould index is calculated using equation (2-18):

$$\Delta M = \begin{cases} -0.00133k_3 \; when \; t_{decl} \leq 6 \\ 0 \; when \; 6 < t_{decl} < 24 \\ -0.000667k_3 \; when \; t_{decl} > 24 \end{cases} \tag{2-18}$$

where

k_3 = mould index decline coefficient specific to the material surface

t_{decl} = number of hours from the moment when conditions for mould growth changed from favorable (T_s > 0°C and $RH_s > RH_{crit}$) to unfavorable (T_s < 0°C or $RH_s < RH_{crit}$).

For the mould index decline coefficient, in the absence of specific test data for the material surface, the recommended value of k_3 is 0.1. Further details about the model for mould calculation can be found in ASHRAE 160 (2010).

Table 2.2: Mould sensitivity classes and example materials (Source: ASHRAE 160, 2010)

Mould sensitivity class (RH threshold)	Example of materials
Very sensitive (80%)	Untreated wood; includes lots of nutrients for biological growth
Sensitive (80%)	Planed wood, paper-coated products, and wood-based boards
Medium resistant (85%)	Cement or plastic-based materials, mineral fibers
Resistant (85%)	Glass and metal products, materials with efficient protective compound treatments

Viitanen et al., (2011) presents the mould growth modelling on different materials and considering the effect of unfavourable conditions for mould growth e.g., seasonal, long period dry or cold periods. They used pine sapwood as the reference material and the experimental results were used to improve the existing numerical model for mould growth. It was found that for resistant materials, the threshold value for mould growth could be set to 85 % RH. Lähdesmäki et al., (2011) examined mould growth on different materials and at the interfaces of two materials within assemblies using field tests. They found that at higher humidity levels i.e., 97-98% RH, mould growth was seen irrespective of the choice of material. For lower humidity levels (89-90% RH) and high temperature levels (20-22ºC), with the exception of pine sapwood, the mould index remained low (0-1). Further, the authors examined the effect of unfavourable conditions on mould growth. They found that for most of the materials, a dry period resulted in the lowering of mould index value. However, the decrease in mould index during the dry period was found to be more intense with the model than the experimental results.

Adan (1994) introduced Time of Wetness (TOW) to indicate the availability of water under high relative humidity periods. He suggested that TOW below 0.5 would reduce the growth of mould to a large extent. Clarke et al., (1999) and Rowan et al., (1999) in their model divided the mould fungi in the buildings into 6 different categories based on the relative humidity and temperature. Experimental data was later curve-fitted using a third-order polynomial function. It was suggested that when the relative humidity and temperature from the experimental data lie above this polynomial curve, it will lead to mould growth. There are a few other models developed to predict mould growth on the surface of wood, metal, or any other material. Bio-hygrothermal model (IBP) developed by (Sedlbauer, 2001; Sedlbauer, 2002) considers the intermediate drying out of the spores and provides the critical humidity level within a spore for the wood material. Mould Germination Graph Method (Moon and Augenbroe, 2005) calculates the exposure time for a different group of materials based on the surface relative humidity and temperature. Exposure time is used as a criterion to determine the mould growth risk i.e. if the total exposure time is greater or equal to the required exposure time, mould will grow. Other models include the Max-days model (Geving, 1997), Gobakken et al. model (Gobakken et al., 2010), and Johansson et al. model (Johansson, 2010). These models involve fitting the data into a regression model to define the level of mould growth based on exposure time, temperature, and relative humidity.

The mould index suggested by (Viitanen et al., 2010) is most commonly used for a quantitative assessment of mould growth risk. However, for evaluating the performance of the building envelope when exposed to different moisture loads, it is imperative to have a quantitative measure that could differentiate different simulation results. ASHRAE suggested a mould index of 3 as a threshold limit (TenWolde, 2008). To compare the hygrothermal performance, different statistical outputs are made on the hourly time series of mould index. The widely used method (i.e. performance indicator) is to evaluate the maximum or average mould index that might have happened during the course of the simulation (Hansen et al., 2018; Wang and Ge, 2018; Abdul Hamid and Wallentén, 2017; Salonvaara et al., 2010). Another method to compare the wall performance is to compute the number of hours when the mould index is above a threshold limit (Aggarwal et al., 2020). These are a few methods that are used in the literature to identify the level of performance and to make a comparison between different simulation results.

2.2.2. Moisture Content in the critical wall layer

Moisture content is the total amount of moisture (liquid, vapor, and ice) accumulated in the material under consideration. It is widely used to evaluate the moisture performance of the building envelope. The critical layer e.g. OSB panel in wood frame walls is evaluated for its moisture content level. During the course of the simulation, usually, the highest moisture content level is noted and is used as a performance indicator for the wall. The higher the moisture content in the structure at any given year, the greater the likelihood of high moisture loads and/or poor drying capability (ASHRAE RP-1325). The maximum moisture content as the performance indicator has been widely used to evaluate the wall response (Glass, 2013; De Mets et al., 2017; Wang and Ge, 2018; Salonvaara et al., 2010).

2.2.3. RHT Index

Hygrothermal simulations can provide the temperature and relative humidity at any layer of the wall that is under consideration. However, the performance of the wall is impacted by the combination of temperature and relative humidity. To incorporate the combined effect, (Mukhopadhyaya et al., 2003c) proposed an index called the RHT index. The index calculates the integral of temperature and humidity difference from a threshold level.

$$RHT = \sum (T - T_L)(RH - RH_L) \tag{2-19}$$

Here, T and RH represent the temperature and relative humidity. T_L and RH_L are the limiting values of temperature and RH above which the wall poses a risk. The limiting values further depend on the degradation mechanism. For metal corrosion, the limiting values for temperature and relative humidity are 0°C and 80% respectively (Garverick, 1994). For the decay of wood material to occur, temperature and relative humidity should be above 0°C and 95 % respectively (Viitanen et al., 2011). RHT index has been a part of many studies to analyze wall performance (Zhou et al., 2017; Kesik et al., 2006; Kumaran et al., 2002; Salonvaara et al., 2010).

2.3. Review of Moisture reference year (MRY) selection methods

One of the parameters that influence the moisture performance of the building envelope is the outdoor climate. However, having a large number of climate parameters and estimating the effects of these parameters over the entire service life would result in a large simulation effort. One of the approaches to reduce the simulation time and cost is to select a year or combination of years called Moisture Reference Year(s) (MRYs). The selection of representative climate data is necessary to provide an accurate assessment (Delgado et al., 2012) and they are assumed to represent the entire set of long-term climate data. An MRY is usually selected from existing long-term climate data to represent a climate that allows a correct evaluation of the moisture stress on the building envelope (Zhou et al., 2016).

Many different ranking methods are available in the literature and are used in MRY selection. The π-factor method suggested by Hagentoft and Harderup, (1996) compares the absolute humidity at the external wall surface with the absolute humidity of the outside air in order to compute the drying potential of the wall surface. They suggested that drying out potential is higher for a higher value of π-factor. Kalamees and Vinha, (2004) used a method similar to the π-factor method for selecting the MRY in terms of evaluating the risk of water vapor condensation. Carsten Rode (1993) proposed a construction-dependent method, which compares the integral moisture content values for different wall constructions and orientations. He suggested that the higher the value of moisture content for a particular year, the more severe the year is in terms of the moisture performance of the wall. Cornick et al., (2003) used an index called the Moisture Index (MI) to categorize the years in terms of severity. MI method uses the wetting and drying function to compute MI and then further categorizes the year as dry, average, and wet. From a dataset of years, the years having MI value in the range of more than one standard deviation (+/-) from the mean MI value are considered dry and wet years, while those years having a value within (+/-) one standard deviation are referred to as average years. The year having the highest, lowest, and mean MI is defined as the wettest, driest, and average year, respectively. The wetting index (WI) is represented by the mean annual total horizontal rainfall or the annual wind-driven rain load. In the Dryness Index (DI), the drying function is given by the annual sum of hourly Δw in [kg_{water}/kg_{air}], the difference between the humidity ratio at saturation and the humidity ratio present in the ambient air. For humidity ratio at saturation, saturation vapor pressure, p_{vs}, was calculated as follows (Cornick et al., (2003)):

$$\Delta w = w_{sat}(1 - \mu) \tag{2-20}$$

$$DI = \sum_{h=1}^{k} \Delta w \tag{2-21}$$

Where,

Δw: the difference between the humidity ratio at saturation and the humidity ratio of ambient air (kg_{water}/kg_{air}),

w_{sat}: humidity ratio at saturation,

μ: degree of saturation,

k: number of hours in the particular year.

DI and WI are further normalized to have similar units using the following equation:

$$I_{normalized} = (I - I_{min})/(I_{max} - I_{min}) \tag{2-22}$$

Where, I is the index of interest, and I_{min} and I_{max} are the lowest and highest values of the index in the dataset respectively.

Finally, MI is computed using equation (2-23)

$$MI = \sqrt{(1 - DI_{norm}^2)^2 + WI_{hnorm}^2} \tag{2-23}$$

A method suggested by (ASHRAE 160, (2010)) combines the climate load and durability to choose the "severe" weather years and provides a more representative ranking of the climate data. This approach, called the Severity Index (I_{sev}), uses an equation to predict the RHT value as a damage function. Salonvaara et al., (2010) suggested the I_{sev} equation (equation (2-24) as a reliable method of selecting representative years. A regression equation generated for computing the RHT value considers different climate parameters. The yearly average value of each climate parameter is used in the correlation and the years are arranged in the descending order of the RHT values. However, I_{sev} was calculated only for the orientation receiving the least solar radiation i.e. North. The year with the third highest (top 10% year among 30 years) RHT value is selected as MRY for the hygrothermal simulations.

$$\begin{aligned} I_{sev} = 108307 - 241\, Rad - 1391\, Cloud - 312326\, RH + 183308\, Rain \\ + 15.2\, P_v + 27.3\, T \cdot T + 261079\, RH \cdot RH - 0.00972\, P_v \\ \cdot P_v \end{aligned} \tag{2-24}$$

Where, Rad is the solar radiation (W/m^2) incident on the wall; $Cloud$ is the cloud index (0-8); RH is the relative humidity; $Rain$ is the wind-driven rain (kg/m^2.h) on the wall; P_v is partial vapor pressure (Pa), and T is the ambient temperature (°C).

Salonvaara et al., (2010) further compared their method with three other existing methods (ANK/ORNL Karagiozis, (2002), π-Factor, and Moisture Index MI) and concluded that their method performs better in selecting severe years than other methods. Another index called, the Climatic Index suggested by Zhou et al., (2016) comprises wetting and drying components. The wetting component includes annual wind-driven rain (WDR). WDR load for different wall orientations is calculated according to ASHRAE 160 (ASHRAE 160, (2016)). The WDR is calculated using the following equation:

$$WDR = R_h * F_E * F_D * 0.2 * V_{10} * \cos\theta \tag{2-25}$$

Where, R_h is the horizontal rainfall amount (kg.m^{-2}.h^{-1}); F_E is the rain exposure factor; F_D is the rain deposition factor; V_{10} is the wind speed at 10 m above ground (m/s); θ is the angle between the wind direction and the normal to the façade. Hourly data was obtained for WDR, and the annual sum was taken as the wetting index (WI).

$$WI = \sum_{i=1}^{n} WDR \tag{2-26}$$

The drying component is based on the potential evaporation calculated using the Penman equation shown below:

$$E = \frac{\Delta}{\Delta + \gamma}\frac{K + L - A}{I} + \frac{\gamma}{\Delta + \gamma} h_m(e_a - e) \tag{2-27}$$

Where, $\frac{\Delta}{\Delta+\gamma}\frac{K+L-A}{I}$ represents the radiation term and $\frac{\gamma}{\Delta+\gamma} h_m(e_a - e)$ represents the turbulence term. The radiation term comprises energy balance at the surface and the turbulence term incorporates the effect of the atmospheric conditions.

E is the drying index (DI), K is the net short-wave radiation (Wm^{-2}), L is the net longwave radiation (Wm^{-2}), A is the conductive heat flux to the porous material (Wm^{-2}), I is the latent heat of vaporization (Jkg^{-1}), γ is the psychometric constant (PaK^{-1}), Δ is the slope of the relationship between saturation vapor pressure and air temperature, e_a is the saturated vapor pressure of the air, e is the partial vapor pressure in the air (Pa) and h_m is the convective vapor transfer coefficient (sm^{-1}).

The CI is calculated as the ratio of the Wetting Index (WI) and Drying Index (DI) (equation (2-28)), where WI is annual WDR, and DI is the potential evaporation calculated using equation (2-27).

$$CI = \frac{WI}{DI} \tag{2-28}$$

Unlike the MI method, this index takes into consideration the effect of many climate parameters such as net short-wave and long-wave radiation, temperature, humidity, wind speed, wind direction, and orientation of the façade. Zhou et al., (2016) made a comparison with the MI method in terms of accuracy in selecting the MRY and suggested that the year selected using CI gives better results than the MI method. Another study by (Aggarwal et al., 2020) tested CI, MI, and I_{sev} in terms of their capability in selecting the worst year from a series of weather data. They tested brick cladding walls for three cities in Canada under historical and future projected climates. It was observed that none of the methods provides the worst year with 100% accuracy, however, for most of the cases, I_{sev} method performs better than the other two methods in terms of the worst year selection.

2.3.1. Review of the effect of climate uncertainties on hygrothermal performance

A major challenge at present is to compile trustworthy technical information as a means of quantifying the environmental effects on the long-term performance of buildings. Considering the impact of climate change, it is evident that future climate will significantly affect the existing infrastructure. This further leads to quantifying these impacts to have sustainable building performance over the long term (Lacasse, 2019). Existing buildings are constructed considering the climate from the past, however, in the context of climate change, these buildings need to be renovated to make them capable of sustaining under the future climate. All these factors lead to the conclusion that it is of utmost importance to consider climate change when evaluating the hygrothermal performance of buildings.

Having understood the importance of climate change and its potential impacts on building envelope performance, a reliable projected future climate is required. General Circulation Models or GCMs are used as numerical climate models to generate future data. GCMs representing the physical processes in the atmosphere, ocean, cryosphere, and land surface, is the most advanced tools currently available for simulating the response of the global climate system to increasing greenhouse gas concentrations (IPCC, 2014). However, GCM data is simulated at a very coarse tempo-spatial resolution and hence this data needs to be downscaled to a regional scale to be used for modeling purposes (Gaur et al., 2019).

There are several climate scenarios to be taken into consideration when performing the simulations for generating future climate data. These scenarios include a different set of boundary and initial conditions, emission scenarios, etc. The emission scenarios further depend on the assumptions like human activities, plant coverage, etc. Different weather files will be generated assuming different emission scenarios using the same climate model (Nik and Kalagasidis, 2010). This further leads to high uncertainty in the simulated future climate data. Moreover, as the simulation results are strongly dependent on the climate and hence these results are also prone to large uncertainties.

Many studies have been made to investigate the impact of uncertainties in the climate data for building simulations (Nik and Moussavi, 2012; Tian and De Wilde, 2011; Gaterell and McEvoy, 2005; Nik et al., 2015). The effect of three uncertainty factors used for climate projections by comparing the moisture content in wood-stud walls was investigated. They studied the uncertainties originating from global climate models (GCM), emissions scenarios, and spatial resolutions. Higher moisture content level was found in the walls when simulated for future climate. Moreover, the climate uncertainties caused up to 13% variations in the average moisture content. The authors concluded that with different spatial resolutions, a large variation was observed in the rain and wind data. However, GCM affected the water content of the wall the most. Another study by (Nik et al., 2012) investigated the hygrothermal performance of ventilated attics concerning possible climate change in the Swedish climate. They simulated the conventional attic along with three other attics by modifying the baseline in terms of high insulation and ventilation rate. To analyze the impact of climate data, the authors analyzed the three emission scenarios for the climate model. Mould growth is used as the performance indicator for the hygrothermal simulations. They found that the moisture problems increase in the future climate. Zhou et al., (2020) studied the freeze-thaw risk in masonry in two cities located in Switzerland for two future scenarios obtained using two emission scenarios from ten different GCM-RCM chains. For both cities, they found that the results show a much higher variation for different climate model chains as compared to when considering different emission scenarios. They further recommended using the climate projections from an ensemble of different climate models under the different emission scenarios to cover the entire range of uncertainty linked with the projected climate. Nik and Kalagasidis, (2010) studied the hygro-thermal response of a cold attic for a building situated in Lund, Sweden. They simulated the building under different climate scenarios which were derived assuming different CO_2 emission scenarios. They observed that the trend of variation in the simulation results i.e. attic temperature and relative humidity is different from the one observed in the climate data and a direct correlation was not found. They further concluded that it is not possible to deduce the performance of the attic in the future by assuming only one climate scenario. Vandemeulebroucke et al., (2020) investigated the effect of different initial conditions in generating future climate data. The authors simulated the Canadian initial-condition ensemble CanRCM4 LE using the HAM modeling tool DELPHIN. An effort was made to select the "reduced" ensemble comprising fewer ensemble members to represent the entire data set without losing much of the information. The study was made using two types of wall systems: (i) brick-clad wood-stud wall assembly and (ii) historical solid masonry wall before and after retrofitting. They found that for a few scenarios the "reduced" ensemble was able to represent the entire ensemble, but it was recommended to use the complete ensemble to minimize the loss of information. Javed et al., (2022) evaluated the existing climate zones in Australia using the Moisture Index. They proposed that the current climate mapping is not suitable and is too coarse to reliably provide robust indications for moisture management. They further proposed a new characterization of Australian climates for hygrothermal performance assessment.

From the various studies conducted on analyzing the impact of climate uncertainties on hygrothermal performance, it was observed that relying on a single dataset of future climate might lead to unreliable results. The way future climate is modeled makes it prone to large uncertainties and hence there is a need to consider all the possible variations of climate models for performing the simulations. A few studies lead to the conclusion that GCM variation is more dominating than different emission scenarios, but further investigation is required to reduce the number of simulations.

2.4. Review of the existing regression methods and Partial Least Squares (PLS) regression

To have a reliable performance analysis, it is imperative to deal with the model complexity and it is not a viable option to trade off between the computation time and complexity of the model as this might not result in reliable results. To solve this issue, metamodels are commonly used as a substitute for time-consuming simulations (Simpson et al., 2001; Wang et al., 2007). A metamodel is a simplified mathematical equation that is statistically determined using the original model data and is used to represent the simulation model. With these models, a single output is often predicted based on single-valued inputs. Van Gelder et al., (2014), compared 5 methods i.e., polynomial regression, multivariate adaptive regression splines, kriging, radial basis function networks, and neural networks in terms of their capacity to predict the response for a building energy simulation. Outputs i.e., cumulative heating demand and the number of hours with a temperature greater than 25ºC for a semi-detached dwelling were predicted using

5 methods. Marincioni et al., (2018) constructed a metamodel for moisture risk assessment of interior wall insulation. The moisture risk was evaluated based on the maximum relative humidity and mould index. The authors highlighted the applicability of the developed model; with predicted results being similar to the results obtained from the simulations.

Instead of predicting a single response, several studies focused on using different machine learning algorithms to predict the response time series. The predicted time series is further post-processed to quantify the moisture risk. Dong et al., (2016) used Support Vector Regression (SVR) to develop a model to predict the hourly and daily energy consumption in residential buildings. The authors suggested that their model is better than existing models in predicting energy consumption. Tijskens et al., (2019) considered three types of neural networks i.e., the multilayer perceptron (MLP), recurrent neural networks (RNN), and the convolutional neural network (CNN) to predict the hygrothermal time series. They found that CNN is faster and most accurate among the three types of neural networks and can be applied as a metamodel in the prediction of non-linear hygrothermal time series. Freire et al., (2017) used SVR for the prediction of mould index, vapor flux, and sensible and latent heat fluxes on the roof surface of a building located in Curitiba, Brazil. Climate data was split into two equal sets i.e., training and test and the model results showed a significant R^2 (more than 97%) for all the investigated output parameters. Bansal et al., (2021) explored the potential of SVR to forecast the long-term hygrothermal response of light wood frames and massive timber walls. From a long-term 31-year series of data, the first 5 years were used as training and model development with the prediction made on the remaining 26 years. Temperature and relative humidity profiles were predicted, and the authors found that with a proper selection of training sets, the model can be effectively used to forecast performance. Tijskens et al., (2021) developed a metamodel using convolutional neural network to predict the hygrothermal response of masonry walls. They found that the model can give the response in 4 min which is over 500 times faster compared to the original hygrothermal model. Xie et al., (2022) used multilayer neural network (MLNN) to predict the distribution of mean radiant temperature around buildings. They used first five years of training data and predict the performance for the distribution of mean radiant temperature for the following year. They found that the prediction results are extremely accurate with a Mean Absolute Percentage Error of 0.23%.

Partial Least Squares (PLS) regression was developed in the 1960′s by Herman O.A. Wold, and it was originally used in econometrics. To date, PLS regression is being used in different disciplines for prediction analysis. For instance, PLS algorithms are effectively used for predicting soil salinity (Zhang and Huang, 2019, Fan et al., 2015, Qu et al., 2008). PLS regression is also applied to develop soil quality index models, to determine organic matter content in soil (Morona et al., 2017). Rumpel et al., (2001) used PLS regression to obtain soil properties using data from the infrared spectroscopy technique. The PLS modeling technique is also used in the field of energy-dispersive X-ray fluorescence (Melquiades et al., 2014) and mid-infrared photoacoustic spectroscopy (Geoderma, 2008). The advantage of PLS over other methods is the way it uses the information from the input variables and develops many factors based on the internal relationships between each variable, and then provides a quantitative measure of the explained variance. Unlike simple regression methods, PLS takes into consideration the multi-collinearity among input variables and results in factors that represents the input variables.

2.5. Summary

Given the effect of climate change on buildings and the high uncertainty in the simulated climate data, one way is to simulate all possible scenarios and then perform the statistical analysis. However, in this case, the simulation efforts required will be tremendous and will require high computational cost and time. The other way to avoid detailed hygrothermal simulations is to use a climate-based index. The index solely based on climate data could predict the anticipated range of wall performance or select the representative year, and hence help in reducing the simulation load. Having a climate-based index to select the representative years has been a part of the study by many researchers, which were reviewed in this thesis. However, most of them have their associated limitations and a single method cannot be taken as a universal method to select the representative years. The following sections discuss the identified knowledge gaps in the literature and the scope of this thesis:

Knowledge gaps identified:

- Existing methods to select a moisture reference year (MRY) are developed based on the US or European climate data. Very few studies are made which considers Canadian climate for the method development.
- Existing climate-based indices are supposed to work for all climates, wall types, etc. but

the moisture response can significantly differ when exposed to different climates and for different construction types. To incorporate this, a general index does not work and a specific index for a given climate is required.

- Existing climate-based index e.g., the Severity Index developed by Salonvaara et al., (2010) work only for north-facing walls. The index was developed using data for north-facing walls only but could be adapted to all orientations. An index that does not depend on the wall orientation is required to cover a wider range of data and not limit the analysis to only one wall orientation.
- All the existing MRY selection methods assumed the wall to be perfect i.e. wall without any defect to allow water entry through the exterior cladding. It is imperative to assume a more practical scenario by assuming rain leakage and air leakage.
- To cover the uncertainties in the future climate, a large simulations are required and a metamodel is required to select the moisture reference year and predict the response in future climate. Limited studies have been conducted to develop a meta-model using data from Canadian cities.
- A very few studies have been conducted to evaluate the effect of climate change on moisture performance in Canadian context. A thorough investigation considering typical wall claddings, future climate uncertainties and different global warming scenarios is required.

Research questions:

To address the identified knowledge gaps, this thesis tries to answer the following questions:

1) What is the level of moisture risk under projected future climate, and will the walls designed according to historical climatic data be able to sustain it?
2) Can existing climate-based indices be used for a reliable assessment of moisture risk under future climates considering uncertainties in the projected climate data and different global warming scenarios?
3) If existing methods could not reliably assess the performance, how to develop a new climate-based index and select the most influential climate variables to be used for the new index?
4) Can the newly developed index be used for different wall claddings and climate scenarios?

Chapter 3 Methodology

The study aims to evaluate the reliability of existing climate-based indices and develop the new index for moisture performance assessment. The objective is to develop an index using one representative wall cladding, one moisture loading condition to cover other types of walls, and moisture loading scenarios. Further, the model should be able to cover the uncertainties in the projected future climate data. Finally, to have an estimation of the maximum mould growth risk that the wall can be subjected to considering the climate uncertainty and future climate so as to develop an appropriate retrofit plan. The study includes 15 runs, with each run having 31 years of historical and future climate. The goal is to develop a predictive model that can estimate the worst-case scenario for mould growth on different types of cladding under a broad range of climatic conditions. To achieve this, the model would need to incorporate data on various cladding materials and climatic factors that could impact moisture levels in wall assemblies.

Hygrothermal simulations were undertaken to investigate the hygrothermal performance of wood-frame wall assemblies. Two (2) wall assemblies typical of Canadian residential building practice were selected for this study. The two walls differ only in their cladding type i.e. brick-veneer and stucco; a description of the common elements of the wall assembly is given in section 3.3. The buildings were supposed to be located in a suburban setting corresponding to terrain category III as defined by the ISO standard. Hygrothermal simulations were performed using the DELPHIN HAM simulation tool (version 5.9.5). Only a one-dimensional horizontal configuration of the wall was simulated. The amount of rainwater impinging on building façades was determined using the ASHRAE method under historical climate (1986-2016) and projected future climate when global temperature increases by 3.5ºC (2062-2092). Comparisons were made using relative humidity (RH) and temperature (T) of the outer surface of the OSB sheathing which accounts for the risk of mould development on the OSB sheathing. It was assumed that the wall was perfectly air tight. In the following sections, details and considerations are provided of the various parameters needed for simulations and the evaluation of the risk of premature degradation of the respective wall assemblies.

Figure 3.1 shows a brief description of the methodology followed in the present work. Certain cities, walls, and climate data were chosen for this work and details for the cities and climate data are presented in the subsequent sections. Simulations were carried out and the output from simulations i.e., response-based indices (RBIs) were correlated with climate-based indices (CBIs). There are several methods that are used as CBIs, but the reliability of these indices to match the hygrothermal response remains questionable (discussed in section Chapter 4). In this study, these indices along with newly developed indices are analyzed in terms of their ability to assess the wall performance.

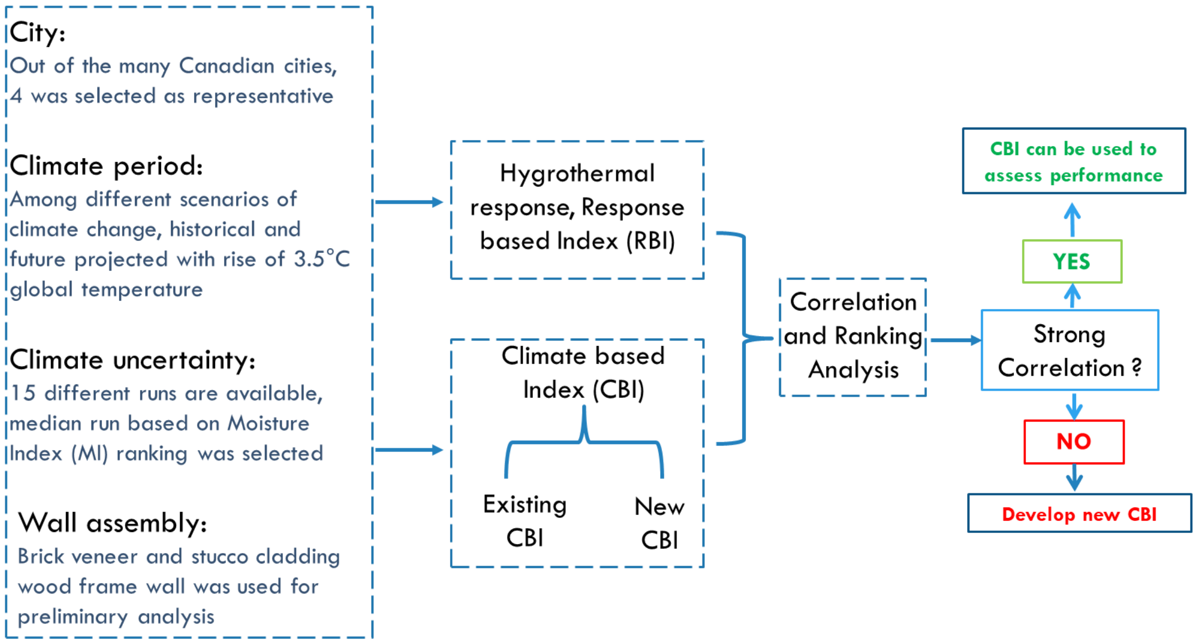

Figure 3.1: Proposed methodology to assess the wall performance using climate-based indices

3.1. City Selection

Four Canadian cities belonging to different climate zones (Figure 3.2) were selected for this study; this included: Calgary (AB), Ottawa (ON), St. John's (NL), and Vancouver (BC). Their location and respective climate characteristics are provided in Table 3.1. The moisture index (MI) and Heating Degree-Days (HDD) are 0.37 and 5000, 0.84 and 4500, 1.41 and 4800 and 1.93 and 3100, for Calgary, Ottawa, St. John's, and Vancouver, respectively (National Building Code, 2015). Among the four cities, Vancouver is the wettest city with a moisture index (MI) of 1.93 and Calgary is the driest city with an MI of 0.37. Other cities lie between these two values.

Table 3.1: Characteristics of the selected cities

City	Latitude	Longitude	HDD[1]	MI[2]	TZO[3]	CZ[4]	Annual Rainfall (mm)

Calgary	51.05	-114.07	5000	0.37	-7	7A	325
Ottawa	45.25	-75.42	4500	0.84	-5	6	750
St. John's	47.55°	-52.71°	4800	1.41	-4	6	1200
Vancouver	49.28	-123.12	3100	1.93	-8	5	1850

[1]: Heating-Degree Days; [2]: Moisture Index; [3]: Time Zone; and [4]: Climate Zone

Figure 3.2: Location of cities selected for analysis

3.2. Climate data

The historical climate data was sourced from the hourly and daily climate databases of Environment and Climate Change Canada (ECCC). Missing values were filled in using bias-corrected Climate Forecast System Reanalysis (CFSR: Saha et al. 2010). To perform bias correction, multiplicative or additive (depending on the climate variable being corrected) correction factors were calculated for each month and hour by comparing the CFSR data with the observational data, and thereafter the correction factors were applied to correct CFSR data. This data was then used to fill in missing values in the observational database. The direct and diffuse radiation values were derived from global radiation values using the method of Orgill and Hollands (1977). Weather data for the cities was taken from the National Research Council of Canada (NRC). A continuous 31-year long time series of hourly climate data was available for the historical time period from 1986-2016 and similar data for future time-period when global warming of 3.5°C is expected to be reached at the end of the 21st century (Gaur et al., 2019). According to Environment and Climate Change Canada (2018), an increase of 3.5ºC will be reached between 2062 and 2092 under Representative Concentration Pathway (RCP) 8.5.

3.3. Description of wall systems

The procedure involves hygrothermal simulations of a 3.5-storey building located in a suburban setting. A lightweight wood frame wall assembly with either brick veneer or stucco cladding and incorporating an air space behind the cladding (Figure 3.3) was simulated with the assumption that there was no air leakage.

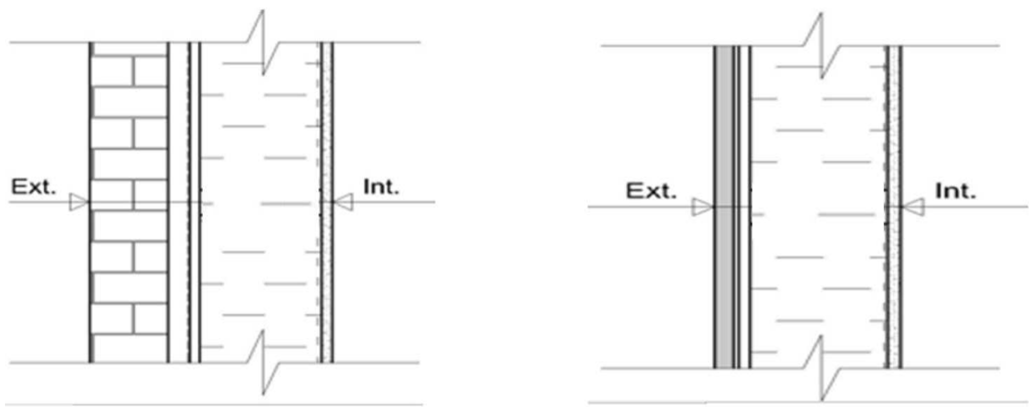

From exterior to interior

- 90 mm brick (red matt clay brick clad.)
- 25 mm air gap
- 30 minute asphalt impreganated building paper
- 11 mm OSB sheathing
- 140 mm fibreglass insulation
- Polyethylene vapor barrier (6mil.)
- 12.7 mm interior finish (gypsum+primer+latex)

From exterior to interior

- 19 mm stucco cladding on metal lath
- 10 mm air gap
- 30 minute asphalt impreganated building paper
- 11 mm OSB sheathing
- 140 mm fibreglass insulation
- Polyethylene vapor barrier (6mil.)
- 12.7 mm interior finish (gypsum+primer+latex)

Figure 3.3: Cross section of brick veneer cladding (left) and stucco cladding wood-stud wall assembly

The walls differ only in their cladding type which included: brick veneer (90 mm) and stucco (19 mm). The general configuration inboard of the cladding consisted of:

- Sheathing membrane (30 Minute paper, 0.22 mm)
- Exterior grade wood-based sheathing panel (OSB, 11 mm)
- Insulation within vertical stud cavities (fiberglass insulation, 140 mm)

- Vapor barrier: polyethylene sheet (0.15 mm)
- Interior grade gypsum panel with latex primer and 1 coat of latex paint (12.7 mm)

A drainage cavity of 25 mm and 10 mm was added to the wall assembly having brick veneer and stucco cladding respectively.

3.4. HAM simulations setting

3.4.1. Overview of the simulation tool

In this study, simulations were performed using DELPHIN 5, v5.9.4. The DELPHIN 5 (Coupled Heat, Air, Moisture and Pollutant Simulation in Building Envelope Systems) was developed during 2004-2006 with funding support from research grants from the U.S. Environmental Protection Agency, U.S. Department of Energy, Syracuse Center of Excellence in Energy and Environmental Systems, EQS-STAR Center/New York State Office of Science, Technology and Academic Research, and Syracuse University. It is maintained by the Institute for Building Climatology, Faculty of Architecture, and the Technical University of Dresden, Germany[1]. It is intended for the coupled heat, moisture, and matter (salts, pollutants) transport in porous building materials. It can solve one and two-dimensional problems and has been successfully validated with HAMSTAD Benchmarks 1 through 5 (Sontag et al., 2013). (Sontag, Nicolai, & Vogelsang, 2013). The model uses either the full sorption isotherm or the water retention function. Material properties are defined as a function of volumetric moisture content and temperature. Climate data is entered as individual files for each climate variable. An important feature of DELPHIN is its ability to handle wind-driven rain deposition and solar radiation as part of its boundary conditions, as well as air leakage, and moisture and heat sources. Cavity walls can also be considered and in the case of a ventilated cavity, the contribution of airflow to heat and moisture transfer in the structure can be done by using either an air exchange rate or an air flow rate.

3.4.2. Material properties

The following material properties were defined for each component of the wall assemblies:

- Density
- Specific heat

[1] DELPHIN documentation, http://www.bauklimatik-dresden.de/downloads.php

- Sorption isotherm
- Thermal conductivity
- Water vapor permeability
- Liquid water diffusivity

The material properties were obtained from the NRC hygrothermal material property database (Kumaran. 2006). The material properties of various layers and claddings are shown in Table 3.2.

Table 3.2: Material properties of the various layers of the wall assembly

Material	**Thickness (mm)**	**Dry density (kg/m^3)**	**Specific heat capacity (J/kg.K)**	**Thermal conductivity (W/m.K)**	**Porosity (m^3/m^3)**
Brick	90	1900	800	0.5	0.21
Stucco	19	1960	840	0.40	0.23
OSB	11	600	1880	0.09	0.96
Fiberglass insulation	140	11.5	840	0.04	0.99
Vapor barrier	0.15	1256	840	0.15	0.001
Sheathing membrane	0.22	909	1256	0.15	0.97

A comparison of the moisture storage capacity, moisture diffusivity, and vapor permeability of the cladding materials used in the wall assemblies is provided, in Figure 3.4, Figure 3.5, and Figure 3.6, respectively. At the lower level of RH, brick has a lower moisture storage capacity than stucco. However, at higher RH levels (RH>95%), brick and stucco have similar storage capacities. For the liquid diffusivity, at a lower level of RH (RH<95%), brick has low liquid diffusivity but above 95% RH, the liquid diffusivity increases sharply. Vapor permeability (expressed in ng/m.s.Pa) for the brick remained almost constant while for stucco cladding, it increases steadily with the increasing relative humidity.

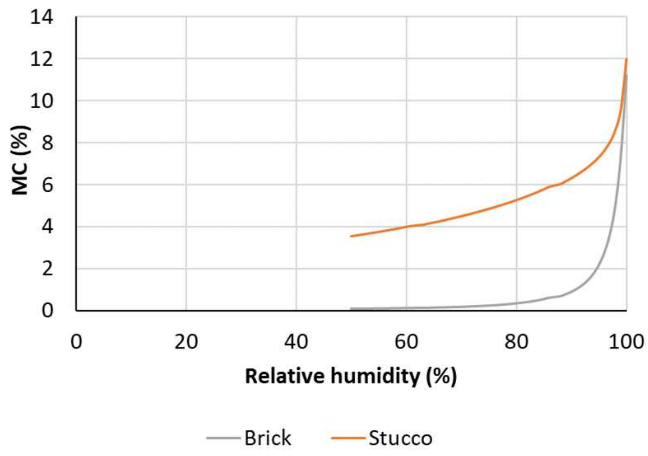

Figure 3.4: The variation of Moisture Content (MC) with relative humidity for brick and stucco

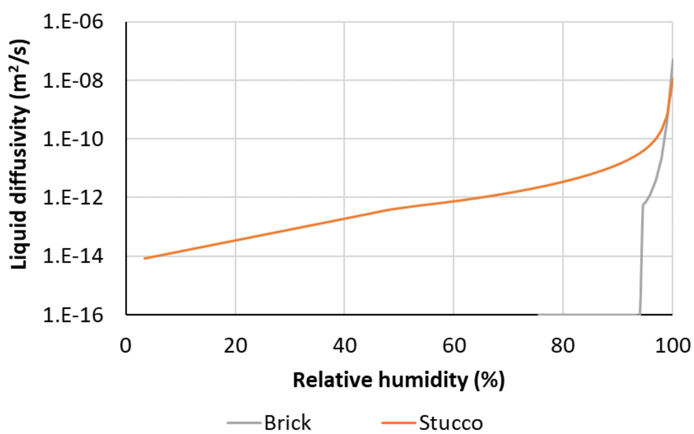

Figure 3.5: The variation of liquid diffusivity with relative humidity for brick and stucco

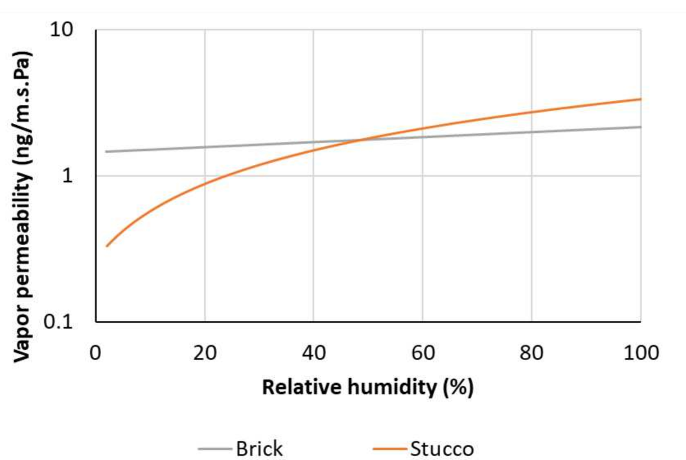

Figure 3.6: The variation of vapor permeability with relative humidity for brick and stucco

3.4.3. Boundary conditions

3.4.3.1.Indoor boundary conditions

Indoor temperature and relative humidity were assumed constant and set to 21°C and 50%, respectively assuming that the residential building was equipped with air conditioning and dehumidification. Following the EN ISO 6946 standard, the indoor surface heat exchange coefficient was set to 8 W/m^2K (convective heat transfer coefficient: 2.5 W/m^2K and radiative heat transfer coefficient: 5.5 W/m^2K).

3.4.3.2.Outdoor boundary conditions

Following the EN ISO 6946 standard, The convective heat transfer coefficient, h_{ce}, on the exterior surface was calculated using equation (2).

$$h_{ce} = 4 + 4\,v \tag{3-1}$$

The outdoor vapor diffusion coefficient was calculated using the convective heat transfer coefficient and Lewis number (Incropera et al., 2015). The reflectance of the surrounding ground (albedo) was set as 0.1 and the solar absorptance of the wall surface was set to 0.6.

3.4.4. Initial conditions

The wall was conditioned by repeating a seven-year simulation using the weather data of the average year (the year with the average MI among the 31 years). The values of temperature and RH for each layer in the wall configuration at the end of the simulation were used as initial conditions.

3.4.5. Moisture source and location

The moisture source used in the simulations was determined assuming water entry beyond the cladding in the wall systems. The water entry was calculated as a function of the wind-driven rain from the climate data. Based on ASHRAE 160, 1% of the wind-driven rain was applied to the exterior side of the sheathing membrane.

3.4.6. Critical location in wall assembly at risk of moisture issues

The OSB sheathing panel plays a structural function in the wall assembly. If water passes through the first defense layer and reaches the sheathing membrane, it can diffuse toward the OSB sheathing and create conditions for mould growth, and ultimately wood decay which can lead to premature deterioration of the component and wall system. The outer layer of the OSB sheathing was therefore selected as the critical location to assess the moisture performance.

3.4.7. Moisture performance assessment

For analyzing the moisture performance of the wall assembly, the mould index was computed at the exterior of the OSB layer, 0.1mm thick element size using the VTT model proposed by Viitanen et al. (2010). The model suggested that the mould index can vary between zero and six, where an index of 0 means no mould growth and 6 means the surface is fully covered with mould. Details of the model can be found in Viitanen et al. (2010). For this study, the calculations were made assuming the “sensitive class” for material and surface and a decline factor of 0.1 when the conditions become unfavorable for mould growth. The maximum mould index (among the hourly values) was used as a measure to compare the performance of different years. It should be noted here that the VTT model used in this study is based on several assumptions and the results can vary from real-world results. Caution is advised while analyzing the absolute values of the results, however, the results can be effectively used for a relative comparison among different scenarios.

3.4.8. Numerical simulation

Spatial discretization: For efficient performance of numerical simulation, it is imperative to have a fine mesh to have a solution as close as possible to analytical solutions. However, having a fine mesh could result in many elements and hence increase the computational time. In this study, different meshes were investigated comprising equidistant and variable mesh discretization. To analyze the response of the different meshing, the moisture content of the OSB layer was calculated and compared for simulations with different meshing. Four meshing were tested, and the details of each of them are shown below:

Equidistant mesh of 1mm minimum size: For brick cladding, an equidistant mesh of 1mm was assumed. There were 279 elements with a thickness of 1 mm each with an exception for the sheathing membrane and vapor barrier. For all the next meshes and cladding surfaces, similar mesh dimensions were kept for the sheathing membrane and vapor barrier, i.e. 3 equal mesh elements of thickness 0.0733 mm and 0.05 mm respectively. There were 285 elements in total.

Similar to the brick cladding, for stucco cladding, a 1 mm equidistant mesh was created. There were 183 elements with a thickness of 1mm each with an exception for the sheathing membrane and vapor barrier. There were 189 elements in total.

Equidistant mesh of 0.5mm minimum size: For brick cladding, an equidistant mesh of 0.5 mm is assumed. There were 558 elements with a thickness of 0.5mm each with an exception for the sheathing membrane and vapor barrier. For the sheathing membrane and vapor barrier, 3 equal mesh elements of thickness 0.0733mm and 0.05mm respectively are used. There were 564 elements in total.

Similar data for stucco cladding involves, 373 elements in total with 367 elements of 0.5 mm mesh each and the remaining 6 for sheathing membrane and vapor barrier as per dimensions mentioned earlier.

Equidistant mesh of 0.1mm minimum size: For brick cladding, an equidistant mesh of 0.1 mm is assumed. There were 2673 elements with a thickness of 0.1mm each. There were 2679 elements in total (including 6 elements from the sheathing membrane and vapor barrier).

For stucco cladding, there were 1833 elements in total with 1827 elements of 0.1 mm each.

Manual discretization: Brick cladding

Table 3.3: Description of meshing for different layers for brick cladding

	Region 1			**Region 2**		**Region 3**	
Layer	**Thickness**	**No. of elements**	**Stretch factor**	**Thickness**	**No. of elements**	**Thickness**	**No. of elements**
Brick (90 mm)	15 mm	19	1.17	60 mm	22	15 mm	19
Air cavity (25 mm)	5 mm	7	1.7	15 mm	6	5 mm	7
OSB (11 mm)	2 mm	4	2.3	7 mm	3	2 mm	4
Insulation (140 mm)	20 mm	25	1.15	100 mm	31	20 mm	25
Gypsum (12.7 mm)	2.5 mm	5	1.9	7.7 mm	4	2.5 mm	5

In the final case, mesh thickness was chosen manually. Different wall layers except for the sheathing membrane and vapor barrier were divided into three regions with the first and last regions of equal thickness. A fine and variable mesh was used for the first and large region while an equidistant mesh was opted for the middle region. For the regions with fine mesh, a minimum thickness of the element was chosen to be 0.1 mm with an equal stretch factor. Table 3.3 illustrates the thickness and mesh details of different regions for different layers of the wall configuration.

Figure 3.7 shows one typical example where the moisture content of OSB was outputted from DELPHIN for brick cladding simulation in Ottawa. Four different meshes were tested to evaluate the response from the simulation and it was found that the result with manual discretization was similar to the one obtained with an equidistant fine mesh of 0.1 mm size. A similar observation was noted with simulations involving different cladding and cities. Manual discretization offers a similar accuracy as obtained from fine mesh but with a much lesser number of elements (2679 vs 192) and hence a lower computational time. Following this, the suggested manual discretization was opted for all the simulations in the thesis work.

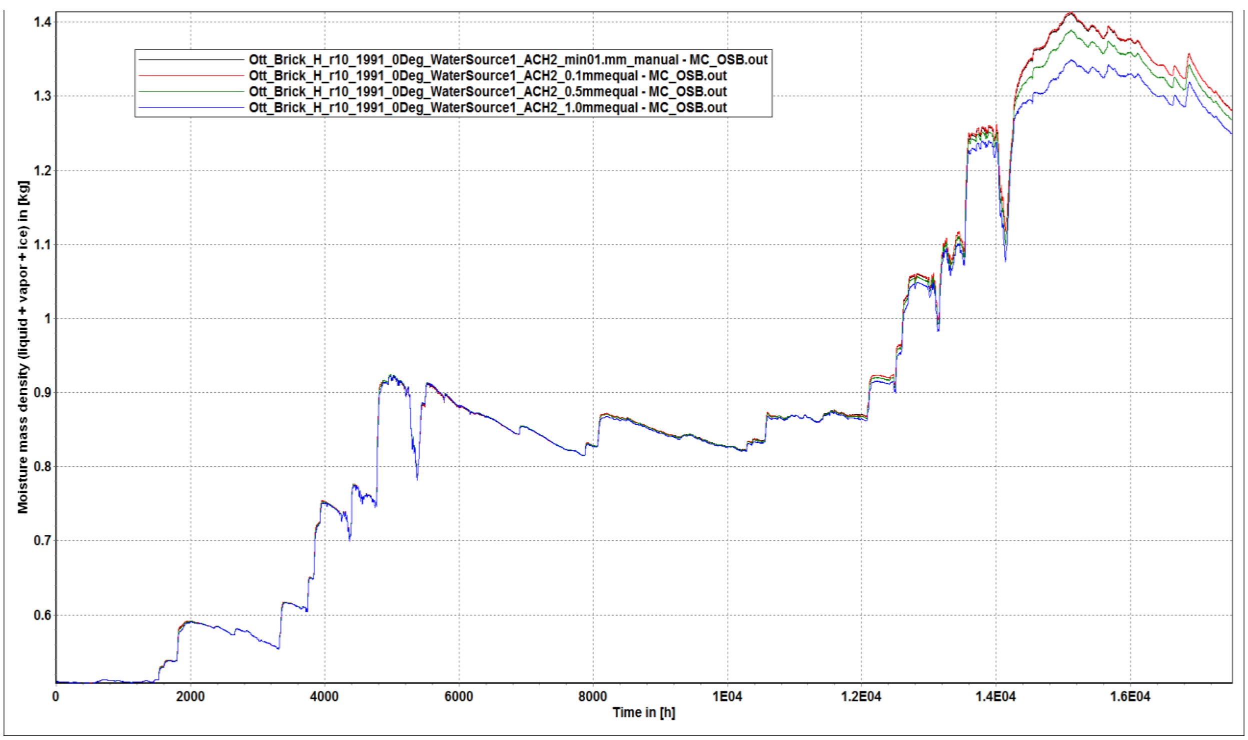

Figure 3.7: Integral moisture content in OSB layer for different mesh discretization for brick cladding wall configuration

Manual discretization: Stucco cladding:

For stucco cladding, similar to the above-shown table, all dimensions and number of elements were kept the same except for the fact that instead of brick, now stucco cladding was used with an air cavity of 10 mm.

For the sheathing membrane and poly vapor barrier layer, similar to the previous meshes, an equidistant mesh of 3 elements was opted for. Using the manual discretization, the total number of elements was found to be 192 and 138 for brick and stucco cladding respectively. For stucco cladding, the following dimensions were used:

Table 3.4: Description of meshing for stucco cladding

	Region 1			Region 2		Region 3	
Layer	**Thickness**	**No. of elements**	**Stretch factor**	**Thickness**	**No. of elements**	**Thickness**	**No. of elements**
Stucco (19 mm)	4 mm	6	1.9	11 mm	4	4 mm	6
Air cavity (10 mm)	3 mm	4	2.9	4 mm	2	3 mm	4

Solver Settings

In this study, simulations were performed using state-of-the-art hygrothermal modeling software, Delphin 5.9. Material properties were defined as a function of volumetric moisture content and climate data was entered as individual files for each climate variable. An initial time step of 0.01s, a maximum time step of 30 min, a relative tolerance of 10^{-7} and an absolute tolerance for moisture mass balance equation of 10^{-8} were selected for all the simulations.

3.5. Assumptions for hygrothermal simulations

The following assumptions are made for the hygrothermal simulations:

- Material properties of various layers of the wall assembly are assumed to be constant regardless of their thickness throughout the simulation period.
- All the layers are assumed to have perfect contact between them.
- The numerically modeled climate data used for the simulations is assumed to represent the possible future climate data.

- The mould index used for performance assessment is calculated based on hygrothermal simulation results. It is assumed that the relative variation among different scenarios is similar to the relative variation as if the mould index is calculated based on measurement results.
- There is no mass or energy transfer through the top and bottom of the geometry.

3.6. Wall orientation selection for hygrothermal simulations

The hygrothermal response of a wall depends on the type of climate to which it has been exposed. A wall could lead to satisfactory performance in one type of climate but the same might not be true for another climate. The response of the wall is affected by many climate variables. Amongst these climate variables, most of these are independent of wall orientation but a few are directly dependent on the orientation of the wall. Wind-Driven Rain (WDR) for a given location is determined by the wind speed, wind direction, rainfall intensity, and the quantity of WDR to which a wall may be subjected is dependent on the wall orientation in relation to the prevailing WDR direction. Moreover, WDR and solar radiation serve as important orientation-dependent boundary conditions when performing any hygrothermal simulation. Therefore, the need to have the appropriate wall orientation when undertaking an analysis of the moisture performance of a wall becomes a critical task to help ensure a durable building envelope design. Different methods are available in the literature to select the wall orientation for simulations. An orientation chosen based on any available method was assumed to lead to the worst performance of the wall i.e., having the most severe moisture problem that could be defined using damage functions such as moisture accumulation, mould growth, and wood decay.

Most studies have suggested using the orientation (called default orientation in this work) that receives the highest amount of WDR or the least solar radiation for the simulations without considering the climate data, type of cladding, structure of the wall, moisture source, etc. The objective of the thesis was to verify these assumptions for different wall assemblies under different climates for different rain scenarios. Further, different methods were investigated to choose the default orientation. The intent was to identify whether the results using these methods are consistent with each other and also, can the use of any of these methods results in a wall orientation that leads to the worst moisture performance when compared to the simulation results.

Hygrothermal simulations were performed to assess the effects of wall orientation on the moisture performance of wood-frame wall assemblies. Four cladding types and eleven Canadian cities (representing the whole of Canada) were selected for analysis (Aggarwal et al. (2021) and Aggarwal et al. (2022)). The results with the three cities and 2 wall claddings are discussed and detailed in this thesis. The results obtained for other cities and wall cladding can be found in the appendix A3.

Three scenarios were simulated: (i) no WDR and no water source, (ii) only WDR, and (iii) both WDR and water source. The water source considered was 1% of wind-driven rain applied on the exterior side of the sheathing membrane as per ASHRAE 160. Simulations were performed for four cardinal orientations (North, East, South, and West) and one default orientation (orientation with the highest amount of WDR).

The WDR in a specific direction was calculated using four methods (equations (3-2) to (3-5)) i.e., ASHRAE (ASHRAE 160 (2016), ISO (ISO (2009), CI (Zhou et al., 2016) and R*v (Aggarwal et al. 2020)).

$$WDR_{ASHRAE} = F_E . F_D . F_L . U_{10} . \cos\theta . R_h \tag{3-2}$$

Where, F_E: rain exposure factor; F_D: rain deposition factor; F_L: empirical constant; U_{10}: hourly mean wind velocity at 10 m (m/s); θ: angle between the wind direction and the normal to the façade; and R_h: total hourly horizontal rainfall intensity (mm).

$$WDR_{Iso} = \frac{2}{9} . U_{10} . R_h^{8/9} . C_R . C_T . O . W . \cos\theta \tag{3-3}$$

Where, U_{10}: hourly wind speed at 10 m (m/s); R_h: total hourly horizontal rainfall intensity (mm), θ: angle between the wind direction and the normal to the façade; C_T: topography coefficient; O: obstruction factor; W: wall factor; and C_R: terrain roughness coefficient.

$$CI = \frac{WI}{DI} \tag{3-4}$$

Where, WI: wetting index and DI: drying index.

$$WDR_{R*v} = R_h . U_{10} \tag{3-5}$$

Where, U_{10}: hourly wind speed at 10 m (m/s); R_h: total hourly horizontal rainfall intensity (mm).

3.6.1. Results with different rain scenarios

The results are presented firstly for the cases without WDR and water penetration, secondly for the case with WDR only, and finally for the case with WDR and water source. It was found that the results obtained with the different performance indicators were generally in good agreement. Therefore, only the results obtained using maximum moisture content (amount of moisture in kg) as a performance indicator are discussed. The results obtained with other performance indicators can be found in the Appendix.

3.6.1.1.Scenario with no WDR and moisture source

The first analysis is based on the case where there was no WDR or moisture source. Figure 3.8 shows the maximum MC in the OSB layer obtained at different wall orientations for three cities and two claddings. Table 3.5 shows, for brick cladding, the maximum MC for the default orientation and the maximum MC for the orientation which has the highest value of maximum MC among the orientations compared. For all the cities, irrespective of the cladding type, the highest value of maximum MC was observed when the wall is facing the North orientation. This is due to the significantly lower amount of solar radiation in the North direction. The results are consistent with the one found by Lepage et al. (2017).

Table 3.5: Maximum moisture content (MC) values in the OSB layer for brick cladding with no WDR and no water source for the wettest year

City	Default orientation		Orientation with Max. MC	
	Orientation	**Max. MC (kg)**	**Orientation**	**Max. MC (kg)**
Ottawa	22.5° (NNE)	0.56	0° (North)	0.57
St. John’s	202.5° (SSW)	0.60	0° (North)	0.64
Vancouver	157.5° (SSE)	0.51	0° (North)	0.51

For Vancouver, it was observed that the maximum MC is relatively lower than in other cities. As there is no rain the only factor which results in moisture accumulation is vapor diffusion. Furthermore, for brick cladding, it was seen that the values are similar irrespective of the orientation in these two cities. This is due to the low vapor permeability of brick cladding for the outdoor RH range (Figure 3.6). Considering the brick cladding is 90 mm thick brick, the transport of vapor via diffusion is further limited. Therefore, irrespective of the orientation, the moisture accumulated in the OSB for brick cladding is almost the same.

Figure 3.8: Maximum moisture content of OSB layer for three cities with no WDR and no water source

3.6.1.2.Cases with WDR but no water source

In this section, the results are discussed where wind-driven rain (WDR) is taken into consideration while assuming no deficiency in the cladding and correspondingly no water penetration. In general, it was observed that, unlike the previous case where the north orientation always leads to the worst performance irrespective of city or cladding, in this case, the results are not as consistent. Table 3.6 shows the result for maximum moisture content in the OSB layer for brick cladding walls in three cities. It was observed that for all three cities, the default orientation resulted in the worst performance.

Table 3.6: Maximum Moisture content (MC) values in the OSB layer for brick cladding with WDR but no water source for the wettest year

City	Default orientation		Orientation with Max. MC	
	Orientation	Max. MC (kg)	Orientation	Max. MC (kg)
Ottawa	22.5° (NNE)	0.96	22.5° (Default)	0.96
St. John’s	202.5° (SSW)	1.48	202.5° (Default)	1.48
Vancouver	157.5° (SSE)	1.71	157.5° (Default)	1.71

Figure 3.9 shows, for each city and two claddings, the maximum moisture content obtained in each orientation. In general, the maximum MC was highest for the stucco cladding. This is because stucco has the highest liquid diffusivity up to a certain range (approximately 95%) of RH (Figure 3.5) and is later superseded by brick for higher RH levels. However, as the thickness of brick is approximately five times more than stucco, it takes longer for the moisture to transport through

brick. This results in the highest maximum MC in the stucco cladding for all the orientations and cities.

Figure 3.9: Maximum Moisture content of OSB layer for three cities with WDR but no water source

3.6.1.3.Cases with WDR and water source

In this scenario, WDR was assumed, and the walls were assumed to have some deficiencies that allow water to penetrate the structure. The water source was calculated as 1% of WDR and deposited at the exterior layer of the sheathing membrane. Table 3.7 shows, for the brick cladding, the max. MC in the OSB layer was obtained with the default orientation and with the orientation having max. MC in different cities. For all the cities, default orientation led to the worst moisture performance.

Table 3.7: Maximum Moisture content (MC) values in the OSB layer for brick cladding with WDR and water source for the wettest year

City	Default orientation		Orientation with Max. MC	
	Orientation	**Max. MC (kg)**	**Orientation**	**Max. MC (kg)**
Ottawa	22.5° (NNE)	1.35	22.5°(Default)	1.35
St. John’s	202.5° (SSW)	1.86	202.5° (Default)	1.86
Vancouver	157.5° (SSE)	2.39	157.5° (Default)	2.39

A further illustration of all the simulated cases can be found in Figure 3.10. As observed from Figure 3.10, the worst response occurs in the default orientation. Hence, based on these analyses, it can be said that choosing the default orientation based on the highest WDR is a good assumption.

Figure 3.10: Maximum Moisture content of OSB layer for three cities with WDR and Water source

3.6.2. Results comparing default orientation with different WDR methods

Default orientation selection with 4 methods

In this section, different methods of selecting the default orientations were tested and compared with each other. Figure 3.11 shows the directional WDR distribution (for the wettest year) at sixteen orientations (with an interval of 22.5º) for the three cities. It can be seen that WDR distribution with the "R*v" method showed a greater variation as compared to the other three methods, for which the variation amongst the different orientations remained small.

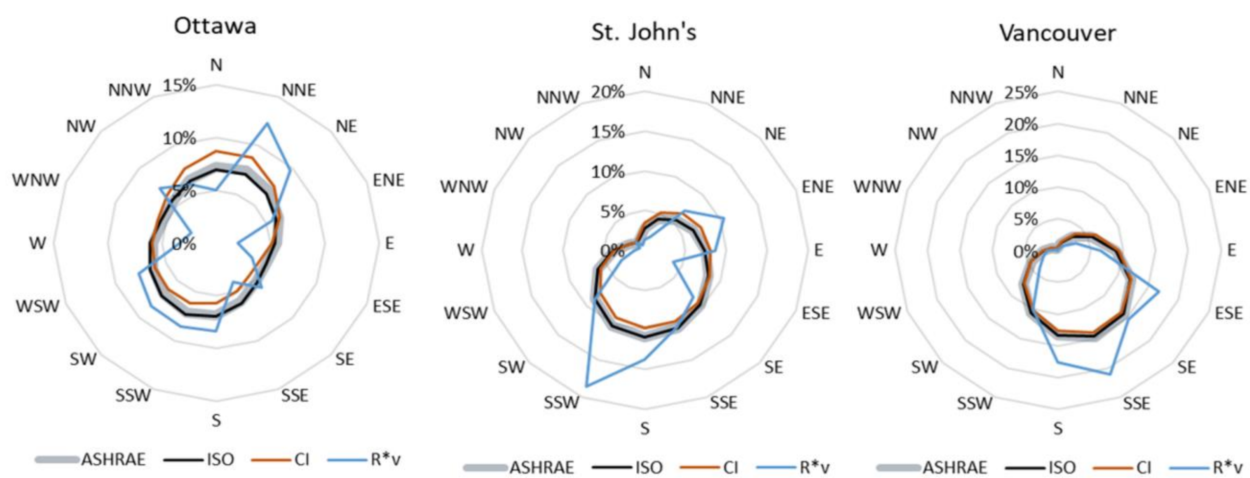

Figure 3.11: Wind-driven rain distribution for the wettest year for 3 cities using 4 methods

Table 3.8 shows the default orientation selected when using any of the 4 orientation selection methods. It can be seen that amongst the 4 methods, ASHRAE and ISO methods were consistent in the selection of the default orientation except for Ottawa. However, a closer look at Ottawa shows that although the orientation chosen was different, the difference in WDR between the two orientations was small i.e., approximately 2% (Figure 3.11).

Table 3.8: Default orientation for 3 cities with 4 methods

City	ASHRAE	ISO	CI	R*v
Ottawa	22.5º (NNE)	202.5º (SSW)	22.5º (NNE)	22.5º (NNE)
St. John's	180º (S)	180º (S)	180º (S)	202.5º (SSW)
Vancouver	157.5º (SSE)	157.5º (SSE)	157.5º (SSE)	157.5º (SSE)

Comparison of default orientation with 4 methods and actual simulation results

In the previous section, a comparison was made between the default orientation selected by different methods. In this section, the default orientation selected using different methods is compared with the orientation that leads to the worst performance when hygrothermal simulations are performed. For this purpose, simulations were performed for 4 cardinal orientations and the default orientation (selected by each method). For a given method, should the worst performance occur in any of the suggested default orientations; the method is deemed satisfactory, otherwise, the orientation that results in the highest value of the performance indicator is marked as the orientation that leads to the worst performance.

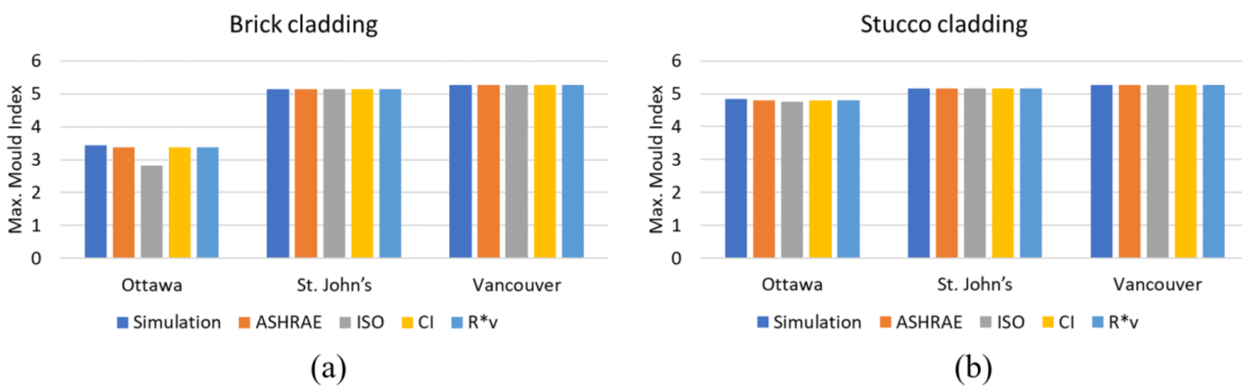

Figure 3.12: Maximum mould index with default orientations from different methods and simulations for (a) brick veneer wall and (b) stucco cladding wall

Figure 3.12 (a) shows the maximum mould index values obtained with default orientations suggested by different methods along with the one having the highest value of maximum mould index based on simulations for a brick cladding wall. It was observed that for all the cities, except for Ottawa, the worst performance occurs in the default orientation suggested by one of the investigated methods. For Ottawa, although the worst performance occurred in the north (different from default by any method), the value of the maximum mould index in the north and default orientation was similar. In general, it was observed that the default orientation suggested by the ASHRAE method results in the worst performance when simulations are performed, meaning that the orientation selected using the ASHRAE method can be used to analyze the worst-case scenario. Figure 3.12 (b) shows the same results as were presented for the brick cladding wall, but for the stucco cladding wall. Similar to the results with the brick cladding, the worst performance occurred in one of the default orientations except for Ottawa. However, the difference in the maximum mould index remained small amongst orientations selected using different selection methods and the simulation results. Further, the ASHRAE method was consistent in terms of leading to the wall orientation resulting in the worst performance.

To analyze the wall performance, it is essential to select the worst wall orientation to quantify the maximum risk. Based on the above-mentioned analysis, it was found that the ASHRAE method results in an orientation that also leads to the worst performance when simulations are performed and hence it is recommended to select the wall orientation for the hygrothermal analysis. Further, to assess the moisture risk of walls, it is essential to perform the hygrothermal analysis under the given climate period. However, many factors can significantly influence the analysis. In other words, the moisture risk for a given city and a given wall configuration might not be the same for any other city and wall configuration. To solve this, the thesis focused on selecting a few cities that are representative of different climate zones across Canada. Further, for the analysis, the two most commonly used wall configurations i.e., brick veneer cladding and stucco cladding wood frame walls were investigated in this work. In terms of climate periods, the work was limited only to historical (1986-2016) and future periods (2062-2092) i.e., when the global temperature is supposed to increase by 3.5°. Finally, the projected future climate data is prone to uncertainties, and hence to incorporate this, 15 climate data realizations are available. This study focused on only one realization which is supposed to have a median value of Moisture Index (MI). Further, to evaluate the uncertainties in the projected climate data, remaining climate realizations were tested in the later stages of the work.

In the following chapter, a detailed description is provided to discuss the methods used to evaluate the reliability of existing climate-based indices along with their corresponding results. The steps involved in developing the new climate-based index and the corresponding results are discussed in subsequent chapters.

Chapter 4 Evaluating the reliability of existing climate-based indices

The content of this chapter is published in the journal paper "*Aggarwal, C., Ge, H., Defo, M., & Lacasse, M. A. (2022). Reliability of Moisture Reference Year (MRY) selection methods for hygrothermal performance analysis of wood-frame walls under historical and future climates*". Building and Environment, 207(PA), 108513. https://doi.org/10.1016/j.buildenv.2021.108513. The abstract and introduction from the originally published paper is not included in this chapter and to avoid the repetition, the wall assemblies, climate-based index, model settings, etc. included in the originally published paper are excluded since these are already provided in Chapter 3 "Methodology".

Methodology

The modeled building was assumed to be a 3.5-storey structure located in a suburban setting. A lightweight wood frame wall assembly with brick veneer cladding and incorporating an air space behind the cladding was simulated with an assumption that there was no air leakage. Three cities representing three different climates across Canada were chosen: Ottawa (ON), Vancouver (BC), and Calgary (AB). One-dimensional section through the insulation of the wood-frame wall was simulated. The water infiltration through the cladding as the moisture source was assumed to be 1% of the WDR and applied to the exterior side of the sheathing membrane. Further details can be found in Chapter 3.

There are several methods to rank the years based on their moisture severity. However, the reliability of these methods remains questionable; for example, will the worst year as per the climate-based index result in the worst moisture risk, is the question that needs to be answered. This section focuses on evaluating the reliability of the existing climate-based indices in assessing the moisture risk of different years.

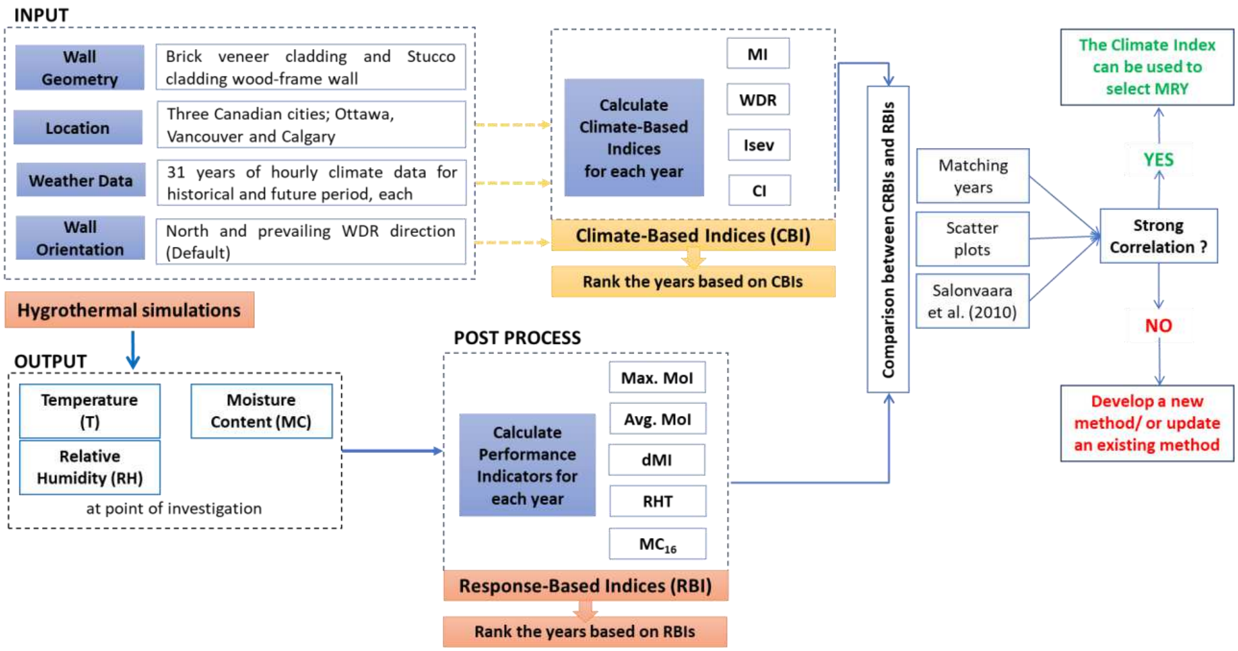

Figure 4.1: Flow chart describing the methodology followed to assess the reliability of existing climate-based indices

To gauge the potential of climate-based indices commonly used to rank the years, different approaches were used. Response-based indices (results from simulations) were evaluated, and the results are compared with the existing climate-based indices. Later, if any of the existing climate-based indices are deemed to be robust, then a procedure is developed to select MRY. The framework for evaluating the reliability of existing climate-based indices is illustrated in Figure 4.1.

To quantify the moisture risk, damage criteria and performance indicators are required. These performance indicators are computed at the critical wall layers and are further used as response-based indices. Mould Index, Moisture content, and RHT Index were used as response-based indices. Except for moisture content, the other two indices are not directly outputted from Delphin, and post-processing is required to obtain them. Accumulated moisture content in the entire OSB layer was calculated. While, for mould index and RHT index calculation, temperature, and relative humidity at the exterior layer of OSB (0.1 mm thick) were evaluated. In this present analysis, 5 performance indicators were used which include 3 variants of mould index along with moisture content and RHT index. Details of these indicators are given below:

1. **Mould Index**

The hourly MoI was calculated using hourly temperature and relative humidity outputted from the simulations. Later, three statistics of MoI i.e., maximum MoI, average MoI, and dMI was used as response-based indices. The maximum and average values of MoI were selected for each year for comparison. The higher the value for MoI, the higher the moisture damage risk. dMI is defined as the summation of the deviation of hourly MoI from a threshold value, as shown in equation (4-1). A threshold value of 3 was used in this study because above 3, mould growth can be visually seen.

$$dMI = \sum (MoI - 3) \tag{4-1}$$

Only the hours with MoI greater than 3, i.e., positive hourly values, were counted, and MoI less than 3, i.e., negative values were set to zero. It should be noted here that the simulated mould index using DELPHIN was used throughout this thesis for performance analysis. The mould from simulation was earlier validated (Wang et al., 2018) with measurement results and hence in this study, only simulated mould index was used.

2. RHT Index

The RHT index was calculated using the following equation:

$$RHT = \sum (T - T_L)(RH - RH_L) \tag{4-2}$$

Where, T and RH represent the temperature and relative humidity, respectively, on the surface of OSB. T_L and RH_L are the limiting values of temperature and RH, above which there is a risk of the onset of mould growth. In this work, the values for T_L and RH_L were chosen as 5°C and 80%, respectively.

3. Mean value of MC above 16% dry mass (MC_{16})

MC_{16} is calculated as the summation of the deviation of MC (in kg) in OSB from the 16% dry mass threshold in kg (Equation (4-3)). A 16% MC in OSB corresponds to the equilibrium moisture content (EMC) at about 80% RH and 21ºC temperature (Service, 2005), above which there could be moisture problems. For an 11-mm thick OSB panel with a 1m^2 area, having a density of 600 kg/m^3, the dry mass is 6.6 kg. A 16% MC in OSB, which is 1.056 kg (16% of 6.6), is subtracted from the hourly MC in the OSB sheathing and the yearly average is then taken (Equation (4-3)).

$$MC_{16} = \frac{\sum_{i=1}^{n} MC_{hourly} - 1.056}{n} \tag{4-3}$$

Where, MC_{hourly} is the hourly MC (kg) in OSB, and n is the total number of hours in a year (8760).

4.1. MC and mould index profiles

To better understand the results and correlation between response-based and climate-based indices, the variation of MC (Figure 4.2) and mould index (Figure 4.3) in the OSB layer located towards the exterior side of the panel were analyzed throughout the year.

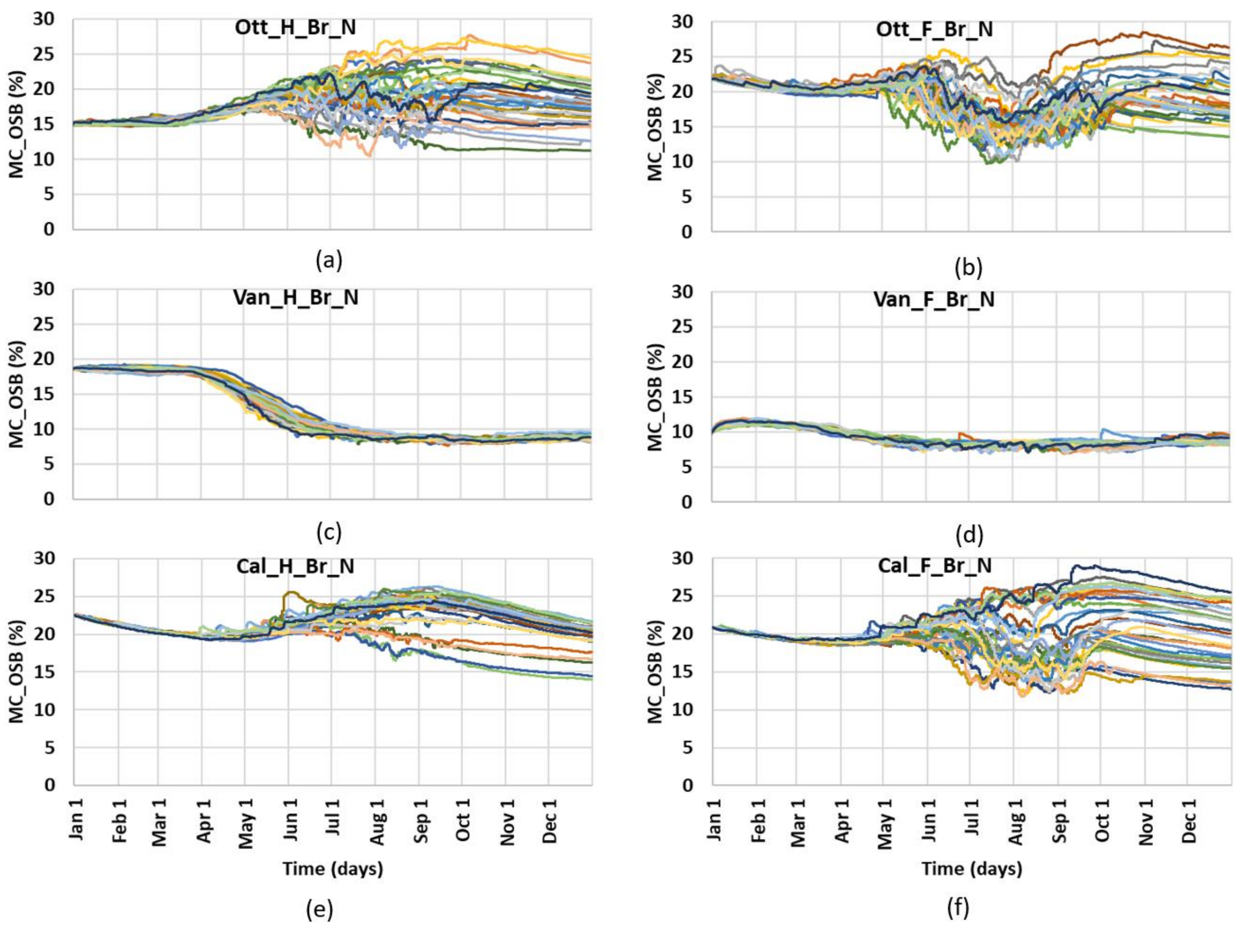

Figure 4.2: MC profile of OSB sheathing for brick cladding facing north orientation for 3 cities under 2 climate periods (Ott: Ottawa, Van: Vancouver, Cal: Calgary, H: Historical, F: Future, Br: Brick, N: North)

Figure 4.2 shows the MC (in % of dry mass) in the OSB layer for brick veneer cladding facing north orientation in the three cities under historical and future periods. It was observed that for Ottawa and Calgary, the MC remained almost constant in the first four months (winter) and it started to increase in spring. Depending on the climate loads corresponding to a given year, the MC either increased or decreased by the end of the year compared to the initial MC. Moreover, in terms of the spread of MC from the historical to a future period, a greater spread was observed for the future period due to more climate variability in future weather data. Vancouver showed a different trend in comparison to the other two cities. MC in OSB in Vancouver remained significantly low due to the extremely low amount of WDR impinging on the north-facing wall. In terms of climate period, there was a more significant decline in the MC, i.e. drying during the spring and summer time, for the historical period than in the future.

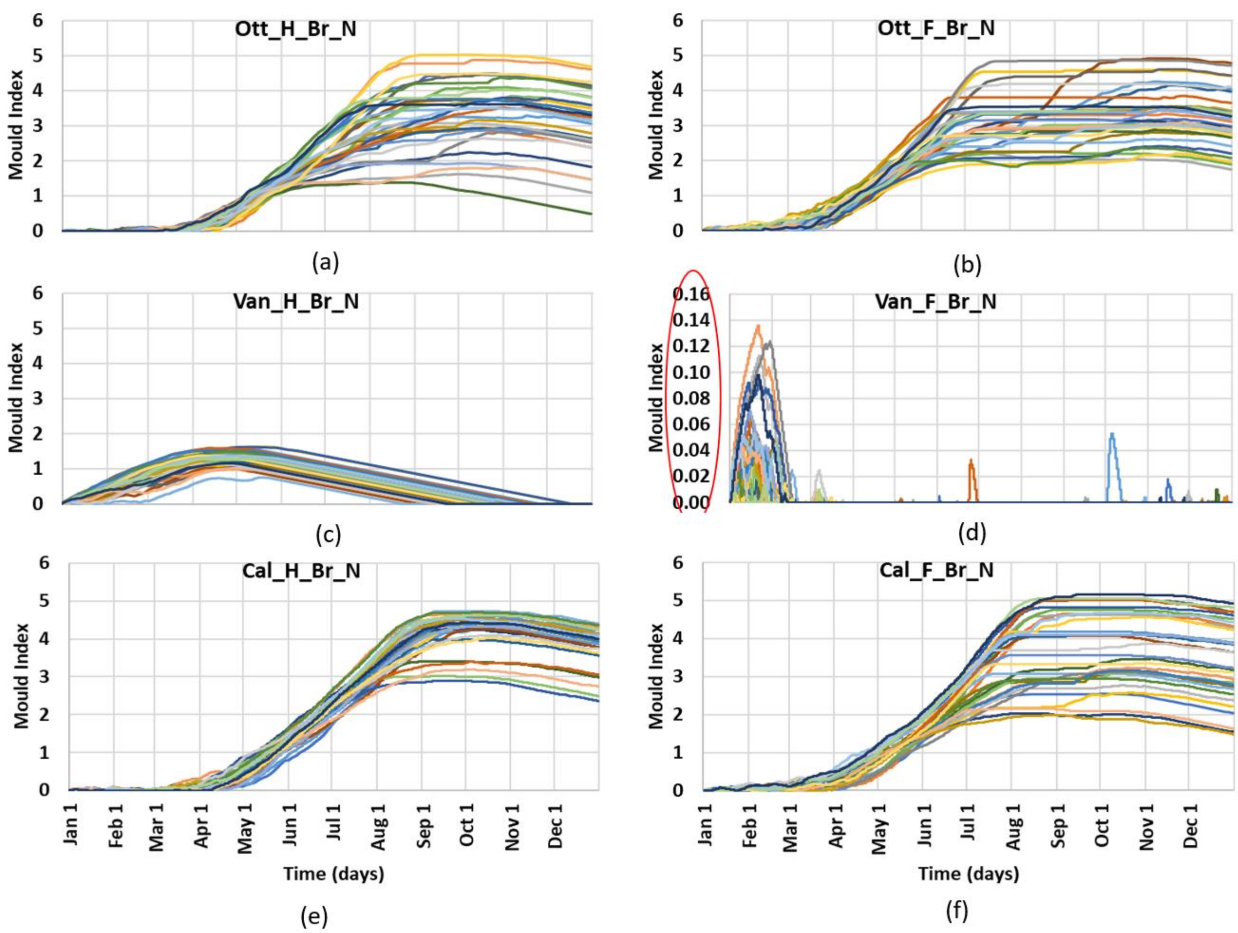

Figure 4.3: Mould index profile of OSB sheathing for brick cladding facing north orientation for 3 cities under 2 climate periods (Ott: Ottawa, Van: Vancouver, Cal: Calgary, H: Historical, F: Future, Br: Brick, N: North)

Figure 4.3 shows MoI results for the same wall. Except for Vancouver, MoI increases to a certain level and then stabilized for the rest of the year. For Ottawa, the range of MoI for historical climate (maximum MoI: 1.3-5) was larger than the corresponding values for future climate (maximum MoI: 2.2-4.9). On the other hand, the opposite trend was observed for Calgary. A similar trend was observed between MC and MoI meaning that the year having the highest/lowest MC corresponds to the same level when compared using MoI. For Vancouver, MoI increased in the beginning, but then fall to zero. The reason behind the initial rise was because of the effect of initial conditions, which provided favorable conditions for mould growth, but the lack of rain in the north thereafter could not sustain the mould growth and hence the values fall to zero.

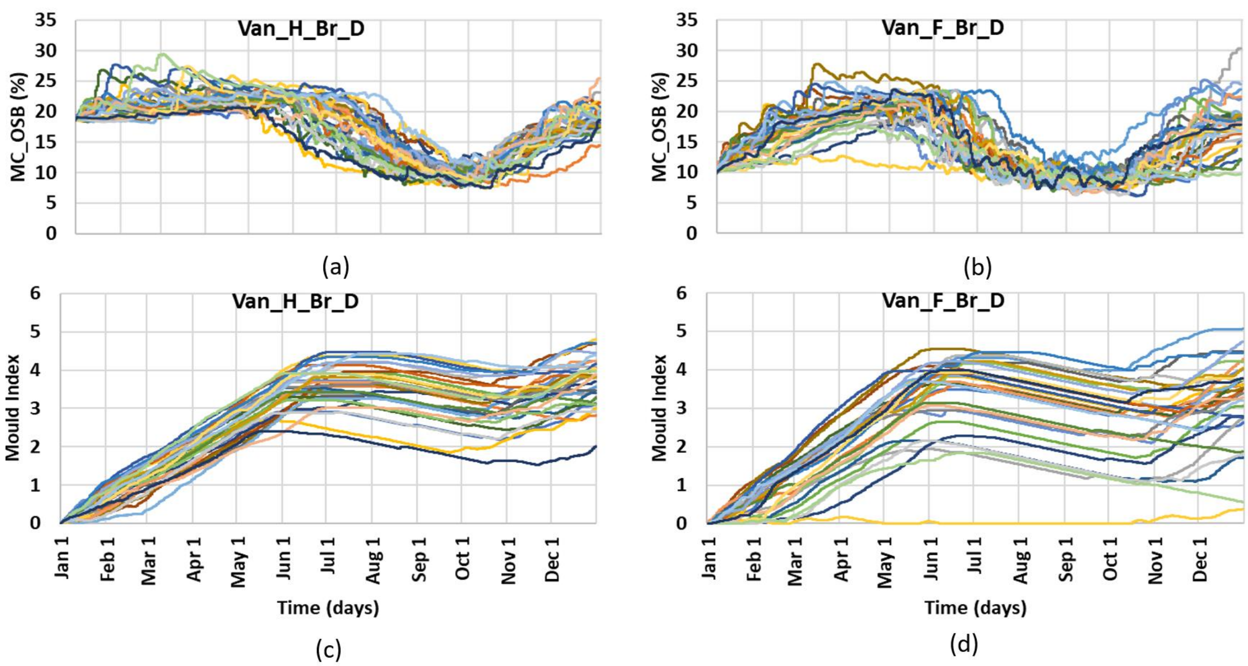

Figure 4.4: MC and MoI profiles of OSB sheathing for brick cladding facing default orientation (i.e. the prevailing WDR) for Vancouver

For a better assessment of the moisture risks in Vancouver, simulations were carried out and results were plotted for brick veneer cladding facing the default orientation (Figure 4.4). The MC and MoI showed a similar trend in terms of variation throughout the year. It was observed that from January 1 until the spring, MoI continuously increased because of favorable conditions of temperature and moisture. During summer, owing to drying conditions, MC decreases significantly and MoI decreases only slightly before both start to increase during the fall season. A similar trend was observed irrespective of the climate period. However, it can be noted that the MoI had a greater spread for the future due to more climate variability. As shown in Figure 4.3 and Figure 4.4, MoI sustained at a particular value for most of the years at the end of simulations, and hence the maximum MoI as a performance indicator could be used when comparing the severity of a particular year with another. The results obtained with default orientation in Ottawa and Calgary showed a similar trend as in the north i.e., MoI increased after a certain time and then stabilized along with a slightly higher spread of data in the future. Similar to brick veneer cladding, results for stucco cladding wall showed a similar pattern.

In summary, it was never apparent that MoI and MC reached a peak over a short period of time and then declined, with the exception of Vancouver (north-facing wall); i.e., in most cases, it stabilized. Therefore, both maximum and average MoI can be used as an index to rank the years based on their severity.

4.2. Comparison between climate-based indices and response-based indices

In this section, results are discussed in two sub-sections. Section 4.2.1 discusses the results related to the direct correlation between response-based and climate-based indices. The coefficient of determination (R^2) was used to determine the degree of correlation between the two indices. Section 4.2.2 presents the results related to the ranking of years using the climate-based index and simulation results.

4.2.1. Correlation method (Coefficient of determination)

A direct correlation between response-based and climate-based indices helps determine the accuracy of predicting the hygrothermal responses using the climate-based index. The higher the coefficient of determination, the more accurate the climate-based index is in predicting the response-based index. The correlation among different response-based indices (Table 4.1) was analyzed using the coefficient of determination.

The correlation among different indices was high for most of the cases with a few exceptions, which indicates that hygrothermal response evaluation using these indices was consistent. In general, the maximum MoI, average MoI, and RHT had a higher coefficient of determination, in the range of 0.76 to 0.98 than with dMI and MC_{16}, which was in the range of 0.64 to 0.98, with the exception of Calgary historical period where the correlation between RHT and other indicators was low (0.08 to 0.25). Missing values in the table indicate that the correlation cannot be established because of zero values. A more in-depth analysis considering all the simulated cases showed that the maximum MoI correlated slightly better with other indices and hence was used as the sole response-based index for further analysis in this work.

Table 4.1: Coefficient of determination (R^2) among different response-based indices for all the simulated cases for brick cladding facing north orientation

City	Indicator	Historical					Future				
		Max. MoI	Avg. MoI	dMI	MC_{16}	RHT	Max. MoI	Avg. MoI	dMI	MC_{16}	RHT
Ottawa	Max. MoI	1.00	0.98	0.77	0.91	0.90	1.00	0.90	0.82	0.93	0.87
	Avg. MoI		1.00	0.76	0.91	0.93		1.00	0.81	0.84	0.93
	dMI			1.00	0.95	0.64			1.00	0.88	0.75
	MC_{16}				1.00	0.80				1.00	0.85
	RHT					1.00					1.00
Vancouver	Max. MoI	1.00	0.96	0.00	0.77	0.81	1.00	0.92	0.00	0.00	0.75
	Avg. MoI		1.00	0.00	0.82	0.78		1.00	0.00	0.00	0.78
	dMI			---	---	---	---	---	---	---	---
	MC_{16}				1.00	0.49				0.00	0.00
	RHT					1.00					1.00
Calgary	Max. MoI	1.00	0.87	0.97	0.97	0.09	1.00	0.98	0.91	0.96	0.94
	Avg. MoI		1.00	0.94	0.86	0.25		1.00	0.89	0.93	0.95
	dMI			1.00	0.97	0.15			1.00	0.97	0.86
	MC_{16}				1.00	0.08				1.00	0.90
	RHT					1.00					1.00

Table 4.2 shows the coefficient of determination (R^2) between the maximum MoI and various climate-based indices for brick veneer and stucco cladding wall facing north and default orientation. In general, the correlation between the maximum MoI and climate indices was not particularly good, especially for the wall facing north in Vancouver. The maximum value for R^2 was 0.79 using MI for the stucco wall facing the default orientation in Calgary for the historical climate.

Table 4.2: R^2 between maximum MoI and climate-based indices for brick veneer cladding facing north & default, and stucco facing default orientation for 3 cities for the two periods (Highest is marked in bold for each case)

City	Cladding	Orientation	Historical				Future			
			CI	WDR	MI	I_{sev}	CI	WDR	MI	I_{sev}
Ottawa	Brick	North	0.47	0.42	**0.64**	0.57	0.20	0.72	0.25	**0.74**
		Default	**0.54**	0.51	0.08	0.06	0.62	**0.64**	0.35	0.28
	Stucco	Default	**0.45**	0.39	0.10	0.01	**0.63**	0.59	0.49	0.27
Vancouver	Brick	North	0.00	0.00	0.01	0.00	0.20	0.00	0.01	0.19
		Default	0.36	0.31	**0.37**	0.00	0.48	**0.52**	0.20	0.01
	Stucco	Default	**0.55**	0.47	0.45	0.00	**0.69**	0.68	0.46	0.00
Calgary	Brick	North	0.60	0.56	**0.67**	0.30	0.51	0.42	**0.60**	0.52
		Default	0.62	0.57	**0.74**	0.38	0.51	0.42	**0.61**	0.52
	Stucco	Default	0.67	0.57	**0.79**	0.40	0.56	0.47	**0.71**	0.52

For the north-facing walls, among all the climate-based indices, MI, led to the highest value for R^2 for most of the cases, except for Ottawa for the future climate, where I_{sev} resulted in the highest R^2. Apart from MI, CI also showed a good correlation with all response-based indices with the exception of the north-facing wall in Vancouver.

In terms of cities, the correlation remained poor for Vancouver (for north) irrespective of the selection of a climate-based index. The reason attributed to this observation is the low amount of WDR in the north orientation for Vancouver, which led to much lower MC and MoI as shown in Figure 4 and Figure 5. For Ottawa and Calgary, the correlation remained significantly higher than that for Vancouver. In terms of climate period, a consistent trend was not found. For Calgary, except for I_{sev}, correlation decreased for all other indices under future climate. For Ottawa, correlation is improved for WDR and I_{sev}, but it remained lower for CI and MI. For walls facing the default orientation, the results showed that the best correlation was usually found with CI and MI. The R^2 for Vancouver in the default orientation was significantly improved, in the range of 0.2-0.52 and 0.45-0.69 for brick veneer and stucco cladding respectively, which is comparable to Ottawa and Calgary except for I_{sev}.

The correlation between climate-based indices and hygrothermal response remained weak and no consistent pattern was observed. In terms of cities, for Ottawa, the correlation remained similar irrespective of the orientation and cladding type for all the indices except MI. For Vancouver, results for the north-facing wall remained poor and were significantly improved for the default orientation, and the stucco wall had a slightly better correlation coefficient than the brick wall in the default orientation. For Calgary, the results showed the least variation between cladding types and wall orientations. The default orientation (NNW) being quite close to the north could explain this trend for Calgary. In terms of climate period, the correlation usually increased in the future for Ottawa and Vancouver, however, it remained slightly lower in the future for Calgary.

4.2.2. Ranking methods

The analysis presented in section 4.2.1 shows that the correlation between the response-based index and climate-based indices is generally weak. How well the climate-based index performs in ranking the years in terms of moisture severity is the question investigated in this section. A climate-based index would be effective if it could provide a similar ranking of years as obtained from simulation results. Three different methods of evaluating the ranking of years were investigated and the details are discussed in the following sections.

4.2.2.1. *Number of matching years*

The analysis was based on the total number of matching years in the ranking obtained using a response-based and a climate-based index. A match is considered if the year ranked using a climate-based index is at the same position as that using a response-based index based on the decreasing severity. The total number of matches was counted for each response-based and climate-based index. The higher the number of matches by a climate-based index, the better the method is in providing the correct ranking of the years.

Figure 4.5 shows the number of matching years for brick veneer cladding facing north for three cities and two climate periods. The number of matching years remained low for Vancouver (1 to 3) in the north because of the low WDR load and MoI. The number of matching years was higher for Ottawa and Calgary with a maximum matching years of 7 out of a total of 31. For Ottawa, CI or I_{sev} usually gave the highest number of matches and for Calgary, CI or annual WDR usually led to the highest number of matches under historical climate. Except for Vancouver, the number of matching years increases (with the maximum MoI as the response-based index) for future climate using CI as the climate-based index. A similar trend was observed with WDR and I_{sev}, with the exception of future results in Calgary. With other response-based indices, a general trend was not found but the results were better for future weather for Ottawa while the opposite was true for Calgary. A similar analysis was made for brick veneer and stucco cladding walls facing the default orientation. For the default orientation, CI or MI generally led to the maximum number of matches for all three cities with the highest being 8 matches out of 31 and an average of about 4 matches for most of the indices. For Vancouver, results were better for the default orientation than the north with an average of at least 3 matches for each of the indices evaluated.

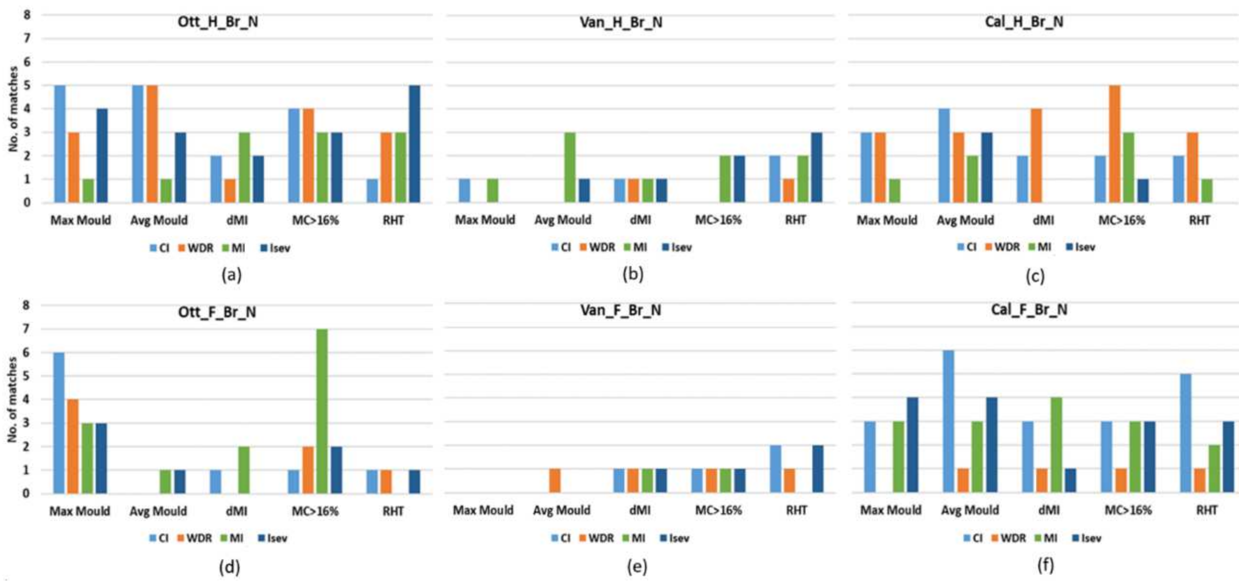

Figure 4.5: Number of matches between the response-based indices and climate-based indices for brick cladding wall facing the north orientation

A further analysis was performed to calculate the total number of times a climate-based index matches with any of the response-based indices. I_{sev} was used only for the simulations considering the north orientation. CI led to the highest number of total matching years considering all the 5 response-based indices followed by MI. By considering only the cases where the wall was facing north, the total number of matching years remained higher for the CI followed by MI and I_{sev}.

4.2.2.2. *Ranking correlation method*

In this section, the correlation in the ranking of years based on MoI (response-based index) and various climate-based indices was further analyzed. The maximum MoI obtained from the actual simulation results was ranked in descending order and these values were compared with the maximum MoI of the year ranked based on climate-based indices. Figure 8 shows the scatter plot of the maximum MoI based on the ranking of years obtained using simulation results and those obtained from the ranking using various climate-based indices for brick cladding wall facing the north in Calgary. For example, the 3rd year based on simulation results is year 1999 which has a maximum MoI of 4.68 whereas, for ranking based on CI (Figure 4.6(a)), the 3rd year is the year 1994 which has a maximum MoI of 4.49. The data point falling on the 45-degree orange line means an exact match between the two indices. A higher number of dots on the line means a greater number of matched years between climate-based indices and simulation results.

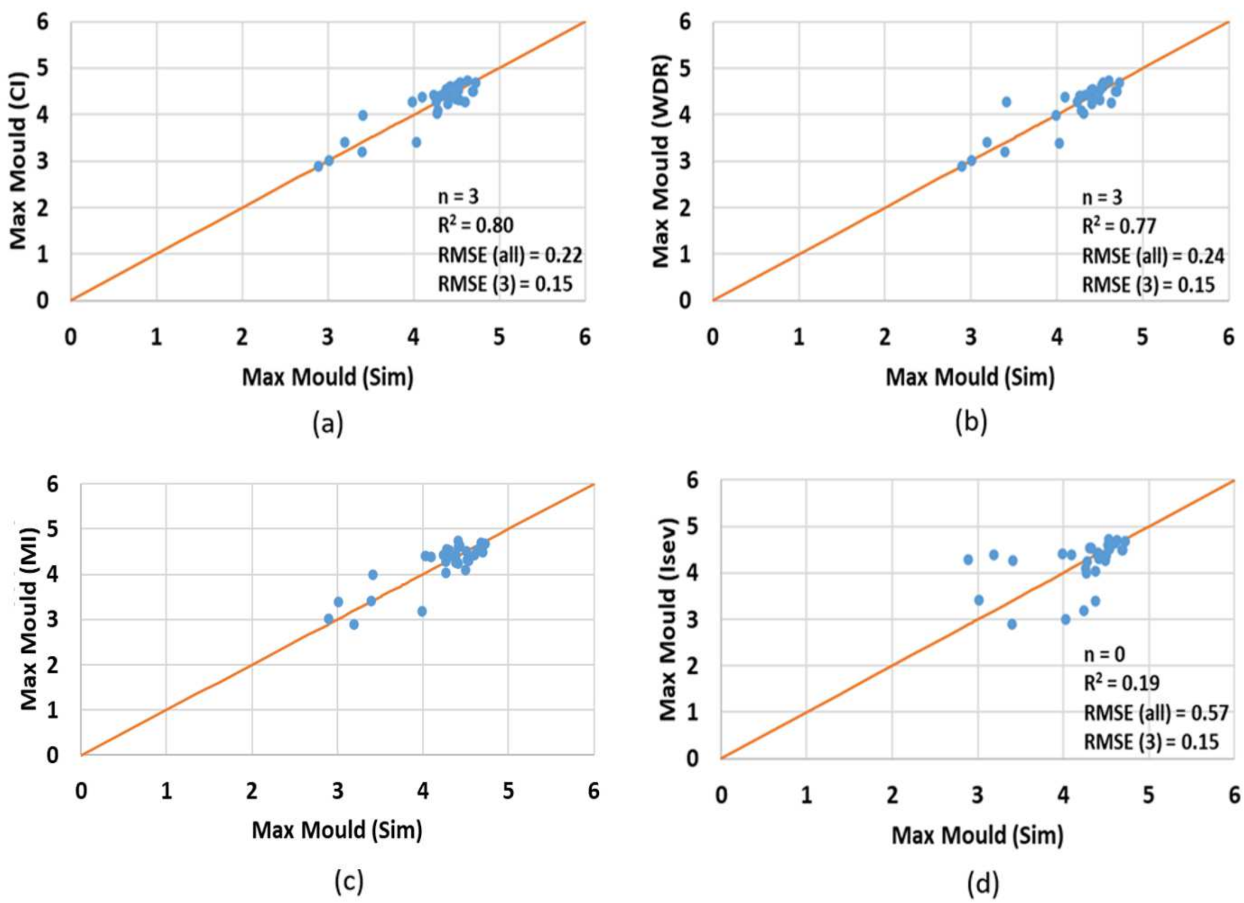

Figure 4.6: Correlation between the maximum MoI when arranged in descending order based on different climate-based indices and simulation results for brick cladding wall facing north in Calgary under historical period. n: number of matching years, R^2: Coefficient of determination, RMSE (all): RMSE considering 31 years, RMSE (3): RMSE considering only the top 3 years

To compare the performance of different climate-based indices, root mean square error (RMSE) was calculated using equation (4-4).

$$RMSE = \sqrt{\sum_{i=1}^{n} \frac{(x_i - y_i)^2}{N}} \tag{4-4}$$

Where, x: predicted values; y: actual values; N: number of observations

Two different approaches were evaluated using this method. Firstly, all 31 years were used to compute the RMSE (RMSE (all)) and the results indicate the reliability of the climate-based index in predicting the same ranking as simulations. Secondly, the RMSE was computed using only the top 3 years (RMSE (3)), for the 10 percentile of 31 years given that the 10 percentile is sometimes used as the MRY. A lower RMSE(3) means a better performance of the climate-based index in selecting the MRY corresponding to the 10 percentile. The number of matching years (n), RMSE (all) for all years, and RMSE (3) for the top three years are given in Figure 4.6. For the cases shown in Figure 4.6, the least RMSE (all) was observed when using CI and MI as the climate-based index to rank the years. Three-year ranking performance was better than all-year ranking for all indices, indicated by a lower RMSE (3) compared to RMSE (all).

In general, for most of the simulated cases, ranking based on CI led to the least RMSE (all) meaning that CI ranks the year in an order that is closest to the actual ranking based on simulations. For walls facing the default orientation, irrespective of the cladding type, CI led to the lowest RMSE for both top-3-year and 31-year ranking. Like Calgary, similar observations were found for Ottawa. For Vancouver, results for the default orientation showed that irrespective of climate period or cladding type, CI resulted in the least RMSE (3). In general, the overall analysis led to the conclusion that although the ranking may not be the same, the year predicted by CI was among the three worst-performing years.

4.2.2.3. *Goodness-of-fit Approach (Salonvaara et al. 2010)*

This approach was suggested by (Salonvaara et al., 2010) and was used to compare the goodness-of-fit in picking the years with the highest value of the performance indicator. The method includes the following steps:

1. Rank the years in decreasing order using the performance indicator from simulations.
2. Normalize the performance indicator to have a range of 0%–100%.

3. Take the top three years as selected by a climate-based index and find the corresponding normalized performance indicator as given by the simulation results.
4. Calculate the average of the normalized performance indicator for the three years.
5. Compare the average normalized performance indicator of the years picked by the climate-based indices. Find out which method picks three years with the highest performance indicator values.

The above-mentioned approach was slightly modified by comparing the average value of the normalized performance indicator (NV) with the corresponding mean value of the three first normalized performance indicators from the simulation results (actual value) and the ratio in the percentage of these two values, i.e. NV divided by the "actual value". The higher the ratio, the better the performance of the climate-based index in ranking the years. The analysis was made using all the response-based indices for brick veneer and stucco cladding. The trend was found to be similar for all response-based indices for both claddings and hence only the results obtained using the maximum MoI for brick cladding wall are discussed here.Table 4.3 lists the ratio of normalized maximum MoI for all simulated cases for brick cladding facing the north and default orientation. The number in the bracket indicates the number of matching years between the actual simulation results and as predicted by the climate-based index. A match is considered if the year predicted by the climate-based index also appears in the top 3 worst years from the simulation results i.e., the order of the ranking within the top three years was not considered. For north-facing walls, for most of the cases, the highest values of ratio were obtained for MI and I_{sev}. For Calgary, although CI did not lead to the highest ratio, its performance was comparable to MI and I_{sev}. A good agreement was found between the actual simulation results and MI with 2 matching years and a high average normalized value. The values remained particularly low in Vancouver because of an extremely low amount of WDR in the north orientation. For Ottawa, I_{sev} resulted in the highest ratio for both historical and future climates.

For walls facing default orientation, similar results were obtained. MI generally had the highest average normalized value whereas CI or WDR generally led to the second-highest normalized average values. I_{sev}, determined only for north-facing walls, was also evaluated in this analysis. The overall results were slightly less promising than those for the north-facing wall, but they were still considerably high. NV for Vancouver in the default orientation increased considerably for all the indices, especially for CI. In general, like north facing wall, MI still performed the best among all indices for most of the cases, however, the improvement in NV (when changing orientation) is lower than the improvement observed in CI. I_{sev} on the other hand has the least correlation for both claddings.

Table 4.3: Normalized value (Average max. mould index for the top three years based on index, NV in %) and Ratio of NV (NV divided by the actual average max. mould index from simulations in %) for various climate-based indices for brick cladding facing the north and default orientation (the highest values are marked in bold for each case and number of matching years in bracket)

City	Climate	Orientation	Actual	CI		WDR		MI		I_{sev}	
				NV	Ratio	NV	Ratio	NV	Ratio	NV	Ratio
Ottawa	Historical	North	93.7	68.7	73.3 (1)	68.7	73.3 (1)	78.1	83.4 (1)	85.0	**90.8 (1)**
		Default	95.5	72.3	75.8 (0)	72.0	75.4 (0)	89.7	**94.0 (0)**	87.5	91.7 (0)
	Future	North	95.5	54.7	57.3 (1)	54.7	57.3 (1)	88.1	**92.1 (2)**	88.1	92.1 (2)
		Default	98.7	85.6	86.7 (1)	81.3	82.3 (1)	91.2	**92.4 (1)**	81.3	82.3 (1)
Vancouver	Historical	North	98.3	40.9	41.6 (0)	40.9	41.6 (0)	68.4	**69.6 (1)**	31.9	32.5 (0)
		Default	97.0	71.6	73.8 (1)	69.4	71.5 (0)	76.8	**79.1 (1)**	50.6	52.1 (0)
	Future	North	90.4	32.5	36.0 (0)	32.5	36.0 (0)	31.7	35.0 (0)	54.6	**60.4 (0)**
		Default	93.8	88.9	**94.7 (2)**	82.9	88.3 (1)	87.0	92.7 (1)	81.6	86.9 (1)
Calgary	Historical	North	98.6	90.9	92.2 (1)	90.9	92.2 (1)	94.4	**95.7 (2)**	90.9	92.2 (1)
		Default	98.1	92.0	93.7 (1)	92.0	93.7 (1)	95.3	**97.1 (2)**	92.0	93.7 (1)
	Future	North	97.5	92.3	**94.6 (2)**	92.3	94.6 (1)	87.5	89.7 (1)	92.3	94.6 (1)
		Default	95.7	90.9	94.9 (2)	91.5	**95.6 (2)**	86.7	90.5 (1)	91.5	95.6 (2)

All the investigated ranking methods led to a similar conclusion. CI and MI generally led to a better correlation i.e., a higher number of matches, lower RMSE, and higher NV. I_{sev} performed fairly well for the north-facing walls and to some extent for the default orientation too when using the goodness-of-fit approach. The choice of method depends on the desired output. If the final outcome is to observe the actual order of ranking, the number of matching years is a good method. If the aim is to analyze the severity of the top 10% percentile year (for the purpose of MRY selection), goodness-of-fit might be a good option as it provides a good estimate of the years based on climate-based index and simulations. The ranking correlation method provides information on the performance of climate-based indices in ranking the severity of years that may lead to potential moisture damage by quantifying the RMSE in addition to counting the number of matching years, which provides information that can be obtained from both the “matching year method” and “Salonvaara method”.

4.3. Discussion on I_{sev}

The Severity Index (I_{sev}) is a method proposed in ASHRAE 160. The equation was developed using training dataset from 8 different cities across the USA and the limiting conditions of temperature and RH were set as 70% and 0ºC , respectively. The developed regression model was tested for one Canadian city (Winnipeg in Manitoba) and one European city (Holzkirchen in Germany) as well and it showed consistent results according to Salonvaara et al., (2010). However, the analysis in the previous section showed that the original I_{sev} model didn’t perform well, especially for Vancouver. One of the reasons could be that in this study 1% moisture source was assumed while the original I_{sev} model was developed for the stucco-wall without rain leakage.

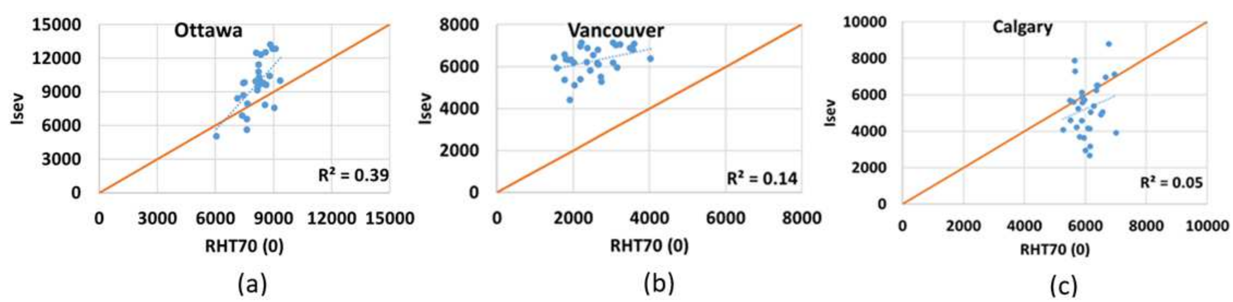

Figure 4 7: I_{sev} (climate-based index) and RHT70(0) (response-based index) for stucco clad wall facing the north in three cities assuming no rain leakage over the historical 31-year period

To verify this assumption, a stucco cladding wall facing the north was simulated for the three cities assuming no rain leakage under the historical climate. As shown in Figure 4 7, I_{sev} is higher than RHT70(0) from simulations (except Calgary) with the same wall configuration under the same moisture loading as originally used in the model. Here, RHT70(0) is the RHT index calculated based on the temperature and relative humidity in the exterior sheathing over time when values of 0ºC and 70% are used as threshold for temperature and relative humidity respectively. These values are same as those used in the development of I_{sev}. For Ottawa, for most of the years (25 out of 31), I_{sev} overpredicted the RHT70(0) meaning that the model depicted the years as more severe than they actually are. For Vancouver, the difference was more significant with I_{sev} being about 1.5 to 3.5 times greater than RHT70(0). The abnormally lower value of RHT70(0) obtained from simulations is because of a very small amount of WDR in the north direction in Vancouver. Finally, for Calgary, unlike other two cities, I_{sev} mostly (23 out of 31 times) underpredicted the RHT70(0). This shows that the original I_{sev} is not applicable for the three Canadian cities used in the study.

A temperature of 5ºC and RH of 80% are typically considered as the limiting conditions for mould growth (Viitanen et al., 1991; Viitanen et al., 2007; Viitanen et al., 2011). Therefore, both RHT70(0) and RHT80(5) were calculated for the brick veneer cladding wall studied in this paper for the three cities under both historical and future years. The RHT index calculated based on simulations are compared with I_{sev}. As shown in Figure 10(a), I_{sev} matches better with the actual RHT70(0) obtained from simulations for Ottawa and Calgary. For Vancouver, I_{sev} is significantly higher than RHT70(0) from simulations because of the low WDR in north orientation. Obviously, with more severe conditions, i.e., 80% RH and 5ºC for temperature, discrepancy becomes greater. This can explain the weak correlation between I_{sev} and RHT index and mould index presented in section 4.2.1, which has the mould growth limiting conditions as 80% RH at 5ºC.

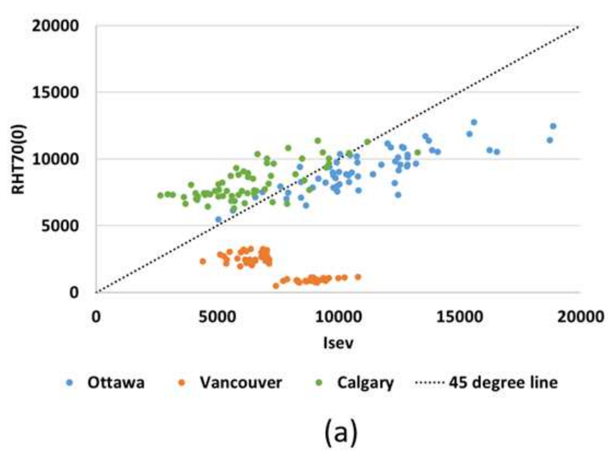

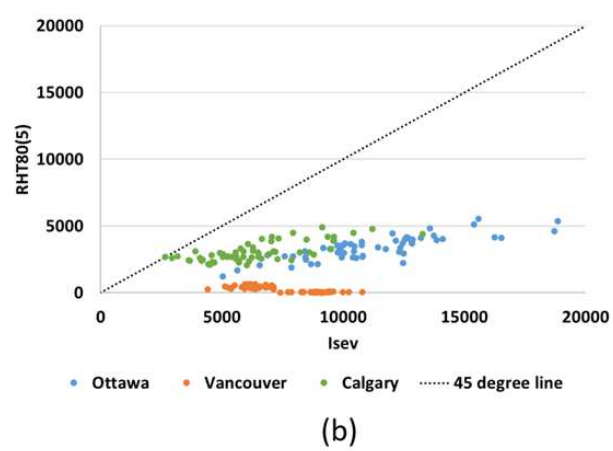

Figure 4.8: Scatter plot of I_{sev} with RHT calculated with limiting conditions of temperature and relative humidity as (a) 0ºC and 70% (b) 5ºC and 80% respectively (combined result for 3 cities and 2 climate periods with 31 years each i.e., 62 points for each city)

The original regression model was generated assuming the worst performance in north orientation. However, for cities such as Vancouver where WDR is minimal in the north orientation, model failed to predict the performance. Furthermore, the regression model was developed assuming the wall structure to be completely flawless i.e., no rain penetration through the external cladding. However, to have a more realistic representation of moisture loads, 1% of rain leakage was assumed to be present on the exterior side of the sheathing membrane in all the simulations. The additional rain load used in the simulations could also contribute to the lower correlation between the performance indicator and I_{sev}.

4.4. Conclusions

A correlation analysis between the performance, i.e. hygrothermal response, and the climate-based indices, i.e. climatic loads, provides a base to understand the reliability of these indices in assessing the moisture risks of walls. In this study, two approaches were used to evaluate this correlation.

The main findings are as follows:

- Correlation between response-based and climate-based indices
  - The correlation between climate-based indices and hygrothermal response was generally weak, with R^2 in the range of 0-0.79. Among all climate-based indices, CI and MI had a better correlation with response-based indices.
  - The correlation remained poor for Vancouver due to the low WDR in north orientation, with R^2 in the range of 0-0.2 for a north-facing wall. Significant improvement was achieved for the prevailing WDR direction with R^2 ranging from 0.2-0.69 (excluding I_{sev}).
  - The correlation varied for different cities, wall types and climate periods. For cities like Ottawa and Calgary, the change in climate-based indices under future climate was consistent with change in the maximum MoI.
- Ranking Analysis
  - Among the three methods used, the choice of response-based index did not change the ranking greatly and usually the maximum MoI led to the slightly better results (higher matches, lower RMSE and higher NV) for most of the cases.

- When using climate-based indices to rank the years, for most of the cases, the accuracy in ranking all years was low with some improvement in ranking the first 3-year
- The number of matching years remained small for all the climate-based indices with the highest being 7 out of 31 using MI.

Using the ranking correlation method, CI in general led to a higher number of matching years, a lower RMSE for both 3-year and all years. The RMSE for 3-year ranking was lower than the RMSE for all-year ranking for all climate-based indices except for I_{sev} with walls facing the default orientation.

- Using the goodness-of-fit approach, MI usually led to the highest normalized value (NV) followed by CI for most of the cases. The moisture severity of the first three worst years selected by climate-based index was similar to that of the first three worst years selected based on simulations for cases where the wall orientation is close to the north, except for Vancouver, although the ranking accuracy (indicated by number of matching years) was generally not very high.
- I_{sev} is proposed in ASHRAE 160 for evaluating the severity of the years. However, for different wall configurations under different moisture loads, it failed to predict the correct ranking. Also, for the three investigated Canadian cities, it didn't perform well even for the same wall configuration and moisture load used in its development.

Analysis in this paper showed that the existing climate-based indices do not show reliability and consistency in ranking the severity of weather years when compared to simulation results. Climate-based indices taking into account more climatic parameters perform better and their performance is influenced by the type of wall constructions, moisture loads and climatic characteristics. Therefore, to assess the moisture risks of building envelope assemblies under future climates, a more reliable climate-based index is needed to better correlate response-based indices with climate-based indices for typical Canadian climates. The future work will include the development of a method to generate climate-based index specific to a cluster of Canadian climates, wall constructions under different loading conditions, i.e., rain penetration, air leakage, etc. For each cluster, the climate-based index will be calculated and correlated with the response-based index to assess the moisture risks for future climate.

Chapter 5 Developing the new index based on PLS modeling

The content of this chapter is published in the journal paper. "*C. Aggarwal, H. Ge, M. Defo, and M. A. Lacasse, "Hygrothermal performance assessment of wood frame walls under historical and future climates using partial least squares regression*," Build. Environ., vol. 223, no. May, p. 109501, 2022, doi: 10.1016/j.buildenv.2022.109501." The abstract and introduction from the originally published paper is not included in this chapter and to avoid the repetition, the wall assemblies, boundary conditions, model settings, etc. included in the originally published paper are excluded since these are already provided in Chapter 3 "Methodology".

The modeled building was assumed to be a 3.5-storey residential building located in a suburban setting. A lightweight wood-frame wall assembly with brick veneer cladding with air space behind the cladding was simulated, assuming no air leakage. To cover different climate zones, three cities i.e., Ottawa, Vancouver, and St. John's belonging to different climate zones across Canada were selected. Ottawa is in the eastern region of Canada and represents cold and dry winter conditions. Vancouver is located in the western coast of Canada and receives high rainfall and has mild winter weather. St. John's is located in the eastern coast of Canada and receives high rainfall, along with windy and cold winter weather. To predict the wall performance, an index based on climate parameters was developed. For this study, an index was developed based on responses (construction-dependent) and then correlated with climatic parameters.

Overview

In most engineering problems, there are many variables/parameters (inputs) that are often used to explain or predict response variables (output). Often, input parameters are correlated with response variables using multiple linear regression (MLR) to turn the data into useful information and later make the prediction when new input parameters become available. In other words, in MLR a direct "least squares" regression is performed between the response and the input matrix. MLR model equation is usually a straight-line equation correlating the input parameters with the response variable. The limitation associated with MLR is that this procedure works well when the input parameters are few in number and the addition of more parameters makes this technique less efficient. In general, for regression analysis, the problem associated with the addition of more parameters is called overfitting of the data meaning that with more variables, the model is likely to fit the sampled data in a precise manner, but it would not be able to predict the response with new data with good accuracy. In such cases, although there are many variables in the model, they are likely to be highly collinear and there may be only a few among those variables that account for most of the variation in the response variable.

To deal with many input variables and their associated collinearity, Partial Least Squares (PLS) regression is often used. It has been frequently used for predicting the response with multicollinear data. This strategy has proved to be efficient with its good prediction ability (Martens et al., 1992; Wold et al., 1982). It is a dimensionality-reduction method that aims to transform a large set of variables into a smaller set while maintaining most of the information. It projects the information contained in a larger set to a smaller set of latent variables called factors. A certain portion of the total content is explained by each factor with the first factor explaining the greatest amount of information. Each subsequent factor explains in order, less information than the previous one. It models both the X (inputs) and Y (output) matrices simultaneously to find the latent variables in X that will best predict the latent variables in Y.

A PLS model is a mathematical equation relating the input parameters with the response variable with each input parameter having a certain coefficient. The coefficients are determined based on a set of input-output combinations. A limited set of these combinations is used, and this data is referred to as training data for the model. Using this training set, a PLS regression equation is generated and is further used for a new set of input data to obtain a predicted response variable. In general, the more representative the training data is, the better the model is in its prediction. However, this is not always true, and the training data might fit very well but the model fails to predict well for future test values.

5.1. PLS scores and loadings

PLS scores are the sample coordinates along the model components in the new X-Y space. The scores describe the data structure in terms of sample patterns and show sample differences or similarities. PLS scores are further classified into T-scores and U-scores. T-scores are the transformed coordinated of data points in X-space and are computed in such a way that it consists mainly that part of X which is most predictive of Y. U-scores on the other hand consists of that part of the structure of Y which is explained by X along a given factor. PLS loadings express how each of the X and Y variables is related to the model component summarized by the T-scores. Like

PLS scores, PLS loadings are of two types. P-loadings; it shows the contribution of each of the X-variable to a specific model component. Q-loadings on the other hand represent the direct relationship between the output (Y) and T-scores. The overall goal of PLS regression is to use the factors to predict the response. To do so, T and U scores are extracted from the sampled factors and responses respectively. Later, T scores are used to predict U scores, and then the predicted Y-scores are used to construct predictions for the responses.

5.2. Selection of most significant variables

In any regression model with many input parameters, not all of the parameters are important for calculating the response variable. Given this, it is important to identify the variables which have the most significant impact on the output. To select the most influential variables, different approaches have been proposed in the literature (Centner et al., 1996; Höskuldsson, 2001; Andersen et al., 2010; Mehmood et al., 2012; Zerzucha et al., 2012). In this study, the variable selection was based on the relative importance of regression coefficients in the regression model, and jack-knifing procedure (Martens et al., 2000; Westad et al., 2000; Anderssen et al., 2006) was used. During the cross-validation process in the regression model, each variable is kept out in turn from the model. Later, the uncertainty variance of PLS model coefficients was calculated using equation (5-1).

$$\sigma^2(B) = \sum_{m=1}^{M} (B - B_m)^2 g \tag{5-1}$$

Where,

$\sigma^2(B)$: estimated uncertainty variance of B

B: the regression coefficient using all variables

B_m: the regression coefficient using all variables except the variable left out

g: scaling coefficient

Student's t-test (Ruiz et al., 2013) is performed for each element in B relative to the square root of its estimated uncertainty variance $\sigma^2(B)$, giving the significance level for each parameter useful to find in which components the Y-variables are modeled with statistical relevance.

Further, for developing the PLS regression, the model requires climate data for different cities. Developing a unique model for each city is not an efficient process and hence various cities are grouped together in such a way that cities with similar weather characteristics constitute a single model. Similarly, for the development of an efficient model, the choice of climate variables and training set plays an important role.

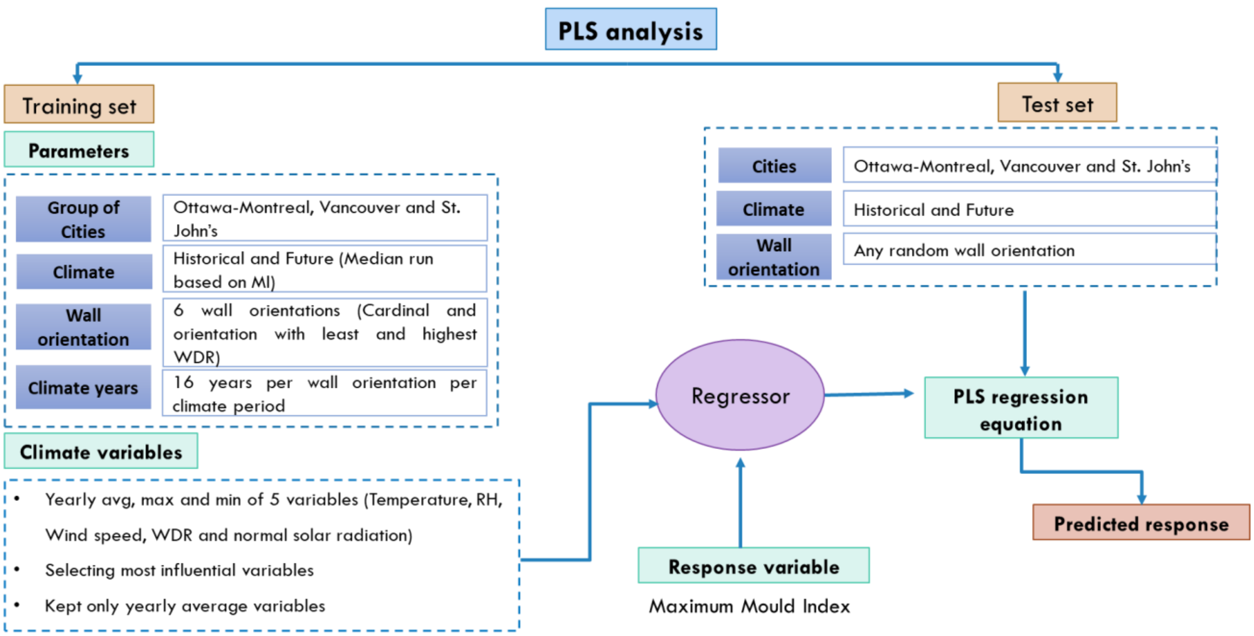

Figure 5.1: Process flow chart for Climate-Based Index development using PLS regression

Figure 5.1 shows the process flow chart for developing the climate-based index using PLS regression. The details of each of the parameters used for the training and test set are provided in the following subsections:

Cities

The climate data was available for 12 cities across different climate zones in Canada. According to the National Energy Code of Canada for Buildings, there are five climate zones across Canada based on heating degree days (NECB). Three cities i.e., Ottawa, Vancouver, and St. John's in three different regions across Canada were selected to represent climate zones 4 and 6. Ottawa is in the eastern region of Canada and represents cold and dry winter conditions (zone 6). Vancouver is located in the western coast of Canada and receives high rainfall and has mild winter weather (zone 4). St. John's is located in the eastern coast of Canada and receives high rainfall, along with windy and cold winter weather (zone 6).

Climate selection

For all 12 cities, modeled hourly climatic parameters were available for the baseline period spanning from 1986 to 2016 and 31-year-long future periods, with different levels of global warming with reference to the baseline period. In this study, the pessimistic scenario with a global temperature rise of 3.5ºC was selected and this scenario is expected to occur between 2062-2092. Further, the climate datasets were generated incorporating the internal climate variability and the effect of initial conditions used in the model hence each timeline comprises 15 realizations or runs. Incorporating all 15 runs for the model development is not a viable option because; (a) the simulation time will be huge and (b) a large amount of training dataset might lead to overfitting of the model. To tackle this issue, for the preliminary analysis, the median run based on MI ranking (as a representative of 15 runs) was chosen for simulations and hence the training dataset.

5.3. Selection of training dataset

For any model to be robust and efficient, it is of utmost importance that the training data used for its development should be comprehensive. In other words, the model should be able to explain all the variations in the data that could arise with the future input data. Different factors i.e., climate scenario, wall orientation, and the number of years were tested for a particular city to select the training set. For all the training sets, the goal was to be as general as possible meaning that the training set is such that various test sets become a subset of it. The following approach was used to select a representative training set:

5.3.1. Cities

Figure 5.2 shows the variability of temperature, RH, wind speed, and annual rainfall of the historical and projected future climate data for the three cities based on the annual average data for each year in the median run. In general, all three cities have different climate characteristics. Vancouver is milder and rainier than Ottawa and St. John's. St. John's is the windiest and the most humid among the three cities. Further, the cities vary significantly in terms of their climate variation from historical to future period. Compared to average historical climatic conditions, an increase of approximately 5°C in annual average dry-bulb air temperature was observed for all three cities under the future climate. From the historical to the future period, mean RH increases by approximately 2% for Ottawa but remained similar for Vancouver and St. John's. Wind speed decreases slightly for all three cities in the future period. Finally, the annual rainfall increases by approximately 15% from the historical to the future period for Ottawa and St. John's but there is a minimal change (less than 1%) in the rainfall for Vancouver. It should be noted that these observations are based on the median run, and they are not representative of climate variation in the full dataset.

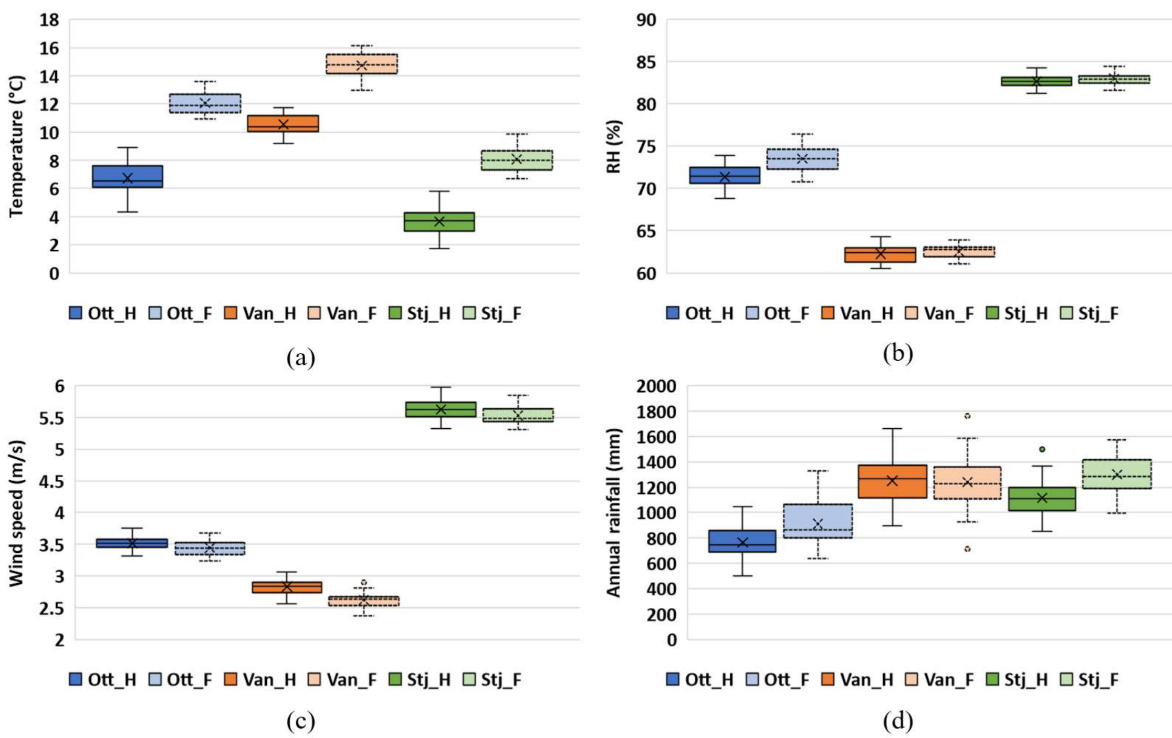

Figure 5.2: Climate characteristics of three cities (Ott: Ottawa, Van: Vancouver, Stj: St. John's, H: Historical, F: Future)

5.3.2. Climate scenario

As observed in Figure 5.2, there is a significant variation between the historical and future climate conditions except for RH and wind speed. However, to cover the entire range of data for other variables, both climate scenarios were included in the training set.

5.3.3. Wall orientation

The impact of wall orientation on moisture performance was part of a few studies (Aggarwal et al., 2021; Aggarwal et al., 2022) and it was found that wall orientation plays a critical role in the outcome. The training set should therefore comprise as many orientations as possible. However, this would lead to large simulation efforts. Based on the extensive evaluation, a trade-off with 6 wall orientations was chosen for the training set to be representative of all orientations. These 6 orientations include 4 cardinal orientations i.e., North, East, South, and West along with the orientations receiving the highest and the lowest amount of WDR called "highest" and "lowest", respectively. The WDR and maximum mould index were plotted for 16 wall orientations separated by an interval of 22.5º and the results were compared with 6 wall orientations. Six orientations could be used as a representative set of 16 orientations if the range of maximum mould index considering all orientations is covered when using only 6 orientations. It should be noted here that the variation of orientation is to represent a range of solar radiation and wind-driven rain received on the façade, while other climate variables are not affected by varying orientations.

Figure 5.3 shows one typical example demonstrating the process of wall orientation selection for the training dataset. The normalized (ratio with values with the maximum) annual WDR and maximum mould index for 16 wall orientations were plotted with encircled orange points being the results for the six selected orientations. It can be seen that the range of WDR and mould index with 16 orientations was covered by the 6 orientations i.e., 4 cardinal orientations along with SW as the highest and NW as the orientation with the lowest WDR. Therefore, to limit the number of simulations, these 6 orientations were chosen for the training dataset.

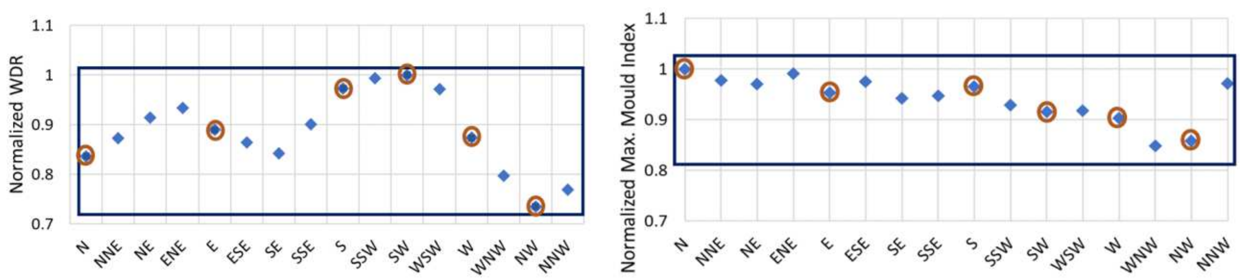

(a) (b)

Figure 5.3: (a) Normalized WDR and (b) Normalized maximum mould index for all 16 and selected 6 orientations for Ottawa

5.3.4. Number of years

Another important factor to consider in the training data is the number of years to be incorporated from each climate scenario and orientation. Based on the trials, it was found that with 31 historical years and each year simulated with 6 wall orientations i.e., 186 training sets, close to 70% of response variation (maximum mould index) was explained with a PLS model using 2 factors and increasing the data points does not increase the explained variance much. A similar observation was found with the future dataset. To cover both, historical and future data, 16 years from each climate period were chosen making a total of 192 (16*6*2) points to obtain the same explained variance. The 16 years were chosen in such a way that the range of the climate parameter values in the selected years covers the entire range of all 31 years among the 6 wall orientations for both climate periods.

5.4. Climate variables selection for model development

For the PLS model, the maximum mould index was used as a response variable. Five weather parameters were used as the input variables. These weather parameters are temperature, relative humidity, wind speed, wind-driven rain, and solar radiation normal to the wall surface. Initially, for all the selected weather parameters, yearly average, yearly maximum, and yearly minimum values were chosen for model development which gave a total of 15 variables. However, a yearly minimum for wind-driven rain and solar radiation cannot be included in the model as these values will always be zero. Similarly, for relative humidity, the yearly maximum is always 100% (or close to that). Eliminating these variables, the final equation consists of 9 variables with 5 being the yearly averages of hourly values, i.e. yearly average temperature, RH, wind speed, WDR, and solar radiation normal to the façade along with yearly minimum temperature, and yearly maximum temperature, WDR, and solar radiation normal to the façade.

A PLS model was generated using the 9 variables. Using the jack-knifing procedure, it was observed that only the yearly averages are the ones that explain most of the variation in the response variable. Figure 5.4 shows the amount of y-variance explained and the corresponding RMSE for maximum mould index with 9 variables in comparison to using 5 yearly average variables for one typical case (Ottawa). As noted, the amount of explained variance was almost constant beyond the 2 factors. Further, a comparison between the models with 9 variables and that with only 5 yearly average variables showed that the amount of explained variance was similar (close to 70%) for both models. Similarly, RMSE remained constant beyond 2 factors and the magnitude was comparable for the model with all 9 variables and the model with only 5 average variables. Hence, the final model was developed using 5 input parameters i.e., a yearly average of temperature, relative humidity, wind speed, wind-driven rain, and solar radiation normal to the wall surface. Further, all the variables were standardized (zero mean and unit standard deviation) before inputting them into the model.

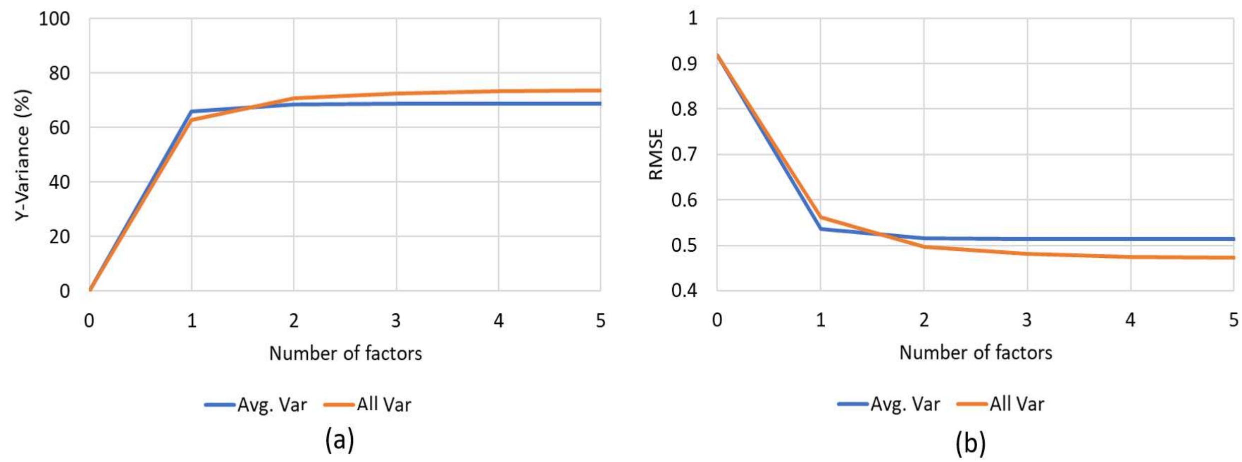

Figure 5.4: (a) Percent of y-variance explained and (b) RMSE of maximum mould index considering all 9 variables and considering only average variables for Ottawa (Avg: Average, Var: Variables)

For all the 5 input parameters, linear and square terms were considered for the model development (Salonvaara et al., 2010) i.e., a total of 10 input variables. Later, based on jack-knifing procedure, the model selects the variables that best explain the variation in the mould index. Figure 5.5 through Figure 5.7 shows the variables that are the most influential to the response for the three cities. For all the cities, the variables highlighted in grey are the most influencing variables and the ones highlighted in blue are the least influencing and hence discarded for the model development. A 5% significance level was set i.e., the variables for which the uncertainty limits cross the zero line do not impact the response variable much at the chosen level of significance. Further, the higher the bar of a particular variable in grey, the greater the significance it holds. In general, it was found that WDR plays a major role in explaining the response variable for all three cities. This is understandable given the fact that no air leakage was assumed from the interior, WDR is the main source of moisture since 1% of WDR was assumed on the exterior layer of the sheathing membrane, which directly impacts the hygrothermal conditions of sheathing for the mould growth. Therefore, the moisture source assumed makes WDR the most significant climate variable influencing the mould growth risk.

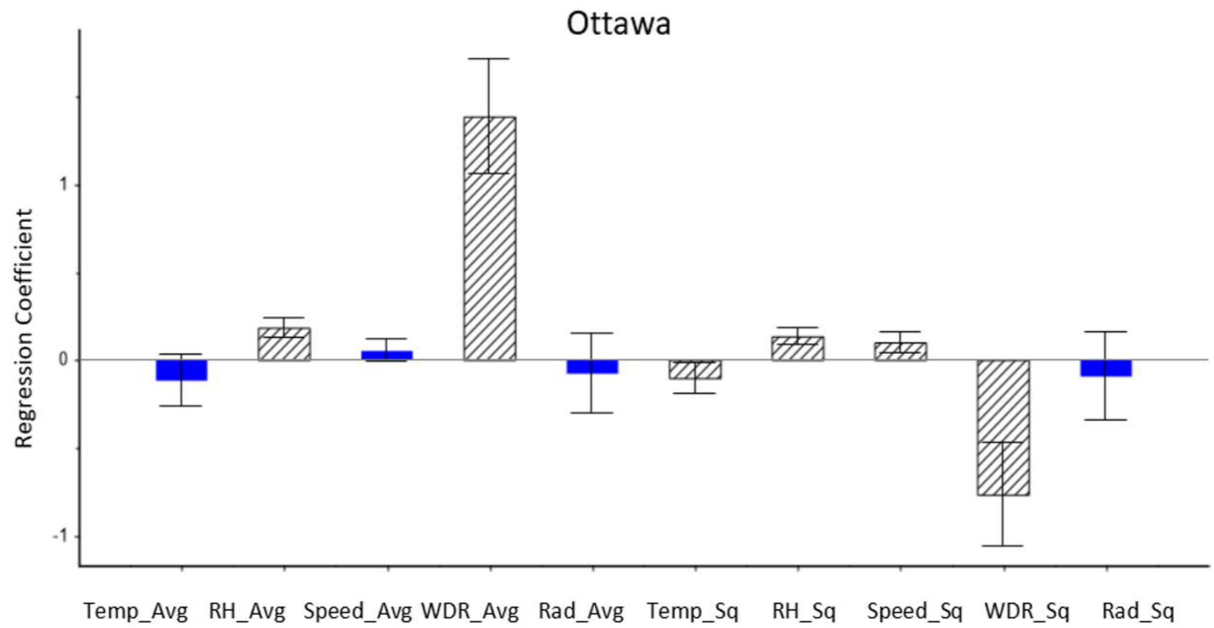

Figure 5.5: Weighted regression coefficients for Ottawa with different input parameters (Sq: Square)

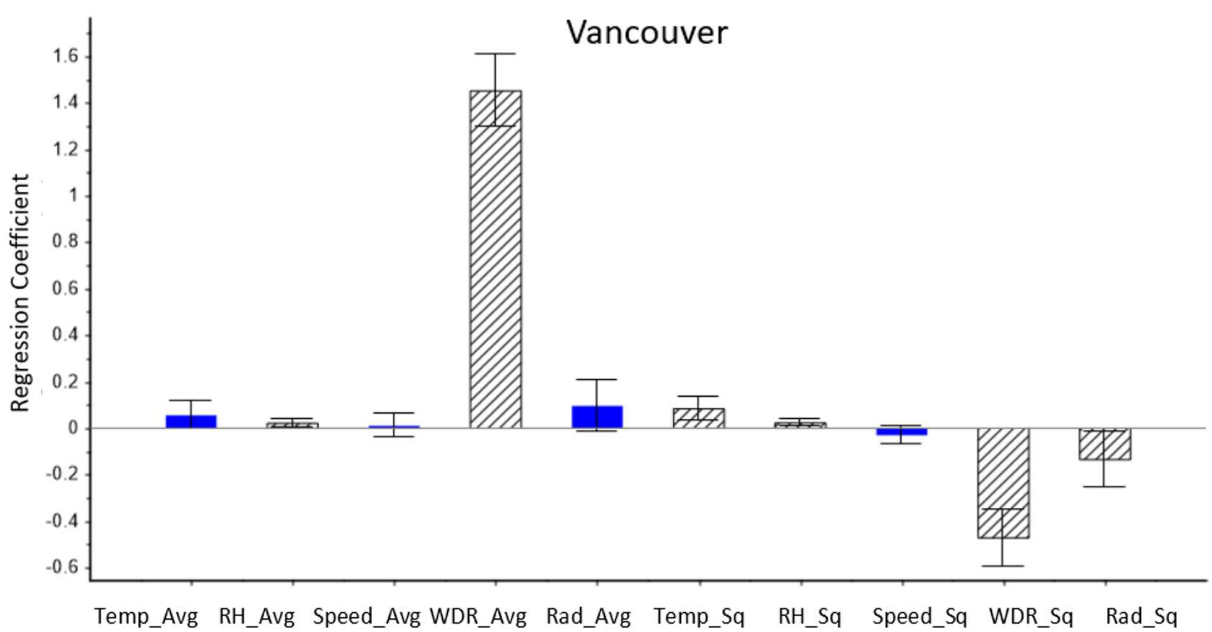

Figure 5.6: Weighted regression coefficients for Vancouver with different input parameters (Sq: Square)

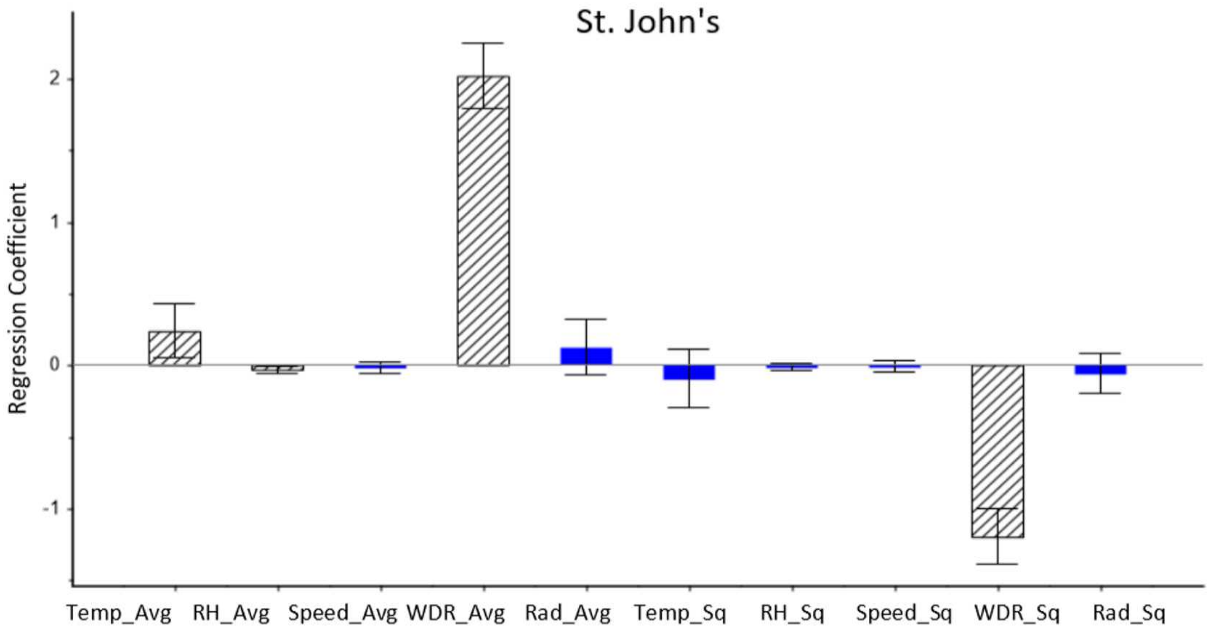

Figure 5.7: Weighted regression coefficients for St. John's with different input parameters (Sq: Square)

The variables selected for each city were further tested and the results were compared with the scenario wherein only the linear average input parameters were considered as inputs. It was observed that based on the type of analysis, the variables selected by the model might not explain the response well. In other words, a further investigation considering important variables and only linear average variables was conducted and it was found that selecting the variables suggested by the model does not always lead to the best prediction results.

Figure 5.8 shows a typical example where the results (actual vs predicted mould index) for two test sets i.e., the historical climate of Ottawa and St. John's, are illustrated. A comparison was made between the results obtained when considering only 5 linear average variables "AvgVar" and when considering the important variables as selected by the model "ImpVar". As observed in Figure 5.8, a better correlation was obtained between the actual and predicted results when only linear average variables were considered for the model development (R^2 of 0.81 and 0.73 "AvgVar" and "ImpVar", respectively). On the other hand, for St. John's better results were obtained with "ImpVar" with a higher R^2 when considering the model based on important variables i.e., 0.89 for "ImpVar" in comparison to 0.78 for "AvgVar". The comparison between the "AvgVar" and "ImpVar" models using different ranking methods results in a similar conclusion i.e., better results with "Avg Var" and "Imp Var" models for Ottawa and St. John's, respectively. Based on these analyses, it was found that for Ottawa and Vancouver, keeping only the linear average variables results in a better explanation of the response. Hence, further analysis was made with model development based on the above-mentioned approach.

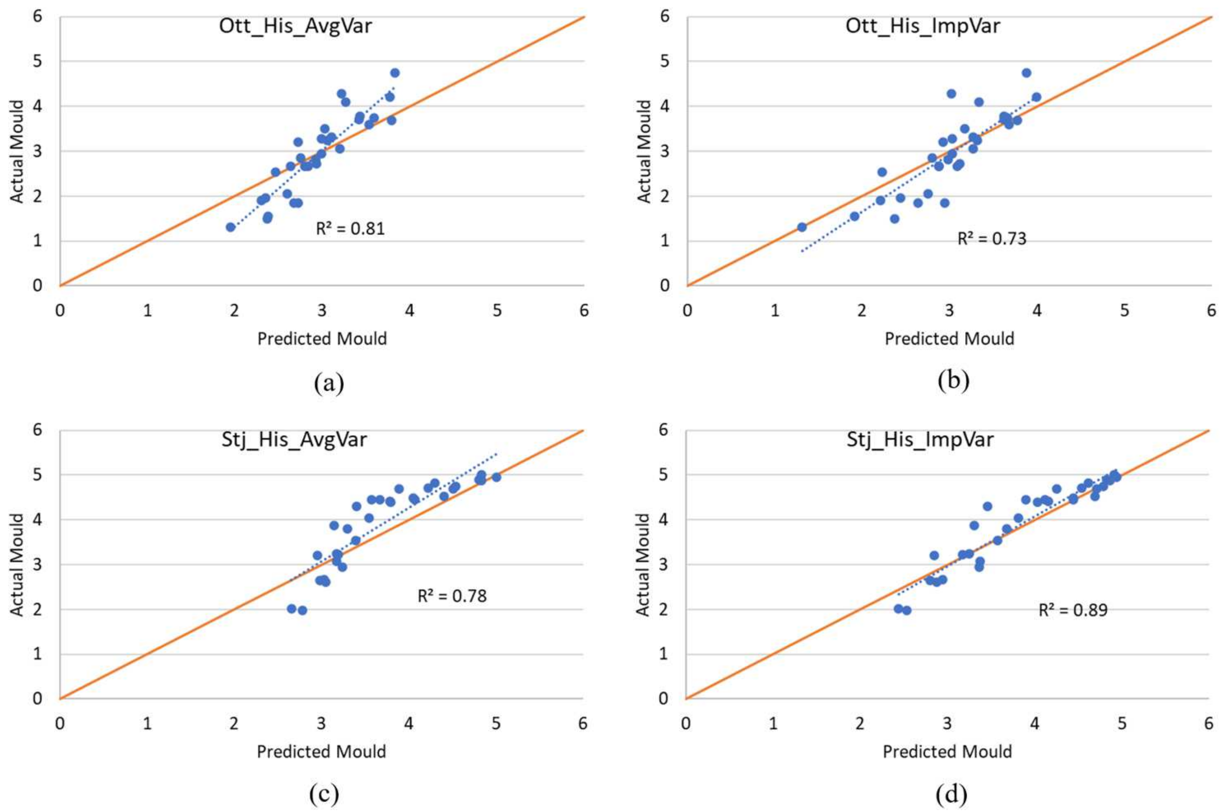

Figure 5.8: Scatter plot results considering only linear average variables (AvgVar) and important variables (ImpVar) for the historical climate of Ottawa and St. John's

5.5. Model Validation

Validating a model based on empirical data means checking how well the model will perform on new data. Regression models are often used to do predictions for the test sets. The validation of the model estimates the uncertainty of such unknown predictions. If the uncertainty is reasonably low, the model can be considered valid.

There are different methods to estimate the model's stability and predictive ability: test set validation, cross-validation, and leverage correction. In this study, the cross-validation method was used. In this method, the same samples are used both for model development and testing. A few samples are left out from the calibration data set and the model is calibrated on the remaining data points. Then the values for the left-out samples are predicted and the prediction residuals are computed. The process is repeated with another subset of the calibration set, and so on until every object has been left out once; then all prediction residuals are combined to compute the validation root mean square error of cross-validation (RMSECV). Further, it is important to understand the level of cross-validation that one requires for validation e.g., how many samples or groups of samples to leave in one validation, etc. In the present study, full cross-validation was used which involves leaving out only one sample at a time. The cross-validation results demonstrate the reliability of the model.

Table 5.1: R^2 and RMSE for calibration and validation for the three PLS models

City	Case	R^2	RMSE
Ottawa	Calibration	0.66	0.49
	Validation	0.64	0.50
Vancouver	Calibration	0.92	0.34
	Validation	0.92	0.35
St. John's	Calibration	0.88	0.32
	Validation	0.87	0.33

The calibration and validation results for the three models are shown in Table 5.1. It was observed that the R^2 and RMSE for the calibration and cross-validation were found to be similar for the three cities meaning that the model could be reliably used to predict performance on the new data.

5.6. PLS regression equation

Following the above-mentioned approach, the PLS model was developed for three cities and the corresponding regression equations for each city are shown below (equations (5-2) through (5-4)):

Ottawa:

$$Mould = -13.77726 - 0.0421 * T_{avg} + 13.8374 * RH_{avg} + 1.7442 * Speed_{avg} + 101.3418 * WDR_{avg} - 0.0038 * Rad_{avg} \tag{5-2}$$

Vancouver:

$$Mould = -3.6923 + 0.1118 * T_{avg} + 3.7850 * RH_{avg} + 0.3543 * Speed_{avg} + 48.5317 * WDR_{avg} + 0.0088 * Rad_{avg} \quad (5\text{-}3)$$

St. John's

$$Mould = 5.71795 + 0.0619 * T_{avg} - 4.7976 * RH_{avg} + 83.1395 * WDR_{avg} - 586.4042 * WDR_{avg}^2 \quad (5\text{-}4)$$

Here, $Mould$ is the maximum mould index (response), T_{avg} is the yearly average temperature in °C, RH_{avg} is the yearly average relative humidity in (-), $Speed_{avg}$ is the yearly average wind speed in m/s, WDR_{avg} is the yearly average WDR in mm and Rad_{avg} is the yearly average normal solar radiation in W/m^2. It should be noted here that the units of coefficients are inverse of the corresponding climate variable so as to have a unitless response i.e., mould index. Further, although the prediction can be made using the PLS equations which eliminates the need of simulations, but the index is construction dependent as it is developed using response from simulations correlated with climate parameters.

5.7. Results from the PLS model

To test the PLS model, the model was used to predict the response on a data set not used in training, called test set. To investigate the robustness of the model, the test set should comprise data that covers a large variation and should be a subset of the training set. To incorporate this, different test sets were identified to cover the variation of climate period i.e., historical, and future climate for all three cities. For all the test sets, 31 individual year simulations were performed for wall orientations which are different from the one used in the training set to build a wall orientation independent model. Three different approaches were used to analyze the results: 1) Direct correlation analysis, 2) Ranking analysis and 3) Risk categorization analysis. Details of each approach along with the analysis of the result are discussed in the following subsections:

5.7.1. Direct correlation analysis

In this analysis, the predicted response variable, i.e. mould index, is compared with the actual mould growth index. Along with the scatter plot, the coefficient of determination (R^2), root mean square error (RMSE), and mean absolute error (MAE) were calculated for statistical comparison. Further, the percentage deviation of the predicted results from the actual results was calculated.

For Ottawa, as shown in Figure 5.9 (a), there was a good correlation between the predicted mould index using the model and the actual mould index for the historical dataset. The coefficient of correlation, R was found to be 0.9, and the corresponding coefficient of determination, R^2 was 0.81. Except for a few years, most of the years lie close to the 45-degree line (orange line) meaning that the results were similar for most of the years. In the lower range (0-3) of mould index, the model overestimated the results and in the upper range (3-5), the model underestimated the results. A mould index of 3 is generally chosen as the threshold, above which the wall assembly is considered as having a moisture risk. A model that can effectively categorize the years with mould index below and above 3 is considered efficient in its prediction. It was noted that, although the mould indices were underestimated in the upper range, the predicted mould index was still above 3 meaning that the model can identify the years which have moisture risk with mould growth.

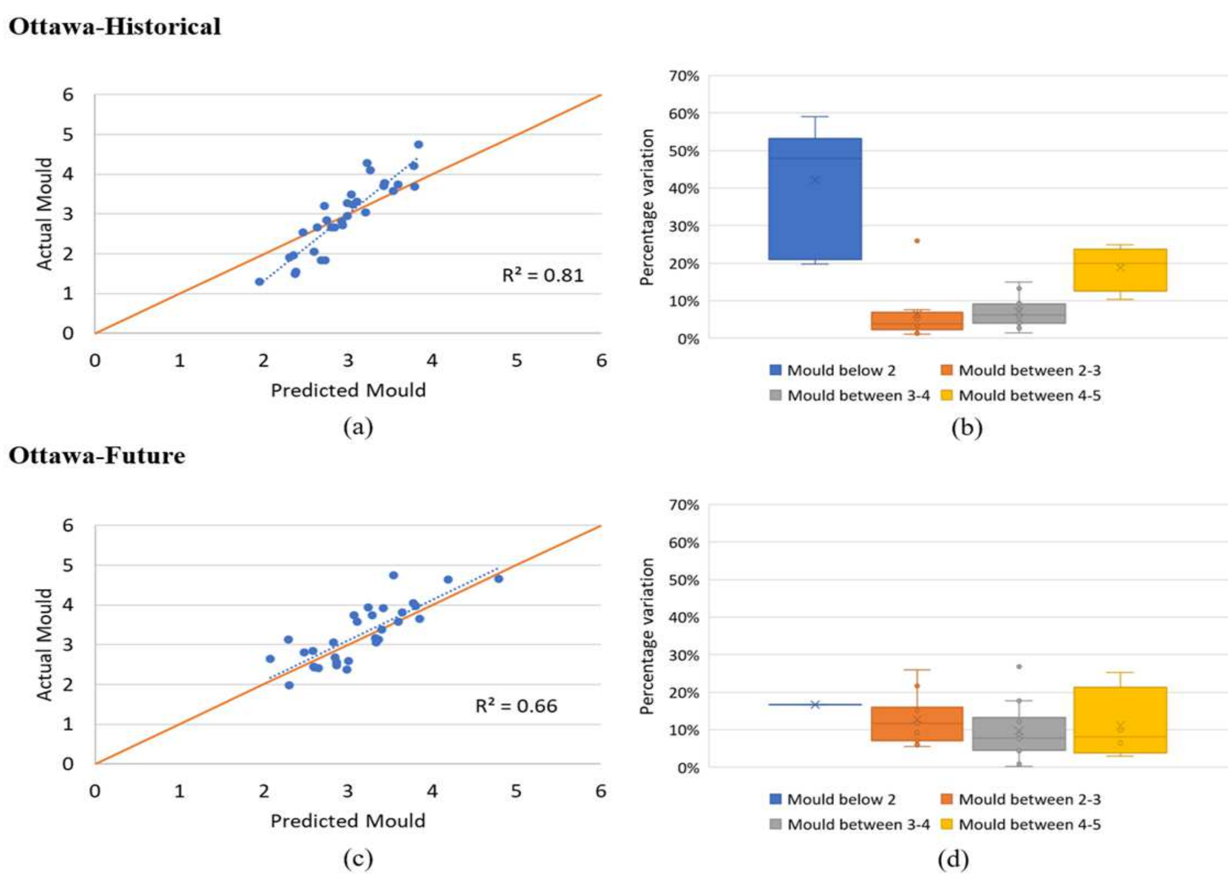

Figure 5.9: Predicted vs. actual mould index and percentage variation between the predicted and actual mould index under Ottawa-Historical and Ottawa-Future climate as the test set

A further analysis was made to analyze the deviation that exists between the predicted and the actual mould index. As shown in Figure 5.9 (b), for the historical dataset, there was a high discrepancy between the actual and predicted mould index with the highest being close to 60%. However, this is less of a concern as a mould index below 2 is generally assumed to be a safe limit and does not possess a significant moisture risk. For mould index between 2 and 4, there was a small discrepancy between the two results with the highest being 18%. For the mould index ranging between 4 and 5, the highest noted error was 27%. Under the future climate (Figure 5.9 (d)), among all the mould classes, the highest error remained below 30%.

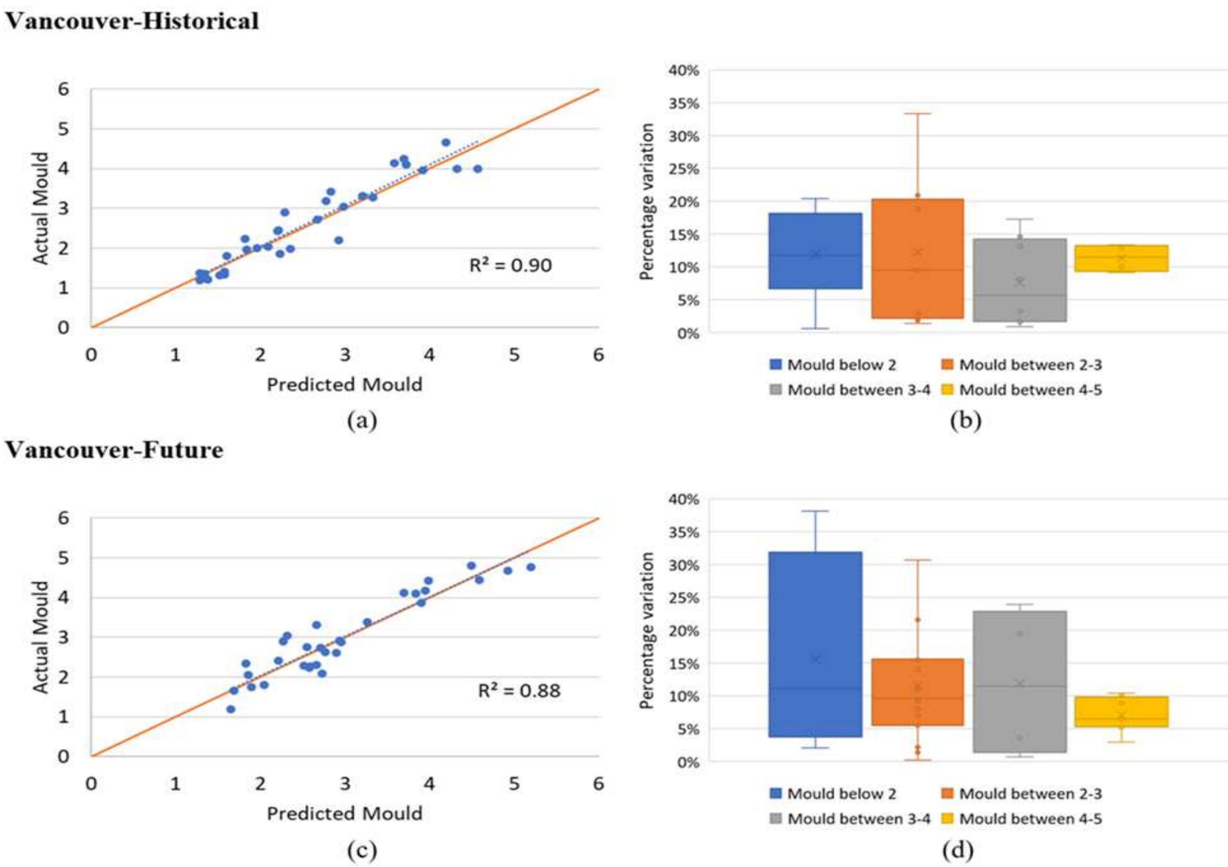

Figure 5.10: Predicted vs. actual mould index and percentage variation between the predicted and actual mould index under Vancouver-Historical and Vancouver-Future climate as the test set

For Vancouver, R^2 of 0.90 and 0.88 were noted for historical and future climate, respectively (Figure 5.10). As noted, most of the points lie close to the 45-degree line meaning that the two results are similar to each other. Further, the percentage variation between the two results for historical climate remained below 20% for all cases except for the mould index range of 2 to 3. For future climate, the variation remained high for the mould index below 2 but as discussed earlier, it is less of a concern. For other classes of mould index, the error range remained below 25%.

Figure 5.11 shows the direct correlation results for the city of St. John's. R^2 of 0.89 was observed for both historical and future simulations. The percentage variation between the two results remained below 20% for historical as well as future climate data. An exception was noted for mould index below 2 for the historical period.

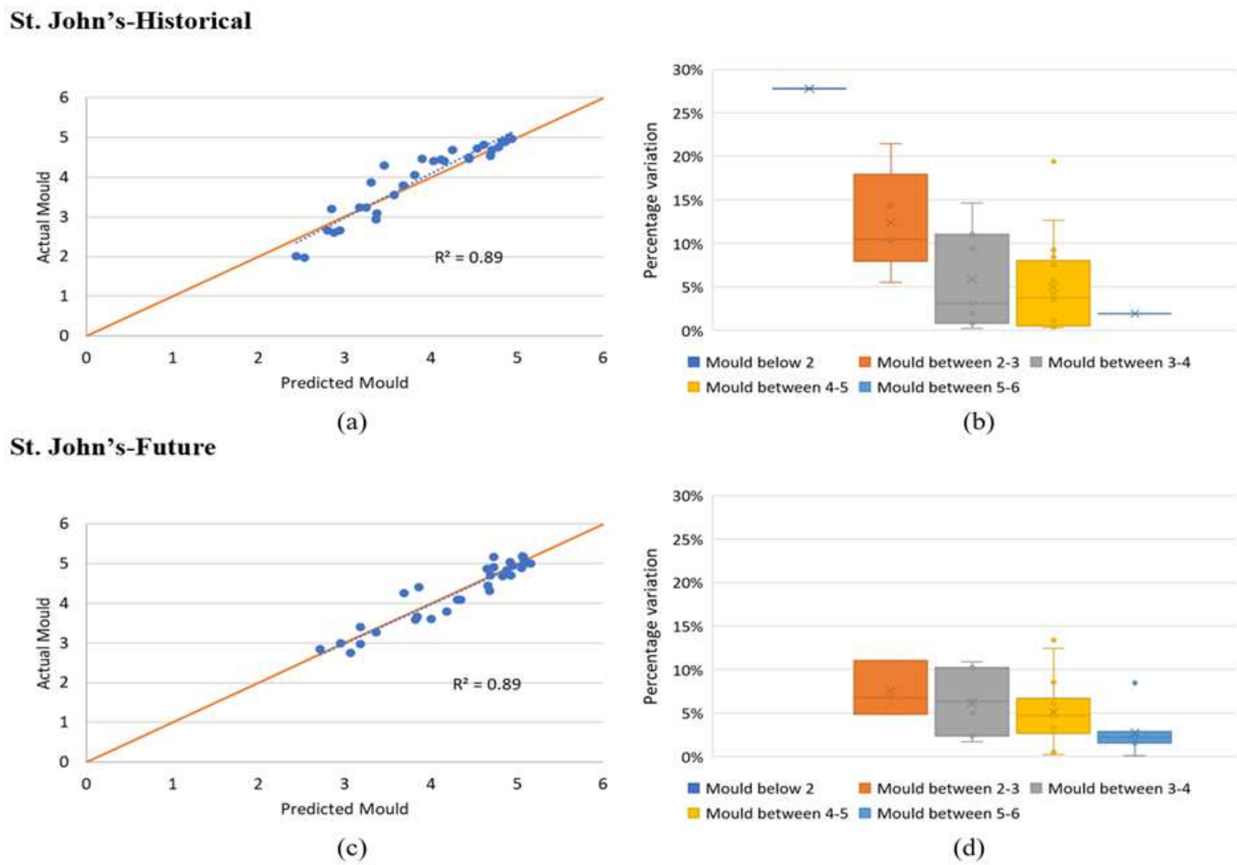

Figure 5.11: Predicted vs. actual mould index and percentage variation between the predicted and actual mould index under St. John's-Historical and St. John's-Future climate as the test set

To further verify the accuracy of the model in predicting the mould index, the RMSE and MAE were also calculated using all 31 years together, the top 3 years only, and the top 5 years only for the three cities (shown in Table 5.2). For Ottawa, the RMSE and MAE were lower when all 31 years were used compared to that when only the top 3 or top 5 years were used. For future climate, the coefficient of determination was slightly lower, while the deviation between prediction and actual mould index was smaller as indicated by a lower RMSE and MAE (Table 5.2) compared to the historical test dataset. For Vancouver, the RMSE and MAE remained lower than in Ottawa indicating better prediction results than Ottawa. For the historical dataset, RMSE and MAE remained low for 31 years in comparison with the top 3 and top 5 years, and for the future dataset, the values were found to be similar irrespective of the number of years used in the calculations. This further implies that the top 3 and top 5 years were predicted with higher accuracy in future climate than that in the historical climate dataset for Vancouver. For St. John's, the RMSE and MAE were minimum among the investigated cities meaning that the actual and predicted mould index values for this city are very close to each other. It was further observed that for the historical dataset when considering only the top 3 and top 5 years, the error was significantly small which indicates that the model had good prediction results for the top years. For the future dataset, the error was higher than the historical results, but it was still lower than the corresponding values for the other two cities.

Table 5.2: Statistical result of the prediction model for three cities under two climate periods as the test set. (RMSE (n): RMSE considering "n" years, MAE (n): MAE considering "n" year)

City	Climate period	R^2	RMSE (31)	RMSE (3)	RMSE (5)	MAE (31)	MAE (3)	MAE (5)
Ottawa	Historical	0.81	0.50	0.85	0.77	0.39	0.81	0.72
	Future	0.66	0.44	0.74	0.59	0.36	0.60	0.45
Vancouver	Historical	0.90	0.34	0.52	0.46	0.27	0.52	0.45
	Future	0.88	0.35	0.33	0.33	0.29	0.33	0.31
St. John's	Historical	0.89	0.31	0.07	0.11	0.24	0.06	0.08
	Future	0.89	0.25	0.27	0.21	0.21	0.22	0.15

5.7.2. Ranking analysis

This analysis focuses on the ranking of years based on the predicted and actual results rather than the actual magnitude of the response variable. The purpose is to see how well the model can rank the years in terms of their moisture severity. The model would be considered as effective if it lead to a similar ranking of years as obtained from simulations. Two different methods of evaluating the ranking of years were investigated and the details are provided in the following sections.

5.7.2.1. Number of matching years

The number of matching years between the prediction and actual results was counted and used as a criterion to evaluate the model's reliability. A match is considered if the year ranked using predicted results is at the same position as that using actual results based on the decreasing severity. The higher the number of matches, the better the model is in ranking the years. The other way to identify the model's effectiveness is to investigate its ability to predict the top 3 or top 5 years. Usually, for the construction of MRY, one is interested in the top years, so if the model can lead to a similar ranking for those top years, it can be considered effective. However, unlike the approach of ranking all years where a direct match is considered when the years are placed at the same place this method does not consider the order of years as long as it is ranked within the top 3 or top 5, it is considered as a match. In other words, if the year "X" is placed at the first position in the predicted results but placed at the third position in the actual results, it is considered a match.

Table 5.3 shows the number of matching years results for the three cities under two climate periods. In general, it was observed that the number of matches considering all 31 years remained low with the highest being 6 matches for Vancouver under the future climate set. Further, when considering the top 3 or top 5 years without considering the order of years, it was noted that there was a good number of matching years. For the top 3 years, among the 6 investigated scenarios, 4 scenarios resulted in 2 matching years. Similarly, when considering the top 5 years, two scenarios resulted in 3 matching years, two scenarios resulted in 4 matching years, and one scenario (Vancouver future set) resulted in all 5 matching years.

Table 5.3: Number of matching years for three cities under two climate periods as the test set. (Matches (n): number of matches considering "n" years)

City	Climate period	Matches (31)	Matches (3)	Matches (5)
Ottawa	Historical	5	2	2
	Future	1	2	4
Vancouver	Historical	4	1	3
	Future	6	2	5
St. John's	Historical	1	2	4
	Future	2	0	3

5.7.2.2. Salonvaara method (Salonvaara et al., 2010)

The approach suggested by Salonvaara et al. (2010) is used to compare the goodness-of-fit in selecting the years with the highest value of the performance indicator. It calculates the normalized mould index, which represents the maximum mould index normalized to have a range of 0%-100%. Further, the average normalized mould index is calculated by taking the arithmetic mean of the normalized values for a given number of years. The higher the average normalized mould index, the better the prediction is. The procedure to compare the results using the Salonvaara method is as follows:

1. Rank the years in decreasing order using the actual maximum mould index results i.e., from simulations.
2. Normalize the actual mould index to have a range of 0%–100%.
3. Take the top three and five years as selected by the prediction model (predicted mould index) and find the corresponding normalized performance indicator as given by the simulation results (actual).
4. Calculate the average of the normalized performance indicator for the top three and five years.
5. Compare the average normalized performance indicator of the years picked by the prediction model with the actual results.

Table 5.4: Ranking analysis results using the Salonvaara approach for three cities under two climate periods as the test set. (Salonvaara (n): Average normalized mould index considering "n" years)

City	Climate period	Salonvaara (3)	Salonvaara (5)
Ottawa	Historical	84.5%	78.1%
	Future	84.6%	80.2%
Vancouver	Historical	87.1%	84.9%
	Future	95.5%	95.3%
St. John's	Historical	98.2%	96.5%
	Future	93.9%	96.2%

Using the Salonvaara approach, it was observed the results were better for Vancouver and St. John's when compared to Ottawa (Table 5.4). In general, for all the investigated scenarios, the average normalized mould index remained above 80% (with one exception of the Ottawa historical set with a 5-year average calculation). For Ottawa, the performance with top 3 years was better than that for top 5 years. For Vancouver, the average normalized mould index remained close to 85% under the historical climate and it is above 95% under future climate. Finally, for St. John's, the results were superior among three cities where the values are above 93% for both climate periods with the highest being 98.2% for the historical set considering three-year average results.

5.7.3. Risk categorization analysis

When assessing moisture risks, from the building practitioner's point of view, one is interested in estimating the risk of the wall instead of knowing the actual mould index value. This analysis aims to compare the risk level based on where a particular year falls when using the predicted and actual results. 5 categories were created based on the mould index value i.e., 0-2, 2-3, 3-4, 4-5, and above 5. For each category, the number of years that fall in the range was counted for both the predicted and actual results. Then the number of years that are common between the actual and predicted results was counted and noted as "common". For instance, as shown in Figure 5.12 (b), for the mould range of 3-4, the simulation results (actual) suggested that 15 years has the mould index in this range, while the PLS model results (predicted) suggested 16 years has mould index in this range. However, between the two results, 13 years were the same and are marked as "common". This implies that the model can categorize well 13 years out of 15 years.

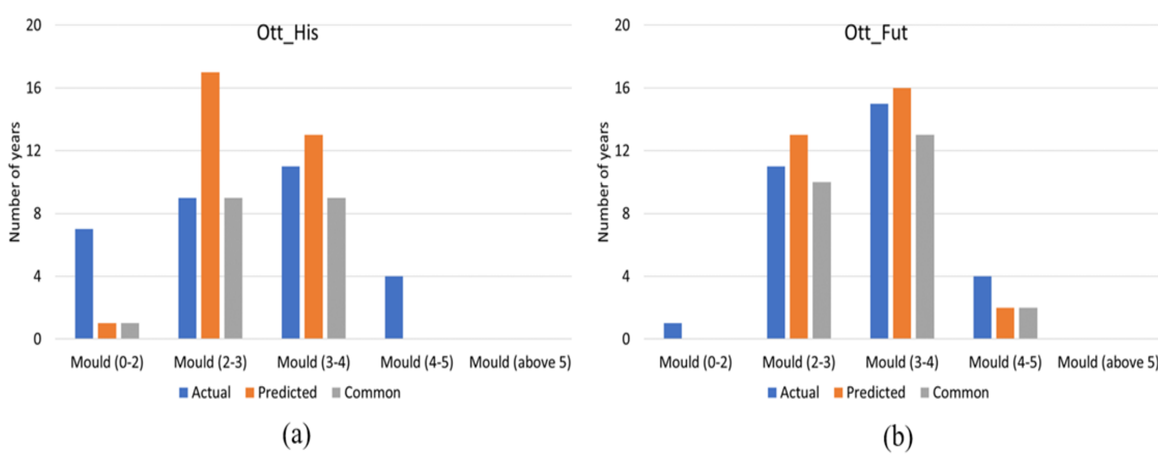

Figure 5.12: Risk category analysis with the number of years in each category for Ottawa-Historical and Ottawa-Future climate as the test set

Figure 5.12 shows the number of years under each category for the predicted and actual results, and the number of years that are in common between the predicted and actual results. For Ottawa historical test set, the model can very well predict the years in the same category for mould range of 2-3 and 3-4, having 9 out of 9 and 9 out of 11 common years, respectively. Under the Ottawa future dataset, a similar pattern was seen i.e., for mould range of 2-3 and 3-4, the model was able to predict 10 out of 11 and 13 out of 15 common years, respectively.

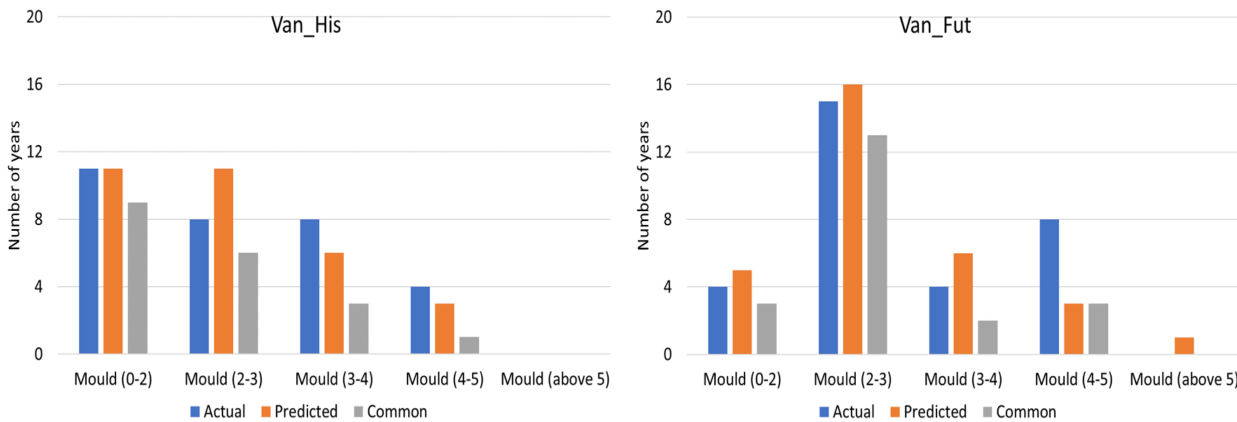

(a) (b)

Figure 5.13: Risk category analysis with the number of years in each category for Vancouver-Historical and Vancouver-Future climate as the test set

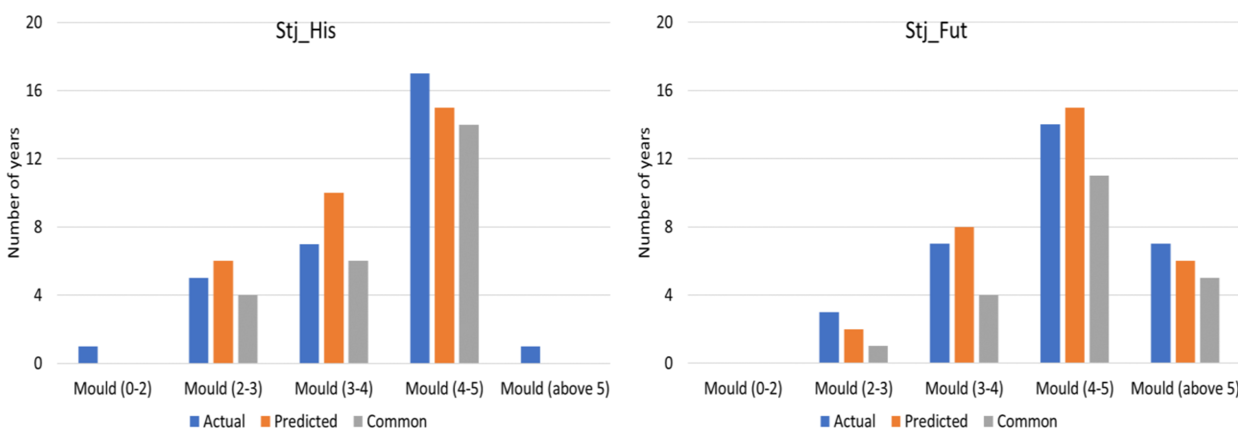

(a) (b)

Figure 5.14: Risk category analysis with the number of years in each category for St. John's-Historical and St. John's-Future climate as the test set

Figure 5.13 and Figure 5.14 show the risk category analysis result for Vancouver and St. John's respectively. For Vancouver, most of the years had mould index ranging between 0 and 4. It was further observed that for Vancouver, the model was able to predict the years in the same risk category for most of the cases. With St. John's, the analysis showed that for historical climate; most of the years had mould index in the range of 2 to 5 and for future climate, the values range between 3 to 6 for most of the years. Further, the model was able to predict the mould class precisely for both, historical as well as future climates.

5.8. Discussion

As observed from the results for Ottawa, Vancouver, and St. John's, it was found that Vancouver and St. John's had better prediction results than Ottawa. To investigate further, the score plot for Ottawa's model was compared with Vancouver's and St. John's models. Any model would lead to a good prediction if the data used in training are grouped well and can explain most of the Y variance. To identify the grouping of data and a pattern within the data set, a score plot was plotted. A score plot is a scatter plot of scores for two specified factors from a PLS regression and helps identify the patterns in the dataset. The closer the samples are in the scores plot, the more similar they are. Conversely, samples which are far away from each other are different from each other. A model is considered reliable if the data is grouped well and can distinguish among the various points used in the test set (Mehmood et al., 2020).

Figure 5.15 shows the score plot using two factors for the three cities. As noted, clear-cut segregation of data based on the orientation was observed in Vancouver and St. John's. One of the reasons for this is that in Vancouver and St. John's, the results vary significantly based on the wall orientation. Also, the orientations with the highest and the lowest WDR were identical among different years for Vancouver and St. John's. On the other hand, for Ottawa, the orientation with the highest and the lowest amount of WDR was different among different years. This further resulted in lower performance in predicting the output for Ottawa compared to the other two cities.

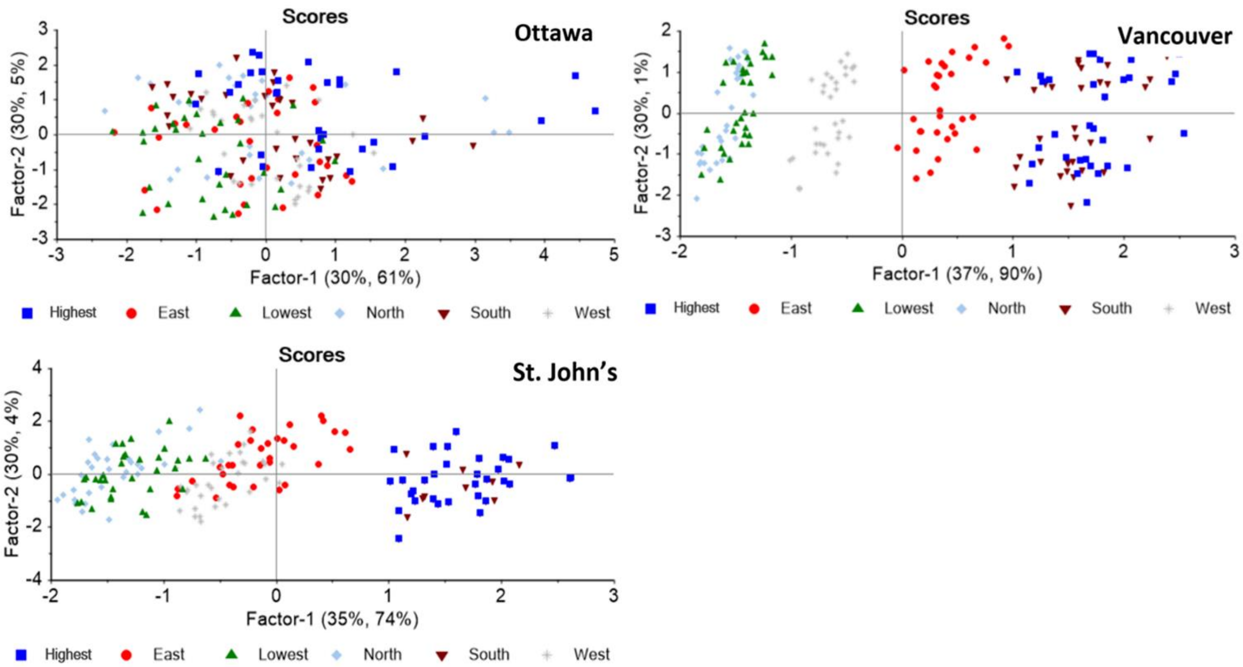

Figure 5.15: Score plot of the training set used for three cities for developing the PLS regression model

5.9. Conclusions

Hygrothermal simulations are commonly used to evaluate the moisture response of the walls, but they can be time-consuming depending on the complexity of situations and hence sometimes becomes computationally expensive. Existing climate-based indices have certain limitations associated with their usage and could not provide a reliable evaluation of the hygrothermal performance of walls. A regression model based on PLS regression was developed in this study to provide an estimated wall performance without performing the simulations and thereby reduce the computation time. The model uses a training set comprising the response variable and the most influential input parameters. Based on the data input to the model, a regression equation is developed, and this can be further used for any new dataset that one can encounter in the future.

The main findings are as follows:

- The prediction results on the investigated test sets showed a good accuracy as depicted by various statistical parameters i.e., R^2 above 65% and an average RMSE below 0.5 for Ottawa, and R^2 above 85% and RMSE below 0.35 for Vancouver and St John's.

- Ranking analysis showed that the model can quite accurately rank the years especially if the primary concern is to identify the top 3 or top 5 worst years for the purpose of Moisture Reference Year selection.
- The model was able to categorize the years in the same mould risk category as depicted by simulation results.

Analysis in this paper showed that the use of the PLS modeling technique to predict the hygrothermal response is an effective way to improve computational efficiency. The model if trained well can help in predicting the wall response and will reduce the simulation efforts. The advantage of regression model is that it is easy to use for practitioners, who may not have the knowledge and experience of DELPHIN or any other hygrothermal simulation programs. It can also be used by the practitioners for screening purposes to reduce the simulation efforts. For example, the predicted mould can be computed using the regression equation and later simulations can be performed only for the cases where the model predicts the mould index above a certain threshold defined by the users. The present study was limited to only one wall assembly and a few cities and hence the future work will include incorporating more cities and different wall assemblies.

Chapter 6 Application of PLS model: Different claddings, climate uncertainties and global warming scenarios

The content of this chapter is submitted to the journal and is under the paper is under proof reading. "*Hygrothermal performance assessment of wood-frame walls under future climates using Partial Least Squares (PLS) regression: Different claddings and climate uncertainties*," Submitted to Building and Environment, under review. The abstract and introduction from the original paper is not included in this chapter and to avoid the repetition, the wall assemblies, boundary conditions, model settings, etc. included in the originally published paper are excluded since these are already provided in Chapter 3 "Methodology".

6.1. Validation of PLS model on stucco cladding

The PLS model regression equations shown in section 2.1 were developed and validated on brick veneer cladding wood frame wall assembly. For a model to be robust, it must work well in terms of its prediction and the ranking ability for other types of walls too. The three PLS models were tested for making predictions on a stucco cladding wall. The applied approach and results are discussed in detail for Vancouver and results of applying the same approach to Ottawa and St. John are also included. .

6.1.1. Application of the brick model to stucco cladding

A test set comprising 31 years of historical and future years from the median run (the run with the median value of MI among 15 runs) was chosen. The PLS model was trained on 6 different wall orientations that cover the entire range of wall orientations. To incorporate the effect of wall orientations in the test set, a random wall orientation was chosen for all the selected years. The comparison of prediction results with simulation results is shown in Figure 6.1.

Figure 6.1 (a) shows the comparison of simulation results and predicted results (PLS model results) for the Vancouver historical climate test dataset. A significant value of R^2 i.e., 0.93 was noted between the two results. Further, as observed, all data points lie below the one-to-one (orange) line, meaning that the brick PLS model overestimated the mould index. However, the model was able to capture the trend of mould index among different years. A similar trend was noted with Vancouver's future climate (Figure 6.1 (b)).

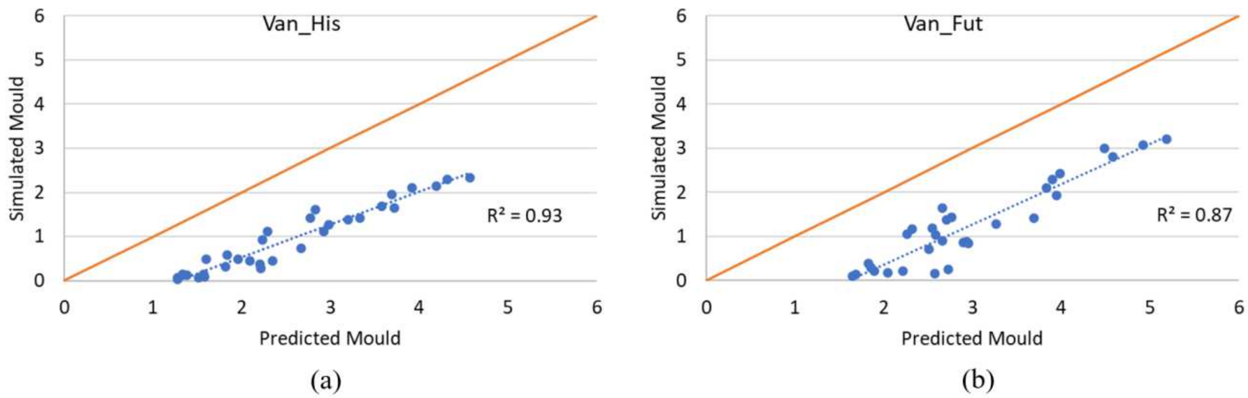

Figure 6.1: Scatter plot of simulation vs predicted mould index for stucco cladding. Predicted results are based on the PLS model developed using brick veneer cladding. (Van: Vancouver, His: Historical, Fut: Future)

Table 6.1 shows the ranking results when simulations are performed for stucco cladding and the simulation results were compared with the predicted result using the brick veneer cladding PLS model. It was found that the PLS model was able to rank well the years i.e., at least 8 matches out of 31 years. Further, when comparing the top 3 and 5 years, the model was able to rank at least the top 2 and 4 years, same as the simulation results.

A further analysis was carried out using Salonvaara method and the procedure to compare the results is as follows:

1. Rank the years in decreasing order using the simulated maximum mould index.
2. Normalize the simulated mould index to have a range of 0%–100%.
3. Take the top three and five years as selected by the prediction model (predicted mould index) and find the corresponding normalized performance indicator as given by the simulation results.
4. Calculate the average of the normalized performance indicator for the top three- and five-years using simulation results.
5. Compare the average normalized performance indicator of the years picked by the prediction model with the simulation results, a ratio between the two results (expressed in %) is shown in Table 6.1.

As noted from Table 6.1, a significant value of ratio of normalized damage functions (above 90%) was noted for both climate periods.

Table 6.1: Number of matching years and results with the Salonvaara approach for Vancouver under two climate periods as the test set. (Matches (n): number of matches considering "n" years, Salonvaara (n): averaged normalized function considering "n" years)

Case	Matches (31)	Matches (3)	Matches (5)	Salonvaara (3)	Salonvaara (5)
Van_His	9	3	4	96.9%	90.3%
Van_Fut	8	2	5	94.3%	90.2%

The above-mentioned analyses suggest that the model can categorize the worst years well but in terms of the actual magnitude i.e., the mould index value, the PLS model overestimates the results. One of the reasons for this overestimation is the ACH assigned in the air cavity, stucco cladding wall has much higher ACH value than the brick cladding wall. This difference in ACH results in a lower mould index in the stucco cladding wall in simulations. Therefore, the original brick PLS regression model could be used in the stucco wall for ranking while the modified brick PLS regression model can bring down the overestimation and used for mould index prediction. This suggests that the developed brick model can be used as a representative for other wall claddings. This approach will be tested for other types of cladding and locations in the future work.

6.1.2. Modified brick PLS model for stucco and its validation

Vancouver's historical and future period were used as a test set and the simulation results for stucco cladding was correlated with the predicted results using the brick PLS model. The detail for obtaining the modified brick PLS model is as follows:

1. Generating the scatter plot distribution between the stucco simulation results and predicted brick PLS model results using historical and future period data (Figure 6.2). The corresponding regression equation representing the fit of two data was noted.
2. Modifying the brick PLS model with the corresponding reduction factor.

Brick PLS model regression equation:

$$\begin{aligned} Mould = \; & -3.6923 + 0.1118 * T_{avg} + 3.7850 * RH_{avg} + 0.3543 \\ & * Speed_{avg} + 48.5317 * WDR_{avg} + 0.0088 * Rad_{avg} \end{aligned} \tag{6-1}$$

Modification step:

$$Mould = \mathbf{0.82} * \left(-3.6923 + 0.1118 * T_{avg} + 3.7850 * RH_{avg} + 0.3543 * Speed_{avg} + 48.5317 * WDR_{avg} + 0.0088 * Rad_{avg}\right) - \mathbf{1.17} \tag{6-2}$$

Note: The multiplication factor and coefficients used for modifying the original brick model are marked in bold.

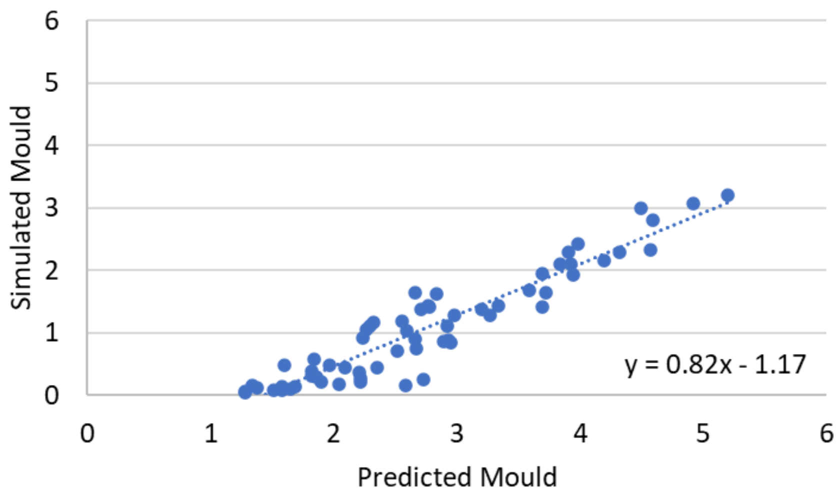

Figure 6.2: Scatter plot between mould index from simulations for stucco wall and the predicted mould index using brick PLS model

Modified brick PLS model regression equation for stucco (historical and future period):

$$Mould = -4.2050 + 0.0917 * T_{avg} + 3.1063 * RH_{avg} + 0.2907 * Speed_{avg} + 39.8299 * WDR_{avg} + 0.0072 * Rad_{avg} \tag{6-3}$$

To validate the modified brick PLS model, the prediction results were compared with the model developed for the stucco cladding wall, the corresponding regression equation with stucco training data is shown below:

$$Mould = -1.4629 + 0.0583 * T_{avg} + 1.8737 * RH_{avg} - 0.0001 * Speed_{avg} + 52.4045 * WDR_{avg} - 0.0091 * Rad_{avg} \tag{6-4}$$

For both models i.e., the modified brick PLS model and the stucco-trained model, the corresponding predicted results from the two models were compared with simulation results, presented in further sections.

6.2. Results and discussion

In this section, the various results of this study are discussed. Firstly, a comparison was made between the modified brick PLS model with the stucco trained PLS model to demonstrate the reliability of the modified model. Secondly, the PLS models are used to predict the mould index for different climate runs to cover the uncertainty in the climate data. For this purpose, the brick PLS model was applied to all 15 runs with each run having 31 years and 16 wall orientations at an interval of 22.5°. This results in a total of 7440 (15*31*16) points for one climate period. The same analysis was applied to historical and future climate periods to compare the risk among different runs and climate periods. Thirdly, the results are discussed for the most conservative scenarios, where the wall is facing the orientation with the highest amount of WDR, to quantify the maximum moisture severity. Finally, the cumulative distribution of mould index among all runs was discussed along with the selection of moisture reference year for simulations.

6.2.1. Comparison of modified brick model and stucco-trained model

Figure 6.3 shows the comparison of the predicted and simulation results for Vancouver's historical and future climate periods. For the historical period, a similar performance was noted for both the models i.e., R^2 of 0.93 vs. 0.95 and RMSE of 0.21 vs. 0.18 for the modified PLS and stucco trained PLS model respectively. Further, a closer investigation showed that with the modified brick model, more points lie close to the one-to-one line meaning that the mould index from simulation and predicted results with the modified PLS model were close to each other. For the future period, the R^2 was found to be 0.87 and 0.92 and RMSE of 0.35 and 0.29 was noted for the modified brick and stucco model respectively.

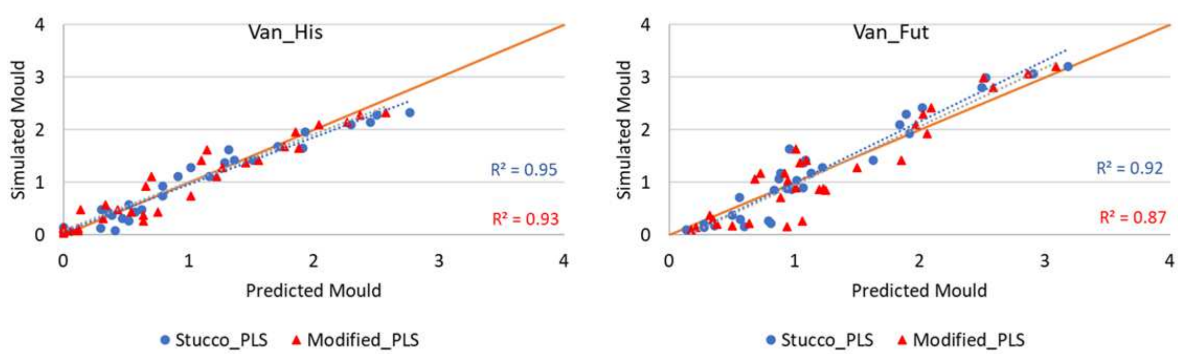

(a) (b)

Figure 6.3: Comparison of predicted results using modified brick PLS model and stucco PLS model with simulation results for Vancouver's historical and future period

Further, RMSE was calculated for the two models considering all 31 years, top 3, and top 5 years (Table 6.2). RMSE considering all the years for the historical period was found to be similar for the two models, while lower RMSE values were noted for the modified model for the top 3 and top 5 years. For the future period, there was not much difference in RMSEs between the two models.

Table 6.2: RMSE with two models for three cities under two climate periods as the test set. (RMSE (n): RMSE considering "n" years)

Case	**Model**	**R^2**	**RMSE (31)**	**RMSE (3)**	**RMSE (5)**
Van_His	Modified_PLS	0.93	0.21	0.17	0.14
	Stucco_PLS	0.95	0.18	0.33	0.27
Van_Fut	Modified_PLS	0.87	0.35	0.31	0.30
	Stucco_PLS	0.92	0.29	0.28	0.32
Ott_His	Modified_PLS	0.57	0.16	0.20	0.26
	Stucco_PLS	0.53	0.16	0.22	0.27
Ott_Fut	Modified_PLS	0.51	0.25	0.33	0.34
	Stucco_PLS	0.57	0.24	0.36	0.35
Stj_His	Modified_PLS	0.84	0.32	0.41	0.38
	Stucco_PLS	0.87	0.30	0.34	0.32
Stj_Fut	Modified_PLS	0.63	0.43	0.87	0.70
	Stucco_PLS	0.75	0.38	0.63	0.57

Based on the above discussion, it can be said that the modified brick PLS model works effectively for stucco cladding, and it might be not necessary to develop the model based on stucco cladding. This implies that the different climate years were ranked in a similar manner in terms of their moisture severity as the relative moisture severity of different years remains the same irrespective of cladding material, brick vs. stucco. What remains is the difference in magnitude of mould index for different years for two claddings and as discussed earlier that as the trend of mould index with stucco cladding simulations and brick PLS model results is the same so a suitable modification factor applied to the brick model could result in a good prediction model for stucco.

Following the above-mentioned approach for Vancouver, the corresponding PLS regression equations for stucco cladding were developed for Ottawa and St. John's i.e., equation (6-5) and equation (6-6), respectively.

Ottawa

$$Mould = -6.86645 - 0.01823 * T_{avg} + 5.991594 * RH_{avg} + 0.755239 * Speed_{avg} + 43.881 * WDR_{avg} - 0.00165 * Rad_{avg} \tag{6-5}$$

St. John's

$$Mould = 3.2493 + 0.0524 * T_{avg} - 4.0630 * RH_{avg} + 70.4108 * WDR_{avg} - 496.6257 * WDR_{avg}^2 \tag{6-6}$$

The same methodology as Vancouver was used for comparing the models for Ottawa and St. John's and it was found that the prediction results with the modified brick model and stucco-trained models were similar for both cities (Table 6.2).

6.2.2. Climate uncertainty and mould growth risks under future climates

The PLS model was based on the MI ranking to select the historical and future climate datasets. The median run with an average MI was used for model development and validation. The median run was assumed to represent the whole 15 runs of data. In this study, to assess the reliability of the model and to validate it on different climate runs, 3 random years were selected from each run for the historical period making a total of 45 years. Further, the effect of wall orientation was also incorporated meaning that among the selected 45 years, 16 different wall orientations were randomly allocated. Simulations were performed using the brick veneer cladding wall assembly and the results of the mould index were compared with the predicted results using the brick PLS model. The analysis was made for the three cities and two claddings. It was found that the results showed a similar trend for three cities and two claddings and hence the detailed analysis was reported only for Vancouver with brick veneer cladding wall.

6.2.2.1. Vancouver brick veneer cladding

Figure 6.4 shows the comparison of the mould index from simulations and predicted mould index for a brick veneer cladding wall using 45 random years selected from the Vancouver historical dataset of 15 runs. As shown in Figure 6.4 (a), the model was able to capture the trend of mould index values among different years. Further, the two results were well correlated with an R^2 of

0.91. This indicates that the model although trained only on the median run can be effectively used to make predictions on any random run, year, and wall orientation.

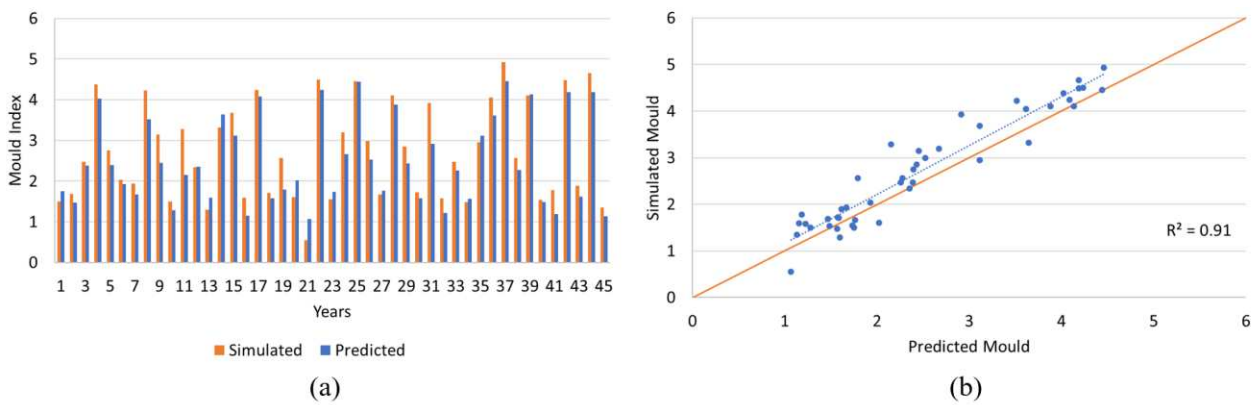

Figure 6.4: Simulated vs predicted mould index for Vancouver historical climate with brick veneer cladding wall assembly using 45 random years. (a) Variation of trend in the mould index, each year is represented with maximum mould index in that year, (b) Scatter plot of simulated and predicted mould index

Mould prediction covering all runs

All the historical and future years of Vancouver were considered and the yearly average for the input variable was computed to predict the mould index using the brick PLS model. Figure 6.5 (a) shows the mould index rosette for the median run of Vancouver (Run 04) for the historical climate. The shaded line represents the 31 years in the run and the average of 31 years in a particular orientation is represented by the black solid line. It was noted that there is a variation in the mould indices among different years. However, a general trend was noticed that the mould index is significantly higher for the ESE to SSW (clockwise) orientations in comparison to the northern side (from West to East, clockwise), which corresponds to the low WDR in the northerly directions in Vancouver.

A similar process was repeated with all the runs and for visual clarity and comparison among different runs, the average value per run (based on the average of all years in a direction) was plotted. Figure 6.5 (b) shows the mould index rosette for each run. It was observed that except for run 07 which is the run with the least amount of WDR in all directions, the mould index does not vary much among the 15 runs. Excluding run 07, the maximum noted variation among the runs was approximately 5%. Further, a mould index below 3 is usually considered a safe limit for design purposes following ASHRAE 160. It was noted that for all the runs, the mould index was above 3 from east to WSW orientations. This further implies that the moisture risk heavily depends on the wall orientation and the wall orientations except east to WSW were at no risk for all the runs.

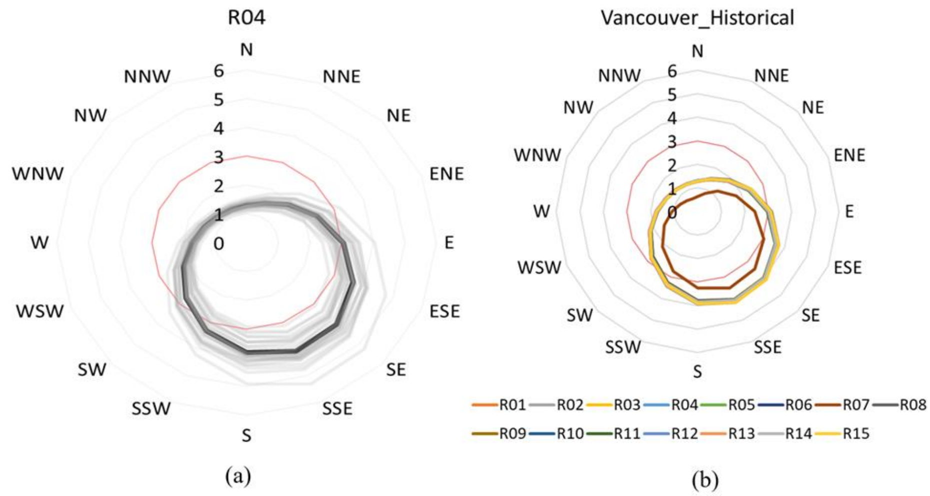

Figure 6.5: (a) Predicted mould index for a brick veneer cladding wall for 31 years of the median run (Run 04) for Vancouver's historical climate. The dark black line represents the average of 31 years in a given orientation, (b) the average value of 31 years of mould index in a run for a given orientation for all 15 runs of Vancouver historical climate

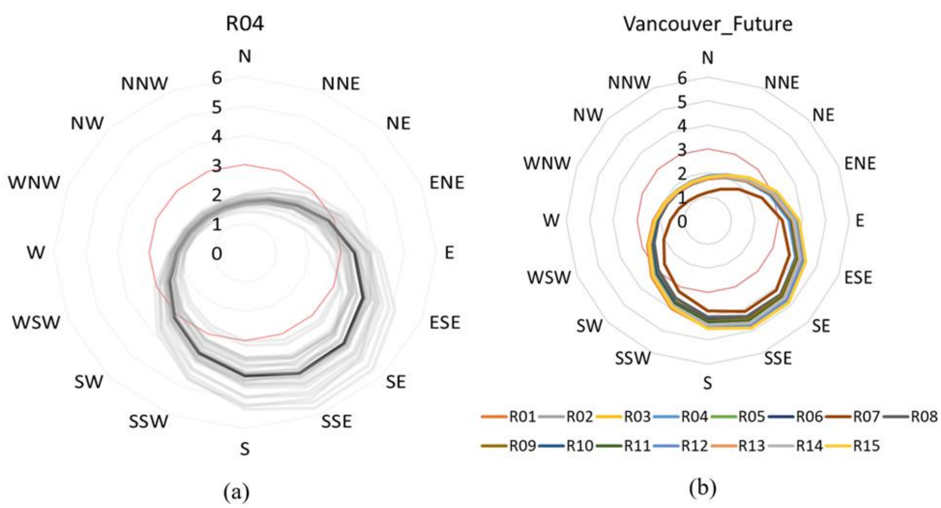

Figure 6.6: (a) Predicted mould index for a brick veneer cladding wall for 31 years of the median run (Run 04) for Vancouver's future climate. The dark black line represents the average of 31 years in a given orientation, (b) the average value of 31 years of mould index in a run for a given orientation

Figure 6.6 shows the results i.e., the variation of mould index among different years in a run and the variation among different runs for Vancouver's future climate. It was observed that similar to results with historical climate, the mould index was significantly higher in the southerly directions. Further, run 07 was still the run with the least value of mould index, however, the variation among different runs was slightly higher than the historical climate i.e., a variation of approximately 12% among different runs in comparison to 5% for the historical climate.

Figure 6.7 (a) shows the comparison in the mould index rosette covering all 15 runs for historical and future periods with a brick veneer cladding wall between the historical and future climates. It was observed that for historical climate, the range of mould index with 15 runs was narrow and it is close to the average of 15 runs. However, for future climate, a wider range of mould index was noticed with different runs, and this demonstrates the higher uncertainty in the projected future climate. It is seen that the mould growth risk will increase in the future for brick veneer cladding walls with maximum risk occurring along the SSE orientation. Further, it was observed that the risk remained lower in the northerly orientations, but the safe zone decreased in the future period. In other words, apart from a higher mould index in the future, the wall orientation which falls under the safe category for the historical period (ENE) would not remain safe in the future period.

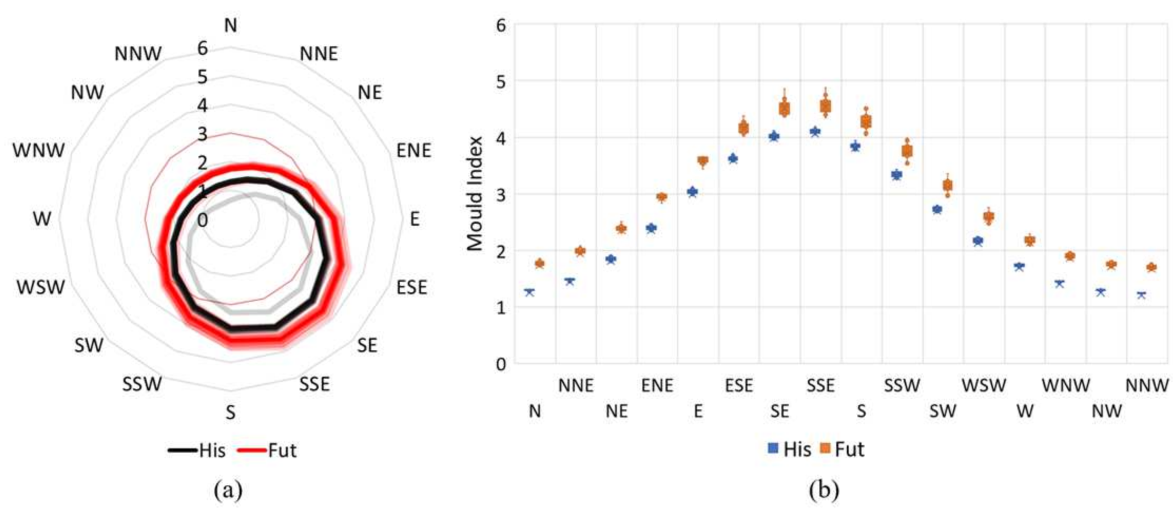

Figure 6.7: (a) Predicted mould index rosette for brick veneer cladding wall for 15 runs with the historical and future period of Vancouver. The dark line represents the average of 15 runs and the shaded region represents each of 15 runs. The red line depicts the threshold limit of the mould index, and it is set at 3. (b) Box plot distribution of mould index for 15 runs along different wall orientations for brick veneer cladding wall

Figure 6.7 (b) illustrates the box plot distribution of mould index for 15 runs of historical and future climate periods among the different wall orientations. The mould index remained below 3 from N to ENE and WSW to NNW (both being clockwise). For the remaining wall orientations, a higher moisture risk is expected with the mould index varying between 3 and 5. Further, for the future period, a higher variation in the mould index was noted and the risk also remained higher in the future period for all wall orientations.

Comparison of maximum mould index among 15 runs

From the design point of view, it is important to estimate the maximum risk that a wall can be subjected to or can experience given the surrounding climate. If the wall can sustain the maximum moisture load that is supposed to occur, it will sustain other possible scenarios without any risk.

Among all the climate parameters, the WDR affects the wall performance the most, and it varies significantly along different wall orientations for Vancouver. For conservative results, the orientation which receives the highest amount of WDR called "default" orientation is identified and it is supposed to pose the highest moisture load to the wall assembly for a given year of climate data. For each year in the 15 runs and two climate periods, "default" orientation was identified. Later, the predicted mould index was computed for all years i.e., 31 years * 15 runs * 2 climate periods = 930 years. These mould index values illustrate the maximum risk a year can witness and if the values are below the threshold limit of 3, then the wall will most likely sustain the moisture loads.

Figure 6.8 shows the predicted mould index for a brick veneer cladding wall assembly subjected to default orientations for all the years in 15 runs and two climate periods. In general, it was seen that the mould index remained above the threshold limit for most of the cases. The value of the mould index varies between 3 and 5 for maximum cases and it can be said that the wall is at risk for all the years. Further, in terms of the impact of climate change, it was observed that for all the runs, an increased risk was seen. The lower mould index value observed in run 07 is due to the significantly lower WDR in historical climate data compared to other runs.

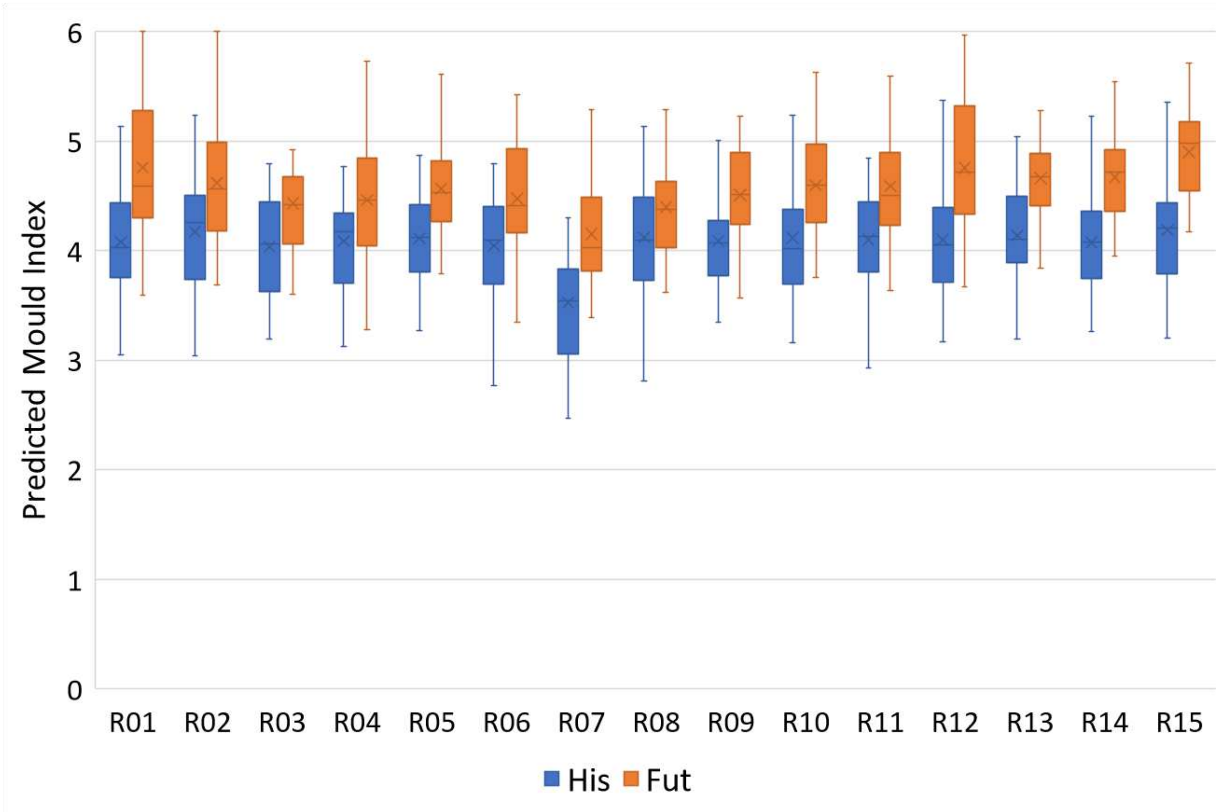

Figure 6.8: Predicted mould index for brick veneer cladding wall facing default orientations for all the runs and two climate periods for Vancouver

6.2.2.2. Vancouver stucco cladding

The modified brick model worked effectively in terms of prediction and can be used as an alternative to the stucco-trained model. Further, as discussed earlier, the brick PLS model worked well for different climate runs and wall orientations. Hence, further analysis was made for stucco cladding covering all the runs and wall orientations. The prediction results were made with the modified regression equation for Vancouver.

Figure 6.9 (a) shows the mould index rosette covering all 15 runs for historical and future periods with a stucco cladding wall for Vancouver. It was observed that for all the runs and two climate periods, the mould index was always below 3. Similar to the results with brick veneer cladding, the mould index was low in the northerly directions, and the risk increased in the southerly orientations. Contrary to the higher risk in brick veneer cladding walls, it was noted that the stucco cladding wall remains in the safe zone for all the investigated cases, however, the risk increases in the future period when compared to the historical period. Further, the mould index has a wider range for future periods as compared to historical period for all wall orientations (Figure 6.9 (b)).

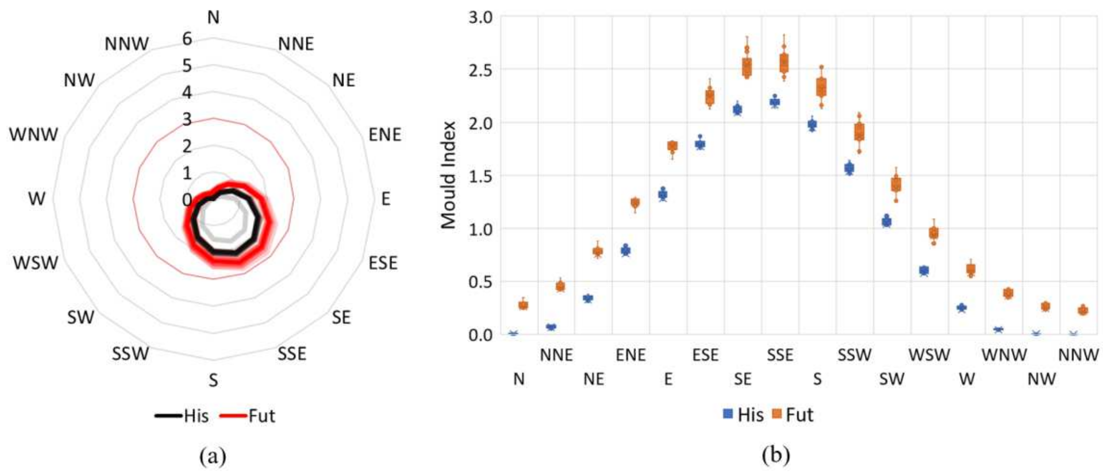

Figure 6.9: (a) Predicted mould index rosette for stucco cladding wall for 15 runs with the historical and future period of Vancouver. The dark line represents the average of 15 runs and the shaded region represents each of 15 runs. The red line depicts the threshold limit of the mould index. (b) Box plot distribution of mould index for 15 runs along different wall orientations for stucco cladding wall

6.2.3. St. John's and Ottawa

The analysis and the performance of the model were further tested with St. John's and Ottawa with brick veneer and stucco cladding walls. In general, both cities are colder and drier than Vancouver. The PLS model developed with brick veneer cladding for these two cities was used to obtain the corresponding regression equation for stucco cladding walls.

Figure 6.10 illustrates the mould index rosette and box plot distribution of mould index for St. John's covering 15 runs with historical and future periods for a brick veneer cladding and stucco cladding wall. For brick veneer cladding, it was noted that the risk remained high for all the wall orientations i.e., the mould index remained above 3 for most of the cases (Figure 6.10 (a)). Further, for the walls facing any orientation between east and west (southern semicircle), the risk was significantly high with an average mould index ranging between 4 and 5. Figure 6.10 (b) illustrates the distribution of mould index across different wall orientations for two climate periods. It was found that the mould risk increases by an average of 10% from the historical to future climate period. Further, a wider spread of mould index values was noted for the future period. For the stucco cladding wall (Figure 6.10 (c)), it was noted that for both climate periods, the mould index remained below the threshold limit of 3. Moreover, similar to the trend noticed with brick cladding wall, the risk increases in the future period by an approximate average of 10% and a higher range of mould index values for each wall orientation (Figure 6.10 (d)).

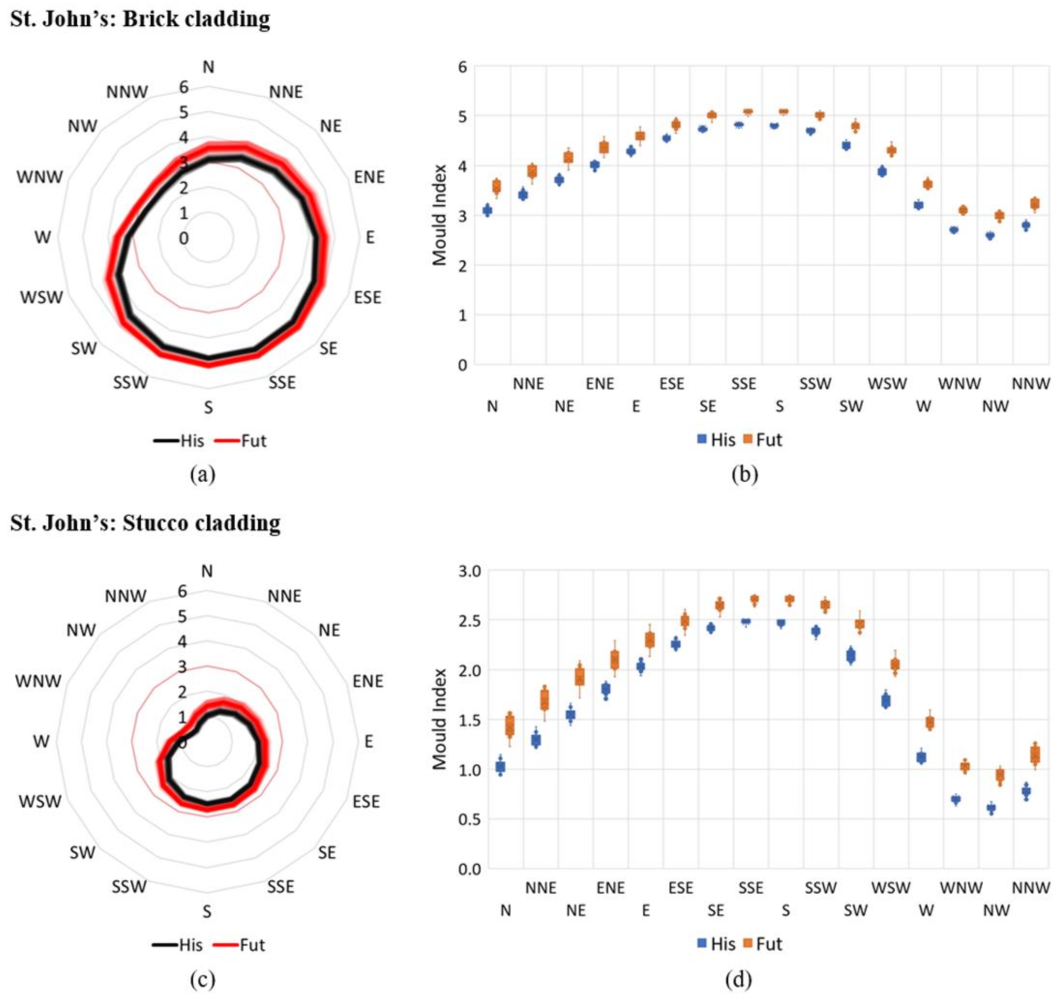

Figure 6.10: (a) Predicted mould index rosette and (b) Box plot distribution of mould index for 15 runs along different wall orientations for brick cladding wall with the historical and future period of St. John's. (c) Predicted mould index rosette and (d) Box plot distribution of mould index for 15 runs along different wall orientations for stucco cladding wall with the historical and future period of St. John's

Figure 6.11 shows the mould index rosette and orientation-wise distribution of mould index with 15 runs of historical and future periods for a brick veneer cladding and stucco cladding wall for

Ottawa. Unlike Vancouver and St. John's, there was not much variation in the mould index across various orientations. The value remained close to threshold limit of 3 and mostly varies between 2.5 and 3.5. Further, the risk increases in the future, however, the increase is not significant (Figure 6.11 (a) and Figure 6.11 (b)). The average mould index in the future period varies between 3 and 3.5 with a similar risk profile across all the orientations. For stucco cladding wall (Figure 6.11 (c) and Figure 6.11 (d)), the wall is safe as the mould index remained well below the threshold limit of 3 for both historical and future periods with slight increase in the risk for the future period.

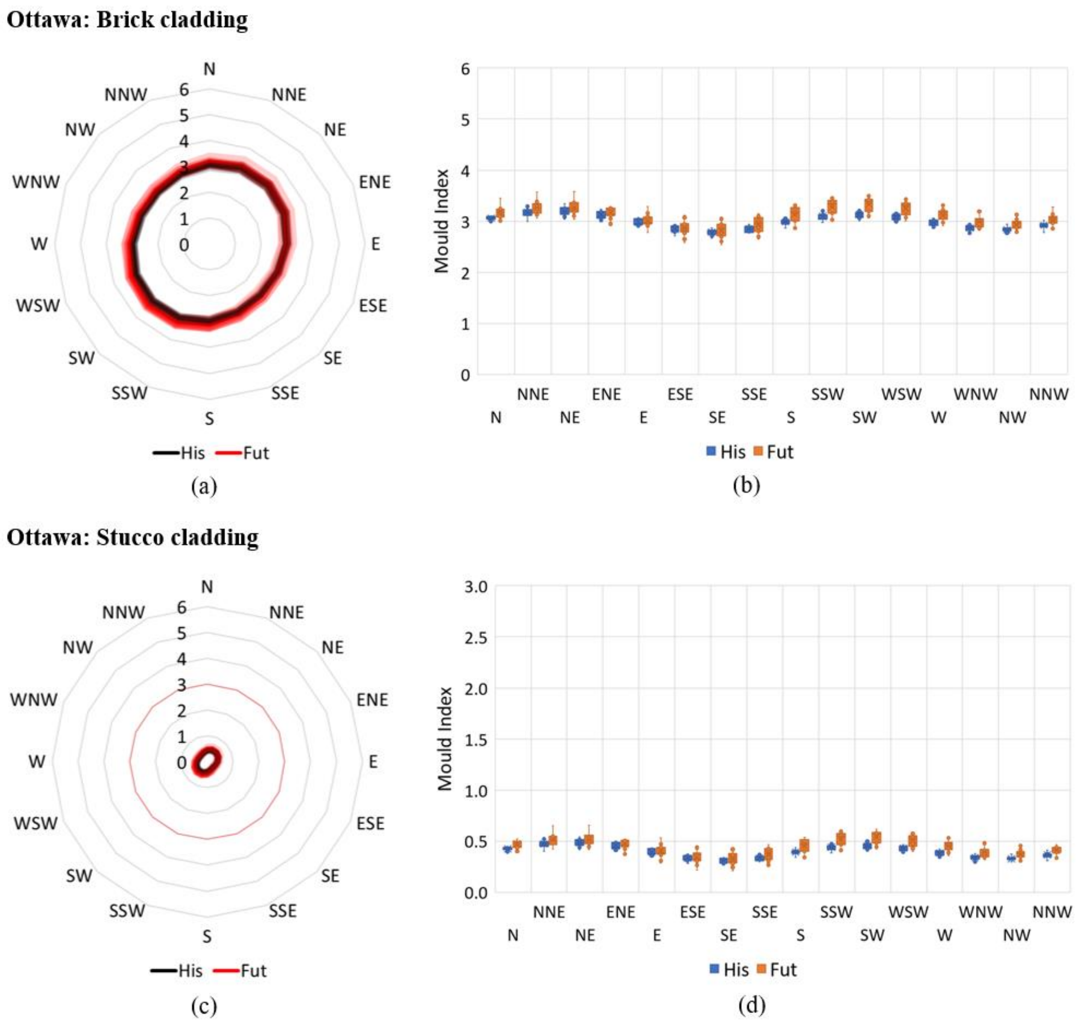

Figure 6.11: (a) Predicted mould index rosette and (b) Box plot distribution of mould index for 15 runs along different wall orientations for brick cladding wall with the historical and future period of Ottawa. (c) Predicted mould index rosette and (d) Box plot distribution of mould index for 15 runs along different wall orientations for stucco cladding wall with the historical and future period of Ottawa

6.2.4. Cumulative distribution of mould index and MRY selection

Figure 6.9 through Figure 6.11 show the distribution of mould index among different wall orientations considering 15 runs. To quantify the impact of climate change on mould growth risk, the probability distribution of mould index between the two climate periods is compared. Figure 6.12 shows the cumulative distribution of mould index for three cities with brick cladding wall assembly considering 15 runs and 16 wall orientations for historical and future periods. As noted, the mould index increased under future climates for all three cities. However, the range of the mould index was different across cities. A wider range of mould index was observed in Vancouver as the mould index varies significantly across different wall orientations with a low amount of mould risk in the northern orientation owing to low WDR in northern orientations. The range was smaller for St. John's and the smallest for Ottawa. For Ottawa, the mould index is uniform across various wall orientations and hence a narrower range of values is noted. Furthermore, as noted from Figure 6.12, the probability of mould growth index above 3 has increased from 30% in the historical period to 40% under future climate for Vancouver, from 80% to 95% for St. John's, and from 40% to about 60% for Ottawa, respectively.

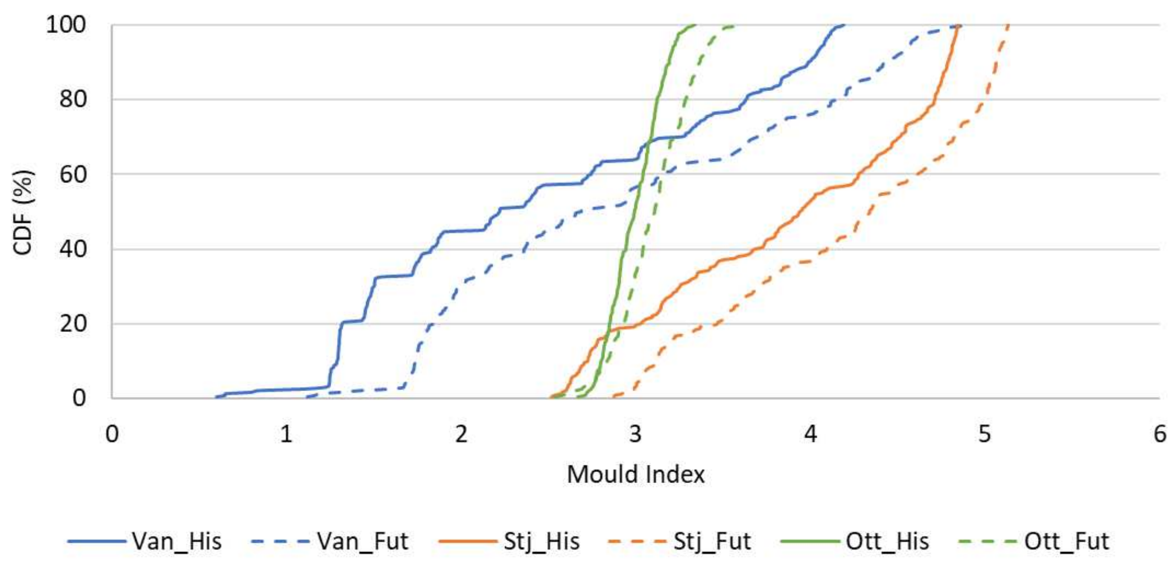

Figure 6.12: Cumulative distribution of mould index considering 15 runs and 16 wall orientations for three cities with brick cladding wall considering historical and future climate periods

One of the applications of the PLS model is to rank the years based on their moisture severity and select the MRY. ASHRAE 160 suggested taking the 93-percentile year as the MRY. This approach is applied to select the MRY for the three cities investigated in the study. Among all the wall orientations, the one with the highest average mould index for the whole run was used to select the MRY. In other words, a total of 465 years were identified i.e., 31 years * 15 runs for the worst mould index orientation based on brick cladding wall, and 93 percentile year was selected for each of the three cities (Table 6.3).

Table 6.3: MRY (93 percentile) selected for three cities under two climate periods based on the PLS model

Climate period	City	Run	Year
Historical	Vancouver	3	2014
Future		1	2089
Historical	St. John's	4	2014
Future		9	2086
Historical	Ottawa	8	1996
Future		4	2077

6.3. Conclusion

The objective of this study is to assess mould growth risks under projected future climates. To account for the climatic uncertainties, various wall designs, and geographical locations, a large number of simulations would be required. To tackle this challenge, a PLS regression model was developed previously and validated for brick veneer walls. This paper expands the previous study to include stucco cladding wall and climate datasets of 15 runs for both historical and future periods.

The main findings are as follows:

- Model performance
    - The PLS model developed with a brick cladding wall can be effectively used for a stucco cladding wall by modifying the regression equation with a suitable factor. The modified model works as effectively as the model trained on stucco cladding. Therefore, the PLS model developed for brick veneer wall can be used for the

assessment of moisture severity, i.e. ranking of a specific location to represent other types of cladding.

  - The PLS model developed for the median run can be used to cover all 15 runs and an R^2 as high as 0.91 was obtained for Vancouver.
  - The model developed can be used to predict the mould growth index directly and also to assess the moisture severity of years for the ranking and MRY selection. This can further help practitioners screen the years and perform simulations for the years with risks.
- Effect of climate change on mould growth risks
  - The model can be effectively used to assess the impact of climate change on mould growth risks without running simulations for all scenarios.
  - A mould growth rosette is used to identify the worst orientation and it was found to be consistent with the WDR rosette.
  - The mould growth risk increase in the future period for all three cities, two claddings, and 15 climate runs.
  - Considering the climate uncertainties, it was noted that the risk varies across different climate runs but in general, a similar trend was noticed. For Vancouver and St. John's the risk is considerably higher in southerly directions while for Ottawa, the risk is uniform across different wall orientations.
  - For the brick cladding wall, the mould index remained above the safe limit for southerly orientations for Vancouver and St. John's and it remained close to the safe limit for Ottawa for all orientations. For the stucco cladding wall, the mould index always remained below the threshold limit and the wall remained safe for all climate runs and periods.

The analysis shows that the PLS models can be effectively used to get an estimated wall response in terms of mould growth for wood-frame constructions under both historical and future climates. PLS models were developed for 3 Canadian cities. The model developed for brick wall cladding can be used for stucco wall as well. However, for other wall claddings e.g., vinyl, fibreboard etc. which has material properties different from brick, a new model might be required. These models can help building practitioners understand the risk involved with a certain type of wall, city, and climate data. The analysis can be used as a first screening to quantify the moisture severity of various years and if needed, simulations can be performed for only critical years for which detailed analysis might be required to reduce computational efforts. The approach developed can be applied to other cities to generate city or region-specific models. A moisture risk map can be generated for Canada, which will be reported in future work.

6.4. Performance analysis considering different global warming scenarios

In the previous sections, results were discussed for the PLS models developed for three Canadian cities and two different wall claddings for yearly simulations. The yearly mould index was predicted using the PLS model and the years were ranked in terms of their moisture severity. The yearly mould index gives a sense of moisture severity of a year in comparison to other years. However, during the service life of buildings, they are exposed to different climates across different years. Hence, it is essential to evaluate the moisture performance of the building over long-term climate data.

This section illustrates the use of the PLS model to predict the wall performance over long-term climate data. To guide building practitioners and to have a decision support tool, a stochastic modeling framework is required to be developed to deal with the uncertainties in the input parameters including material properties, field conditions, and most importantly the climate data. In the previous analyses, the historical and pessimistic global warming scenario (GW3.5) for the future was considered for the analysis. However, for the long-term climate study, all the global warming scenarios were considered to fully capture the variation in the climate data, which allows the practitioners to quantitatively assess the moisture-degradation risks for different global warming scenarios.

As one of the most important stochastic variables for stochastic simulation, the uncertainties of climate data have a significant impact on the hygrothermal performance of the wall. As stated above, these uncertainties are related to different global warming scenarios. The objective of this analysis was to develop a climate ranking system concerning the mould growth risk of the wood-frame wall assemblies, by considering uncertainties associated with different global warming scenarios. This ranking system allows the practitioners and researchers to assess the mould growth risks of the wall assembly under different climate conditions, i.e. different global warming scenarios without running simulations. In addition, this ranking system assists the researchers to pick up the representative climate data set to perform stochastic simulation by considering other uncertainties, i.e. the uncertainties of material properties and boundary conditions.

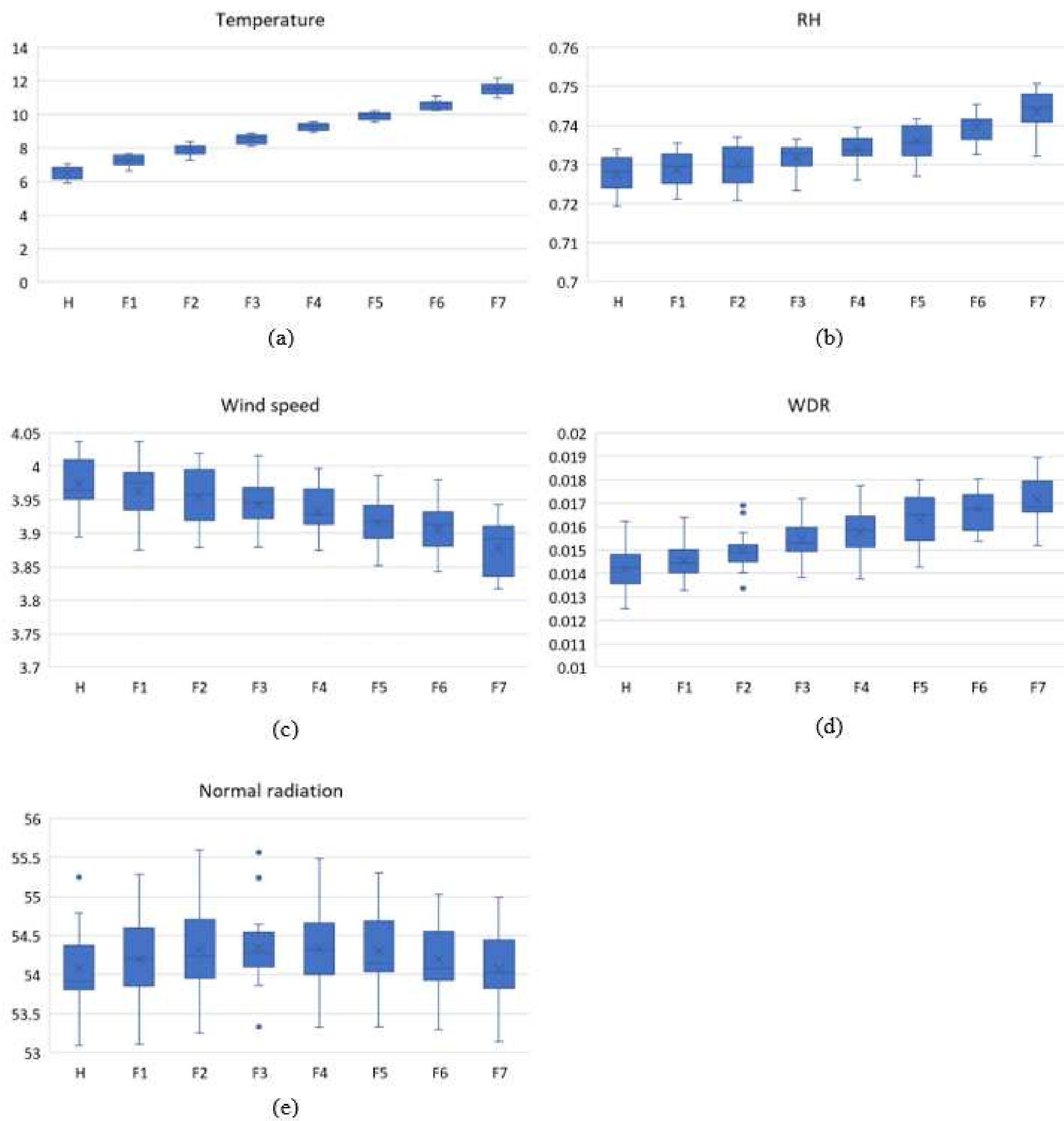

Figure 6.13: Box plot distribution across different global warming scenarios for climate parameters used for PLS model development

For temporally distributed uncertainty associated with the climate data, this work considered historical weather data and all the global warming scenarios from GW0.5 to GW3.5. Figure 6.13

shows the box plot distribution of various climate parameters across different levels of global warming. As expected, a continuous increase was noticed in the temperature across increasing global warming. The relative humidity showed a slight increase from F3 to F7 and remained practically similar from historical to F2 period. Regarding the wind speed, a continuous decrease was noticed across increasing level of global warming with F7 having a mean wind speed of approximately 3.87 m/s which is 0.1 less than the corresponding level in historical period (3.97 m/s). Amount of WDR was found to follow an increasing trend across different global warming scenarios, while normal solar radiation did not show much variation. The range of values was between 53 W/m^2 and 55.5 W/m^2 for normal solar radiation across all the levels of global warming.

For this analysis, a wood frame wall assembly with only one cladding i.e., brick veneer cladding was used to demonstrate the methodology. The temporal uncertainty in the climate data was considered in such a way that the selected data reflects the climate conditions of different global warming scenarios. Three global warming scenarios (Historical, F4, and F7), with each global warming scenario including 15 climate realizations (runs, each run includes 31-year consecutive climate data), were chosen for training a PLS model, which was successfully applied for ranking run wise moisture severity concerning mould growth risk. The 31 years simulations were performed for all 15 runs in the 3 scenarios. The analysis was performed for Ottawa using the method stated above to assess the correlation between climate parameters and the wall response. Three different types of performance-based indices i.e., maximum mould index, average mould index, and dMI (number of hours with mould index greater than 3) were used as the response variable. For the selection of a climate set to represent the temporal uncertainties, historical and 2 global warming scenarios i.e., GW2.0 and GW3.5 was considered for the training dataset. The other global warming scenarios were used to validate the model.

The run-wise simulations were performed for the historical period and all global warming scenarios i.e., a total of 120 simulations (15 runs * 8 periods) for Ottawa. The brick cladding wall facing the default orientation (the orientation which receives the highest amount of WDR) was used for the simulations.

To quantify the moisture risk, mould index was calculated at the exterior layer of OSB (0.1 mm thick) for all 31 years' simulations. The output of mould index (MoI) file is the hourly values of mould index for the 31 years and hence to quantify the moisture severity of a run, three different variants of mould index i.e., maximum MoI, average MoI, and dMI were used as response-based indices. The maximum and average values of MoI were selected for each run for comparison. The higher the value for MoI, the higher the moisture damage risk. dMI is defined as the summation of the deviation of hourly MoI from a threshold value, as shown in equation (6-7). A threshold value of 3 was used in this study.

$$dMI = \sum (MoI - 3) \tag{6-7}$$

Only the hours with MoI greater than 3, i.e., positive hourly values, were counted, and MoI less than 3, i.e., negative values were set to zero.

Figure 6.14 shows the variation of three indices among different runs and global warming scenarios. It was noted that the mould risk increases with the increase in the level of global warming. Further, all three indices resulted in a similar trend i.e., higher risk in future scenarios. The variation in the maximum mould index was found to be the least and the range contracts as the level of global warming increases. However, a significant range was observed for average mould index and dMI.

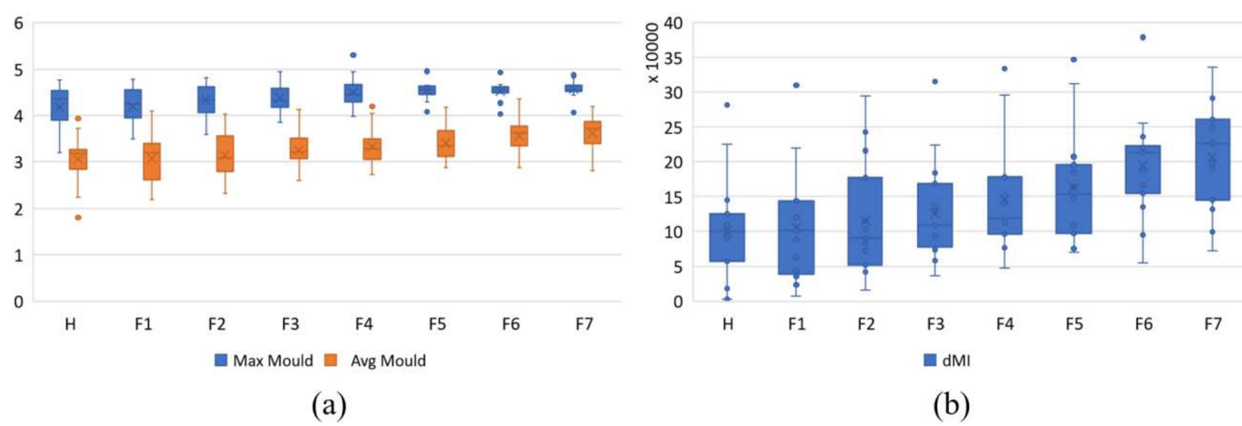

Figure 6.14: Variation of (a) maximum mould index, average mould index and, (b) dMI among 15 runs in historical and each global warming period

6.4.1. Correlation between different performance-based indices

To quantify the correlation among different response-based indices, the following approaches were used:

6.4.1.1.Direct correlation method

For direct correlation, the three response-based indices were calculated for all global warming scenarios and 15 runs. They are further correlated among each other to identify the correlation among themselves, and the results are shown in Table 6.4. It was seen that the R^2 remained high for most of the cases and the highest correlation was obtained between the average mould index and dMI. It was noted that an average R^2 of 0.57, 0.62, and 0.90 was observed with maximum. MoI vs average. MoI, maximum. MoI vs dMI, and average. MoI vs dMI respectively. It further illustrates that the maximum MoI is the least correlated response-based index and the average MoI or dMI can be used as an effective response-based index for moisture performance assessment.

Table 6.4: R^2 among different response-based indices considering 15 runs for all global warming scenarios

Global warming scenario	Max. MoI vs Avg. MoI	Max. MoI vs dMI	Avg. MoI vs dMI
Historical	0.84	0.68	0.82
GW0.5	0.80	0.79	0.89
GW1.0	0.37	0.40	0.85
GW1.5	0.23	0.45	0.91
GW2.0	0.65	0.68	0.93
GW2.5	0.44	0.64	0.88
GW3.0	0.76	0.81	0.94
GW3.5	0.49	0.54	0.94
Average	**0.57**	**0.62**	**0.90**

6.4.1.2.Ranking Analysis

To further confirm the correlation among different response-based indices, a ranking analysis was performed considering all the runs in all global warming scenarios. The total number of direct matches (among 15 runs) for each global warming scenario was calculated. Further, the number of matches when considering the top 3 and top 5 runs (order not considered) was also noted.

Table 6.5 shows the number of matching runs among three investigated variants of mould index. It was found that the number of matching runs was highest when comparing the average MoI with dMI and the least matches were found when maximum MoI was used as the response indicator. The results are in agreement with the R^2 results (Table 6.4). Considering the average MoI and dMI, it was found that on an average there are more than 5 direct matches and above 1 and 3 when considering the top 3 and top 5 runs. This further illustrates that any of the two indicators can be used for performance assessment and as a response variable for the PLS model development.

Table 6.5: Number of matching runs with different response-based indices considering 15 runs for all global warming scenarios

Global warming scenario	Max. MoI vs Avg. MoI			Max. MoI vs dMI			Avg. MoI vs dMI		
	Match (15)	**Match (3)**	**Match (5)**	**Match (15)**	**Match (3)**	**Match (5)**	**Match (15)**	**Match (3)**	**Matches (5)**
Historical	6	2	2	5	2	2	6	1	2
GW0.5	7	3	4	4	2	3	5	2	3
GW1.0	3	2	2	4	2	3	7	2	3
GW1.5	3	1	2	2	1	2	8	2	4
GW2.0	4	0	1	5	1	2	6	1	2
GW2.5	1	0	0	2	0	1	3	1	3
GW3.0	5	2	3	4	2	2	7	2	4
GW3.5	3	2	2	5	2	3	4	2	3
Average	**4**	**1.5**	**2**	**3.88**	**1.5**	**2.25**	**5.75**	**1.63**	**3**

Based on the above analyses, it is clear that any of the average mould index or dMI can be used for PLS model development. To compare the performance of the model, all three response indicators were used in this preliminary study to set a foundation for further analysis.

6.4.2. PLS model development with three response variables

For the PLS model, similar to previous models, five weather parameters were used as the input variables. These weather parameters are temperature, relative humidity, wind speed, wind-driven rain, and solar radiation normal to the wall surface. The average value of the run was used to represent each variable in the run. Among all the global warming scenarios, three scenarios were chosen for the training set i.e., the historical period, the GW2.0 or F4, and GW3.5 or F7. The rationale behind this selection is that the other scenarios lie in between these three scenarios. For the response variable, all the variants of mould index were used and three separate PLS models were generated.

The PLS model was developed with three response indicators and the corresponding regression equations for each indicator are shown below (equations (6-8) through (6-10)):

Maximum MoI:

$$Max.MoI = -13.88511 - 0.0108 * T_{avg} + 11.0378 * RH_{avg} + 2.7257 * Speed_{avg} + 180.5372 * WDR_{avg} - 0.0601 * Rad_{avg} \quad (6\text{-}8)$$

Average MoI:

$$Avg.MoI = -29.5898 - 0.0463 * T_{avg} + 28.3962 * RH_{avg} + 4.1324 * Speed_{avg} + 247.8638 * WDR_{avg} - 0.1413 * Rad_{avg} \quad (6\text{-}9)$$

dMI:

$$dMI = -3727741 - 7509.226 * T_{avg} + 3817636 * RH_{avg} + 570327.6 * Speed_{avg} + 46203700 * WDR_{avg} - 33685.62 * Rad_{avg} \quad (6\text{-}10)$$

Here, T_{avg} is the run average temperature in °C, RH_{avg} is the run average relative humidity in (-), $Speed_{avg}$ is the run average wind speed in m/s, WDR_{avg} is the run average WDR in mm and Rad_{avg} is the run average normal solar radiation in W/m^2.

To test the reliability of the PLS models the model was used to predict the response on the test set which is independent of the data used in training the model. The test set comprises 15 runs from each of the global warming scenarios which were excluded in the training set i.e., GW0.5, GW1.0, GW1.5, GW2.5, and GW3.0. A total of 75 test sets were identified (5 GW scenarios * 15 runs in each). The model was trained using 3 GW and 15 runs in each i.e., using a training set with 45 samples. Two types of analysis were performed to analyze the results: 1) Direct correlation analysis and 2) Ranking analysis. Details of each approach along with the analysis of the result are discussed in the following subsections:

6.4.2.1.Direct correlation analysis

In this analysis, the predicted response variable is compared with the actual response based on simulation results. A scatter plot is generated for predicted and actual response and different statistical parameters were calculated to quantify the model's prediction performance.

As shown in Figure 6.15, there is a significant variation in the prediction results when compared to actual simulation results for the there response variables. The predicted maximum mould index had the lowest R^2 with simulation results. The correlation was higher for dMI and the highest correlation of 0.7 was obtained when using the average mould index as the performance indicator. The results are in line with the analysis made in section 6.4.1.1 where the maximum mould index seemed to be the least correlated indicator with the other two indicators. The average mould index has the best correlation among the three indicators, and it was further noted that among the 75 test points, for the 40 points, the difference in the predicted and actual mould index was less than 0.1 meaning that these points lie very close to the orange one-to-one line and the model was able to predict the exact value. The other points also have a deviation between 0.2 and 0.4 with the highest deviation being 0.51.

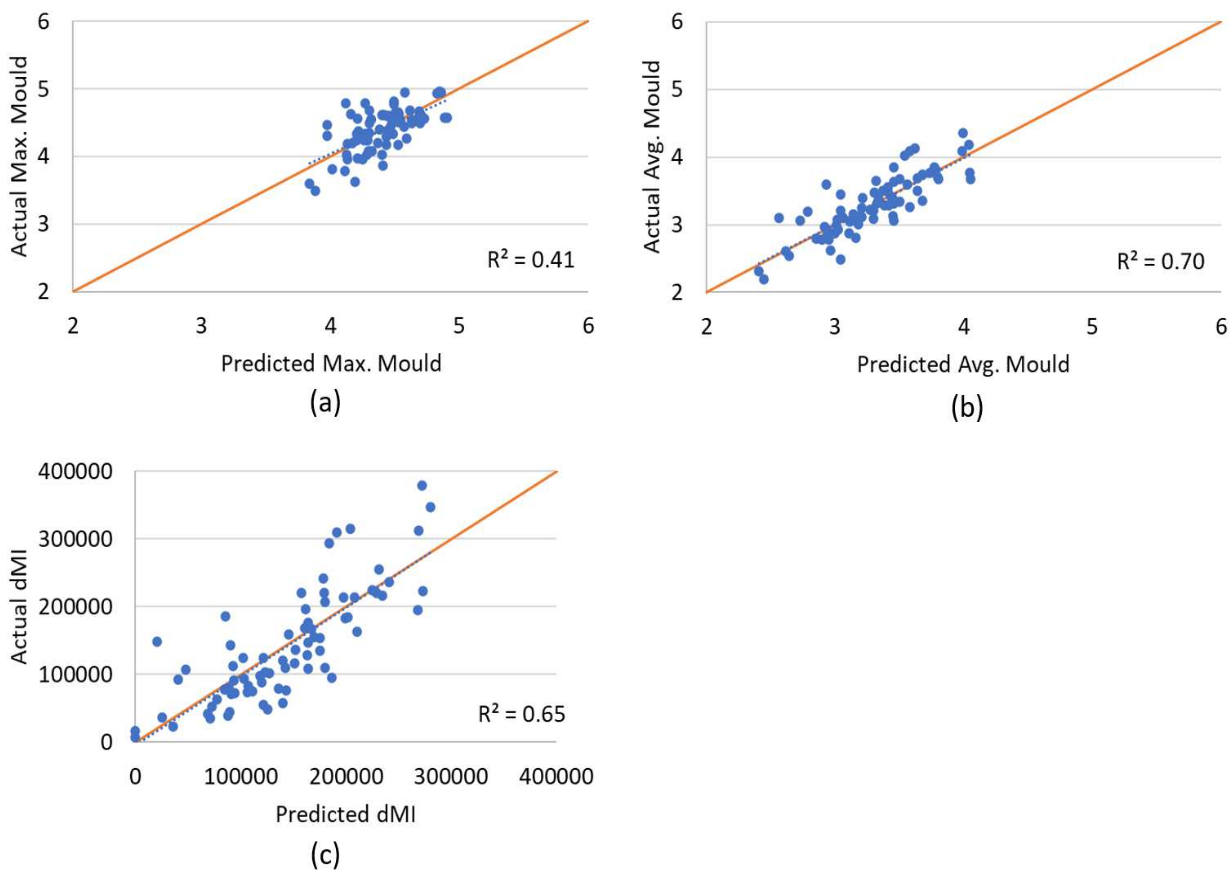

Figure 6.15: Predicted vs. actual value of three performance indicators considering all the runs among different global warming scenarios

To further evaluate the performance of the three models, various statistical parameters were calculated, and the results are shown in Table 6.6. As depicted in Table 6.6, a similar error i.e., RMSE and MAE were noted for maximum and average MoI when all the runs are considered for calculations. However, when considering the top 3 or top 5 runs based on simulation results, it was found that a slightly lower error was noted when considering the maximum MoI as the response variable. Moreover, as the aim of the prediction model is to predict the performance and rank the runs based on their moisture severity level, an additional analysis considering the ranking was performed and is discussed in the following section.

Table 6.6: Comparison of various statistical parameters for three PLS models with different performance indicators as response variable

Indicator	RMSE (all)	RMSE (3)	RMSE (5)	MAE (all)	MAE (3)	MAE (5)
Max. MoI	0.24	0.31	0.28	0.19	0.29	0.25
Avg. MoI	0.23	0.36	0.36	0.17	0.33	0.32
dMI	48812.03	97269.90	94215.74	37808.29	95160.66	89487.50

6.4.2.2.Ranking analysis

This analysis focuses on the ranking of runs based on the predicted and actual results instead of the actual magnitude of different response variables. The purpose is to see how well the model can rank the runs in terms of their moisture severity. The model would be considered as effective if it lead to a similar ranking of runs as obtained from simulations. Different methods of evaluating the ranking of years were investigated and the results are shown in Table 6.7.

The number of matching runs between the prediction and actual results was counted and used as a criterion to evaluate the reliability of the models. The higher the number of matches, the better the model is at ranking the runs. Further, the ability of models to identify the top 3 or top 5 runs was also investigated. A match is considered as long as the run is ranked within the top 3 or top 5 of simulation results without considering the actual order of ranking. As shown in Table 6.7, considering the direct matching runs by considering all the 75 test set points, it was found that the highest number of matches (8) were obtained with average MoI as the response variable. Moreover, considering the top 3 and top 5 runs, average MoI and dMI had similar results and they can rank well the top 3 and top 5 runs in a better way as compared to maximum MoI. Similarly, a higher Kendall W and spearman rho was noted for average MoI and Kendall W.

Table 6.7: Number of matching runs, Kendall W, and spearman rho for three models (Matches (n): number of matches considering "n" runs)

Indicator	Match (all)	Match (3)	Match (5)	Kendall W	Spearman rho
Max. MoI	2	0	2	0.59	0.79
Avg. MoI	8	1	3	0.80	0.90
dMI	4	2	3	0.82	0.91

From these analyses, it is evident that the model trained on only 3 GWs can be used to predict the results of other GW scenarios. Based on the results, it is recommended to use average MoI as a response variable when analyzing the simulation results and generating the PLS model. Using average MoI as a response variable resulted in a higher R^2 as well as it was able to rank the runs in a manner similar to the actual simulation results.

The study can be very helpful as it can be used as a screening measure to avoid performing many simulations. The run-wise simulations (31 consecutive years) can take quite a lot of time to complete e.g., a set of 15 such simulations take up to 36 hours to complete. Using the PLS model, an estimated mould index can be computed and if the need persists, simulations can be performed for only some specific cases.

6.5. Model based on yearly simulations

PLS model based on run wise simulations was originally tested and found to be working well in terms if their prediction ability. An additional study was conducted to determine if a model based on yearly simulations can be used to make run wise prediction. For Ottawa, historical, F4 and F7 data was used, and the median run (run 10) was chosen. For the years (93 years) among the 3 GW scenario for run 10, the years which has default orientation in the range of 247.5deg to 292.5deg was selected. The reason behind this is to be consistent with run wise simulations where the default orientation was 292.5deg. Eliminating the years with wall orientations different from range proposed, a total of 55 years were identified and later were used for the PLS model development. The developed model was later tested using all the runs considering all the global warming scenarios i.e., a total of 120 runs. The PLS regression equations based on run wise and yearly simulations are shown in equation (6-11) and (6-12) respectively.

Based on run wise simulations:

$$Avg.MoI = -29.5898 - 0.0463 * T_{avg} + 28.3962 * RH_{avg} + 4.1324 * Speed_{avg} + 247.8638 * WDR_{avg} - 0.1413 * Solar_{avg} \tag{6-11}$$

Based on yearly simulations:

$$Avg.MoI = -7.55895 + 0.012 * T_{avg} + 8.9676 * RH_{avg} + 0.3283 * Speed_{avg} + 49.5499 * WDR_{avg} - 0.0002 * Solar_{avg} \tag{6-12}$$

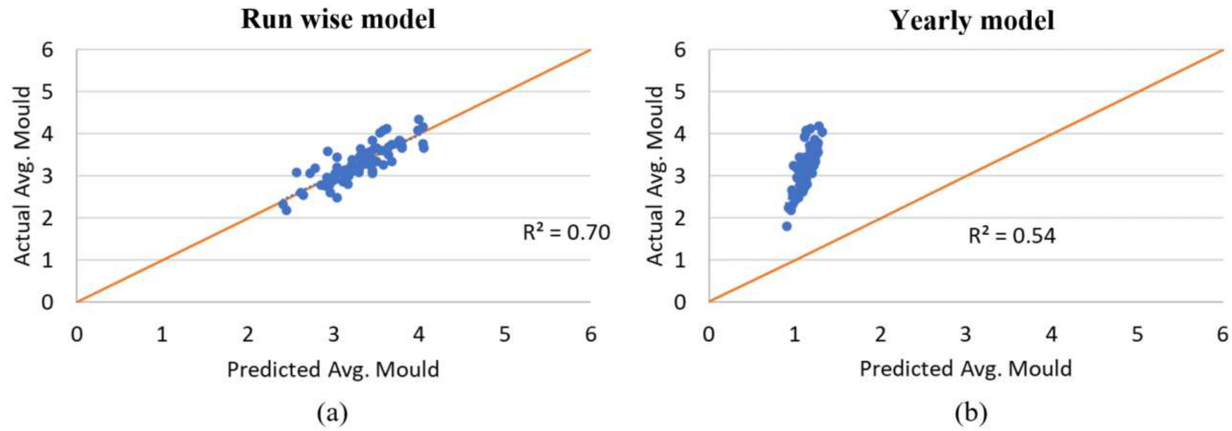

Figure 6.16: Comparison of actual and predicted average mould index for the 15 runs in all GW scenarios using (a) run wise PLS model (b) yearly PLS model

As shown in Figure 6.16, an R^2 of 0.70 and 0.54 was noted for run wise and yearly PLS model respectively. Furthermore, unlike the run wise model where the points like close to one-to-one line meaning the results are similar, the yearly model shows the clustering of data above the one-to-one line. This illustrates that the predicted results underestimate the actual results and are confined in a small range. Table 6.8 shows the RMSE and MAE when comparing the actual and predicted average mould index using the two models. A significant error was noted with yearly model which is in line with the underprediction linked to the yearly model (Figure 6.16 (b)).

Table 6.8: RMSE and MAE using the two PLS models considering all the runs in all global warming scenarios

PLS Model	RMSE	MAE
Run wise	0.238	0.179
Yearly	2.151	2.118

A further analysis was made wherein the two models are used to rank the runs in each global warming scenarios based on their moisture severity. The aim was to quantify the ability of models to identify the worst runs in each global warming scenario. A model might not to be able to predict the absolute value of the mould index but if it can arrange the runs based on their moisture severity, it can be used to select the representative runs.

Table 6.9: Ranking analysis using the run wise and yearly PLS model considering all runs in each global warming scenario

GW	PLS model	Direct matches (15)	Matches top 3	Matches top 5	Kendall W (15)	Spearman rho (15)
Historical	Run	7	3	3	0.86	0.72
	Year	4	3	3	0.87	0.74
GW0.5	Run	2	1	4	0.93	0.85
	Year	2	2	3	0.85	0.69
GW1.0	Run	5	3	5	0.93	0.85
	Year	4	2	4	0.86	0.73
GW1.5	Run	3	3	4	0.97	0.94
	Year	3	2	3	0.93	0.86
GW2.0	Run	3	2	3	0.90	0.80
	Year	2	3	4	0.91	0.83
GW2.5	Run	3	3	5	0.96	0.89
	Year	1	3	5	0.94	0.85
GW3.0	Run	0	1	4	0.89	0.78
	Year	1	2	4	0.88	0.83
GW3.5	Run	3	3	4	0.94	0.89
	Year	3	2	4	0.85	0.71

Table 6.9 shows the number of matches along with Kendall W and spearman rho for 15 runs in each global warming scenario using the two PLS models. For all the measure implemented, in general, it was found that the irrespective of the choice of PLS model, the ranking results were found to be similar. For instance, when considering the number of matches for top 5 years, it was

found that the yearly model lead to same or even higher number of matching runs except for GW0.5, GW1.0 and GW1.5 scenario where the difference is only 1. Moreover, Kendall W and spearman rho were also very close to each other for both the models. These results showed that along with the run wise model, the model trained on year can also be used to predict the run wise ranking for each global warming level.

Based on the analyses shown above, it can be said that the model trained on yearly simulations may not be appropriately used to predict the severity level of runs as the results are found to be underestimated. However, if the purpose is to arrange the runs based on their moisture severity, the yearly model can be used. It should be noted here that to develop a run wise model, simulations with 31 consecutive years are required and a set of 15 simulations requires on an average of 36 hours. On the other hand, 15 yearly simulations takes around 20 minutes to be completed. Hence, a choice is required to be made before performing the analysis. If the goal is to identify the level of severity of each run, the run wise model should be opted as it will lead to more reliable prediction and can also assist with the ranking. However, if the aim is to sort the runs and identify the top runs, a yearly PLS model can be used.

Chapter 7 Conclusions and future work

7.1. Contribution

This research investigates the level of moisture damage risk in the future in comparison to the historical or current risk. Considering the time constraints associated with the traditional hygrothermal simulations, this research presented an approach to predict the hygrothermal performance of the wall assembly using the Partial least squares regression (PLSR). This research developed a climate-based index (CBI) and a framework for the reliable assessment of moisture risks in wood-frame walls under historical and projected future climates using a metamodel that is developed by incorporating the data representing cities belonging to different climate zones across Canada, weather years, and climate change scenarios. These models and methods were validated and demonstrated on different claddings, different cities, different climate runs and global warming scenarios. The potential of the PLSR to predict the response of the wall assembly to the future climate was demonstrated. The contribution include:

- Evaluated the reliability of existing climate-based indices in assessing moisture risk.
- Developed a PLS meta-model which can predict mould growth risks directly; rank the moisture severity therefore select moisture reference year; categorize mould growth risk. In contrast to the traditional hygrothermal simulation, where a single one-year 1D simulation could take anywhere between 10-12 minutes, the model can process the results within seconds. This can reduce the computation time significantly.
- Developed model assessment methods: direct correlation, ranking correlation and risk category analysis.
- Identified wall assembly and moisture load that used can be a conservative configuration for moisture risk analysis.
- The methodology developed can be used for different cities, climates, global warming scenarios, etc. The model can be used by the practitioner as a first screening to eliminate the cases which does not impart much risk to the building performance and can only perform simulations for a limited case.

7.2. Conclusion

The climate-based indices can be used as indicators to rank the severity of moisture loads of different weather years and therefore used for the selection of MRY, if calibrated properly. A correlation analysis between the performance, i.e. hygrothermal response, and the climate-based indices, i.e. climatic loads, provides a base to understand the reliability of these indices in assessing the moisture risks of walls. This thesis investigated the existing climate-based indices and developed new climate-based indices to assess the moisture performance of the wall assemblies. A methodology was developed to assess the reliability of existing indices and to generate new climate-based indices. The main conclusion of this work is categorized into two parts: 1) conclusions regarding existing climate-based indices; 2) conclusions regarding new climate-based indices.

7.2.1. Conclusions regarding existing climate-based indices

Correlation between response-based and climate-based indices

- The correlation between existing climate-based indices and hygrothermal response was generally weak, with R^2 in the range of 0-0.79. Among all climate-based indices, CI and MI had a better correlation with response-based indices.
- The correlation remained poor for Vancouver due to the low WDR in north orientation, with R^2 in the range of 0-0.2 for a north-facing wall. Significant improvement was achieved for the prevailing WDR direction with R^2 ranging from 0.2-0.69 (excluding I_{sev}).
- The correlation varied for different cities, wall types and climate periods. For cities like Ottawa and Calgary, the change in climate-based indices under future climate was consistent with change in the maximum MoI.

Ranking Analysis

- Among the three methods used, the choice of response-based index did not change the ranking greatly and usually the maximum MoI led to the slightly better results (higher matches, lower RMSE and higher NV) for most of the cases.
- When using climate-based indices to rank the years, for most of the cases, the accuracy in ranking all years was low with some improvement in ranking the first 3-year.
- The number of matching years remained small for all the existing climate-based indices

with the highest being 7 out of 31 using MI.

- Using the ranking correlation method, CI in general led to a higher number of matching years, a lower RMSE for both 3-year and all years. The RMSE for 3-year ranking was lower than the RMSE for all-year ranking for all climate-based indices except for I_{sev} with walls facing the default orientation.
- Using the goodness-of-fit approach, MI usually led to the highest normalized value (NV) followed by CI for most of the cases. The moisture severity of the first three worst years selected by climate-based index was similar to that of the first three worst years selected based on simulations for cases where the wall orientation is close to the north, except for Vancouver, although the ranking accuracy (indicated by number of matching years) was generally not very high.
- I_{sev} is proposed in ASHRAE 160 for evaluating the severity of the years. However, for different wall configurations under different moisture loads, it failed to predict the correct ranking. Also, for the three investigated Canadian cities, it didn't perform well even for the same wall configuration and moisture load used in its development.

The analysis showed that the existing climate-based indices do not show reliability and consistency in ranking the severity of weather years when compared to simulation results. Climate-based indices taking into account more climatic parameters perform better and their performance is influenced by the type of wall constructions, moisture loads and climatic characteristics. Therefore, to assess the moisture risks of building envelope assemblies under future climates, a more reliable climate-based index is needed to better correlate response-based indices with climate-based indices for typical Canadian climates.

7.2.2. Conclusions regarding new climate-based indices

A regression model based on PLS regression was developed in this study to provide an estimated wall performance without performing the simulations and thereby reduce the computation time. The model uses a training set comprising the response variable and the most influential input parameters. Based on the data input to the model, a regression equation was developed, and this was further used for any new dataset that one can encounter in the future.

The main findings are as follows:

- The prediction results on the investigated test sets showed a good accuracy as depicted by various statistical parameters i.e., R^2 above 65% and an average RMSE below 0.5 for Ottawa, and R^2 above 85% and RMSE below 0.35 for Vancouver and St John's.

- Ranking analysis showed that the model can accurately rank the years especially if the primary concern is to identify the top 3 or top 5 worst years for the purpose of Moisture Reference Year selection.
- The model was able to categorize the years in the same mould risk category as depicted by simulation results.
- The PLS model developed with a brick cladding wall can be effectively used for a stucco cladding wall by modifying the regression equation with a suitable regression factor. The modified model works as effectively as the model trained on stucco cladding.
- Considering the climate uncertainties, it was noted that the risk varies across different climate runs but in general, a similar trend was noticed. For Vancouver and St. John's the risk is considerably higher in southerly directions while for Ottawa, the risk is uniform across various wall orientations.
- For the brick cladding wall, the mould index remained above the safe limit for southerly orientations for Vancouver and St. John's and it remained close to the safe limit for Ottawa for all orientations. For the stucco cladding wall, the mould index always remained below the threshold limit and the wall remained safe for all climate runs and periods.
- In terms of climate change, the risk increase in the future period for all the cities, claddings, and climate runs.

The results showed that the use of the PLS modeling technique to predict the hygrothermal response is an effective way to improve computational efficiency. The model if trained well can help in predicting the wall response and will reduce the simulation efforts. The advantage of regression model is that it is easy to use for practitioners, who may not have the knowledge and experience of DELPHIN or any other hygrothermal simulation programs. It can also be used by the practitioners for screening purposes to reduce the simulation efforts. For example, the predicted mould can be computed using the regression equation and later simulations can be performed only for the cases where the model predicts the mould index above a certain threshold defined by the user. The model can help in covering all the factors i.e., uncertainties in climate data, climate periods, and types of walls without or with low computational efforts.

7.2.3. Conclusion regarding the model validation on different claddings, considering climate uncertainties and different level of global warming

Model performance

- The PLS model developed with a brick cladding wall can be effectively used for a stucco cladding wall by modifying the regression equation with a suitable factor. The modified model works as effectively as the model trained on stucco cladding. Therefore, the PLS model developed for brick veneer wall can be used for the assessment of moisture severity, i.e. ranking of a specific location to represent other types of cladding.
- The PLS model developed for the median run can be used to cover all 15 runs and an R^2 as high as 0.91 was obtained for Vancouver.
- The model developed can be used to predict the mould growth index directly and also to assess the moisture severity of years for the ranking and MRY selection. This can further help practitioners screen the years and perform simulations for the years with risks.

Effect of climate change on mould growth risks

- The model can be effectively used to assess the impact of climate change on mould growth risks without running simulations for all scenarios.
- A mould growth rosette is used to identify the worst orientation and it was found to be consistent with the WDR rosette.
- The mould growth risk increase in the future period for all three cities, two claddings, and 15 climate runs.

Effect of different global warming scenarios

During its service life, a building is subjected to different climate and moisture loads and hence it is imperative to estimate the risk which the wall is expose to during this period. For a reliable assessment of performance, usually 30 consecutive years simulations are performed. To investigate the reliability of the approach developed for individual year PLS model, a similar model was generated for consecutive years simulations or run-wise simulations. The run average of climate parameters were taken as input to the model and different variants of mould index were taken as response variables. It was found that the among the three models, the model based on average mould index as response could predict the wall performance with a certain level of accuracy and can also help in ranking the run based on their moisture severity. Having the runs sorted based on their severity can assists in proper selection of weather data and to estimate the risk assuming a conservative approach.

7.3. Future work

The future work can include the development of a method to generate climate-based index specific to a Canadian climate, wall constructions under different loading conditions, i.e., rain penetration, air leakage, etc. For each cluster, the climate-based index can be calculated and correlated with the response-based index to assess the moisture risks for future climate. Further, for considering the different global warming scenarios i.e., run-wise simulations, the present analysis was limited to Ottawa only one wall cladding (brick-veneer). The analysis can be further expanded to other cities, wall claddings. Moreover, in the current work, the weather data used for different cities are based on airport location data in the particular city. However, to cover the spatial uncertainties arising due to the local topography e.g., a city center, mountains, station near water bodies surrounding the major city etc. could also be included in the model development.

List of publications

Journal papers

1. C. Aggarwal, L. Wang, M. Defo, T. Moore, H. Ge, M. A. Lacasse, *Long-term hygrothermal performance assessment of wood-frame walls considering climate uncertainties using Partial Least Squares (PLS) regression*, under preparation.
2. C. Aggarwal, H. Ge, M. Defo, *Hygrothermal performance assessment of wood-frame walls under future climates using Partial Least Squares (PLS) regression: Different claddings and climate uncertainties*, Submitted to Building and Environment, under review.
3. C. Aggarwal, H. Ge, M. Defo, M. A. Lacasse, *Hygrothermal assessment of wood frame walls under historical and future periods using Partial Least Squares regression*, Building and Environment, Volume 223. https://doi.org/10.1016/j.buildenv.2022.109501.
4. C. Aggarwal, H. Ge, M. Defo, M. A. Lacasse, 2021. *Reliability of Moisture Reference Year (MRY) selection methods for hygrothermal performance analysis of wood-frame walls under historical and future climates*. Building and Environment, 207 (Part A). https://doi.org/10.1016/j.buildenv.2021.108513.

Conference papers

1. C. Aggarwal, H. Ge, M. Defo, M. A. Lacasse, C*omparison of Different Methods to Identify the Critical Orientation of Wood-Frame Walls in Assessing Moisture Risks*, COBEE 2022, Montreal, Canada. https://www.researchgate.net/publication/362830669_Comparison_of_Different_Methods_to_Identify_the_Critical_Orientation_of_Wood-Frame_Walls_in_Assessing_Moisture_Risks
2. C. Aggarwal, M. Defo, H. Ge, M. Lacasse, *Identifying the critical orientation of wood-frame walls in assessing moisture risks using hygrothermal simulation,* IBPC 2021, Copenhagen, Denmark. https://iopscience.iop.org/article/10.1088/1742-6596/2069/1/012011
3. C. Aggarwal, L. Wang, M. Defo, H. Ge, M. Junginger, M. A. Lacasse, *Sensitivity analysis of hygrothermal performance of wood framed wall assembly under different climatic conditions: the impact of cladding properties*, IBPC 2021, Copenhagen, Denmark. https://iopscience.iop.org/article/10.1088/1742-6596/2069/1/012010

4. C. Aggarwal, M. Defo, T. Moore, M. A. Lacasse, S. Sahyoun, H. Ge, *Validation of Three Methods of Selecting Moisture Reference Years for Hygrothermal Simulations,* DBMC 2020, Barcelona, Spain. https://www.scipedia.com/public/Aggarwal_et_al_2020a.
5. S. Sahyoun, H. Ge, C. Aggarwal, M. Defo and T. Moore, *Effect of Selected Moisture Reference Year on the Durability Assessment of Wall Assemblies under Future Climates,* DBMC 2020, Barcelona, Spain. https://www.scipedia.com/public/Sahyoun_et_al_2020b

Reports

1. C. Aggarwal, M. Defo, *Effects of selected wall orientation on the moisture performance of building envelope,* technical report, NRC, Ottawa, Canada. https://nrc-publications.canada.ca/eng/view/object/?id=5ff6a6ce-ad66-425e-9ff9-9df1557a21dc

References

Abdul Hamid, A., & Wallentén, P. (2017). Hygrothermal assessment of internally added thermal insulation on external brick walls in Swedish multifamily buildings. Building and Environment, 123, 351–362. https://doi.org/10.1016/j.buildenv.2017.05.019.

Adan, O. C. G. (1994). On the fungal defacement of interior finishes.

Aggarwal, C., Ge, H., Defo, M., & Lacasse, M. A. (2022). Reliability of Moisture Reference Year (MRY) selection methods for hygrothermal performance analysis of wood-frame walls under historical and future climates. Building and Environment, 207(PA), 108513. https://doi.org/10.1016/j.buildenv.2021.108513.

Aggarwal, C., Defo, M., Moore, T., Lacasse, M. A., & Sahyoun, S. (2020). Validation of Three Methods of Selecting Moisture Reference Years for Hygrothermal Simulations 1 Introduction. 1–8. https://doi.org/10.23967/dbmc.2020.146.

ASHRAE. (2009). ASHRAE handbook: Fundamentals. Atlanta.

ASHRAE. (2010). Environmental weather loads for hygro-thermal analysis and design of buildings. RP-1325, American Society of Heating, Refrigerating and Air- Conditioning Engineers, Inc. Atlanta.

ASHRAE. (2016). ASHRAE 160 (Criteria for Moisture-Control Design Analysis in Buildings). ASHRAE Standards Committe, Atlanta, GA.

ASHRAE Fundamentals Handbook, Edition, S I. 2017.

Bansal, N., Defo, M., & Lacasse, M. A. (2021). Application of support vector regression to the prediction of the long-term impacts of climate change on the moisture performance of wood frame and massive timber walls. Buildings, 11(5). https://doi.org/10.3390/buildings11050188.

Beaulieu, P., Cornick, S. M., Dalgliesh, W. A., Kumaran, M. K., & Lacasse, M. A. (2001). MEWS methodology for developing moisture management strategies: Application to stucco-clad wood frame walls in North America. (No. NRCC-45213). Ottawa, Canada: National Research Council Canada.

Bizikova, L., Neale, T., & Burton, I. (2008). Canadian Communities ' Guidebook for adaptation to climate change.

Building, N., & Symp, P. (2002). A Methodology to Develop Moisture Management Strategies for Wood- Frame Walls in North America : Application to Stucco-Clad Walls. Physics, 651–658.

Burch, D. M., & Chi, J. (1997). Moisture-A PC program for predicting heat and moisture transfer in building. Gaithersburg, MD: National Institute of Standards and Technology.

C. Aggarwal, H. Ge, M. Defo, and M. A. Lacasse, "Hygrothermal performance assessment of wood frame walls under historical and future climates using partial least squares regression," Build. Environ., vol. 223, no. May, p. 109501, 2022, doi: 10.1016/j.buildenv.2022.109501.

C. Aggarwal, M. Defo, H. Ge, M. Lacasse, Identifying the critical orientation of wood-frame walls in assessing moisture risks using hygrothermal simulation, IBPC 2021, Concordia University, Montreal, QC.

C. Du, R. Linker, and A. Shaviv, "Identification of agricultural Mediterranean soils using mid-infrared photoacoustic spectroscopy," Geoderma, vol. 143, no. 1–2, pp. 85–90, 2008, doi: 10.1016/j.geoderma.2007.10.012.

Cabrera, P., & Samuelson, H. W. (2019). Simulating Mold Risks under Future Climate Conditions. Proceedings of Building Simulation 2019, September.

Canada Green Building Council. (2017). A Roadmap for Retrofits in Canada. www.cagbc.org.

Chen, H., & Garcia, J. (2004). Roots of Mold Problems and Humidity Control Measures in Institutional Buildings with Pre-Existing Mold Condition.

Clarke, J. A., Johnstone, C. M., Kelly, N. J., McLean, R. C., Anderson, J. A., Rowan, N. J., & Smith, J. E. (1999). A technique for the prediction of the conditions leading to mould growth in buildings. Building and Environment, 34(4), 515–521. https://doi.org/10.1016/S0360-1323(98)00023-7.

Cornick, S., Djebbar, R., & Alan Dalgliesh, W. (2003). Selecting moisture reference years using a Moisture Index approach. Building and Environment, 38(12), 1367–1379. https://doi.org/10.1016/S0360-1323(03)00139-2.

C. Rumpel, L. J. Janik, J. O. Skjemstad, and I. Kögel-Knabner, “Quantification of carbon derived from lignite in soils using mid-infrared spectroscopy and partial least squares,” Org. Geochem., vol. 32, no. 6, pp. 831–839, 2001, doi: 10.1016/S0146-6380(01)00029-8.

De Mets, T., Tilmans, A., & Loncour, X. (2017). Hygrothermal assessment of internal insulation systems of brick walls through numerical simulation and full-scale laboratory testing. Energy Procedia, 132, 753–758. https://doi.org/10.1016/j.egypro.2017.10.022.

Delgado, J.M., Barreira, E., Ramos, N.M. and De Freitas, V.P. (2012). Hygrothermal numerical simulation tools applied to building physics. Springer Science & Business Media.

Dong, B.; Li, Z.; Rahman, S.M.; Vega, R. A hybrid model approach for forecasting future residential electricity consumption. Energy Build. 2016, 117, 341–351.Environment and natural resources, C. (2020). Climate-Resilient Buildings and Core Public Infrastructure: an assessment of the impact of climate change on climatic design data in Canada.

Environment and Climate Change Canada. (2016). Pan-Canadian framework on clean growth and climate change: Canada’s plan to address climate change and grow the economy.

Environmental, Canadian, and Sustainability Indicators. 2022. “Global Greenhouse Gas Emissions Data App.” Pollution Engineering 46(4).

Finch, G., & Straube, J. (2007). Ventilated wall claddings: Review, field performance, and hygrothermal modeling. Thermal Performance of the Exterior Envelopes of Whole Buildings, December 2007.

F. L. Melquiades, P. P. González-Borrero, F. R. Dos Santos, W. E. D. De Deus, M. Kalwa, and S. P. Quináia, “Method for sediment texture characterization using spectroscopy techniques and multivariate analysis,” Rev. Virtual Quim., vol. 6, no. 6, pp. 1687–1701, 2014, doi: 10.5935/1984-6835.20140109.

F. Morona, F. R. dos Santos, A. M. Brinatti, and F. L. Melquiades, “Quick analysis of organic matter in soil by energy-dispersive X-ray fluorescence and multivariate analysis,” Appl. Radiat. Isot., vol. 130, no. May, pp. 13–20, 2017, doi: 10.1016/j.apradiso.2017.09.008.

Freire, R.; Santos, G.; Coelho, L. Hygrothermal dynamic and mould growth risk predictions for concrete tiles by using least squares support vector machine. Energies 2017, 10, 1093.

Gaterell, M. R., & McEvoy, M. E. (2005). The impact of climate change uncertainties on the performance of energy efficiency measures applied to dwellings. Energy and Buildings, 37(9), 982–995. https://doi.org/10.1016/j.enbuild.2004.12.015.

Gaur, A., Lacasse, M., & Armstrong, M. (2019). Climate data to undertake hygrothermal and whole building simulations under projected climate change influences for 11 Canadian cities. Data, 4(2). https://doi.org/10.3390/data4020072.

Ge, H., Y. Ye & P. Fazio (2009). Field investigation of the impact of cavity ventilation on the wetting and drying of brick veneer wall systems in the coastal climate of British Columbia. Proceedings of the 12th National Building Science and Technology Conference. May 6-8, 2009. Montreal, Canada. pp. 26-36.

Geving, S. (1997). Moisture Design of Building Constructions: Hygrothermal Analysis Using Simulation Models-Part I and II, PhD thesis, Norwegian University of Science and Technology.

Glass, S. V, Tenwolde, A., & Zelinka, S. L. (2013). Hygrothermal Simulation : A Tool for Building Envelope Design Analysis. Wood Design Focus, 23(3), 18–25.

Glass, S. V. (2013). Hygrothermal analysis of wood-frame wall assemblies in a mixed-humid climate. Research Paper FPL-RP-675. United States Department of Agriculture, Forest Service, Forest Products Laboratory, 27 pp. http://www.fpl.fs.fed.us/documnts/fplrp/fpl_rp675.pdf.

Gobakken, L.R., Høibø, O.A. and Solheim, H. (2010). Mould growth on paints with different surface structures when applied on wooden claddings exposed outdoors. International Biodeterioration & Biodegradation, 64(5), pp.339-345.

Government of Canada, 2020, https://www.canada.ca/en/services/environment/weather/climatechange/climate-plan/net-zero-emissions-2050.html.

Gradeci, K., Labonnote, N., Köhler, J., & Time, B. (2017). Mould Models Applicable to Wood-Based Materials-A Generic Framework. Energy Procedia, 132, 177–182. https://doi.org/10.1016/j.egypro.2017.09.751.

H. Martens, T. Næs, Multivariate Calibration, Wiley, Chichester, 1992.

H. Viitanen, T. Ojanen, and R. Peuhkuri, “Mould growth modelling to evaluate durability of materials,” Proc. 12DBMC - Int. Conf. Durab. Build. Mater. Components, pp. 1–8, 2011, [Online]. Available: http://www.irbnet.de/daten/iconda/CIB22377.pdf.

H. Wold, Soft modeling: the basic design and some extensions, Systems under indirect observation, North-Holland, Amsterdam, 1982, pp. 1–53.

Hagentoft CE, Harderup E. Climatic infuences on the building envelope using the π factor. IEA-Annex 24 Hamtie Task 2, Environmental Conditions. Closing Seminar, Finland, 1996.

Hansen, T. K., Bjarløv, S. P., Peuhkuri, R. H., & Harrestrup, M. (2018). Long term in situ measurements of hygrothermal conditions at critical points in four cases of internally insulated historic solid masonry walls. Energy and Buildings, 172, 235–248. https://doi.org/10.1016/j.enbuild.2018.05.001.

Hao, L., Herrera-Avellanosa, D., Del Pero, C., & Troi, A. (2020). What are the implications of climate change for retrofitted historic buildings? A literature review. Sustainability (Switzerland), 12(18), 1–17. https://doi.org/10.3390/su12187557.

Health Canada. (2011). Dampness, Mould and Indoor Air. Government of Canada.

Hens, H. (1996). Final report of IEA Annex 24- Task 1: Modelling. Leuven, Belgium: KU Leuven University.

Hukka, A., & Viitanen, H. A. (1999). A mathematical model of mould growth on wooden material. Wood Science and Technology, 33(6), 475–485. https://doi.org/10.1007/s002260050131.

IEA. (1991). IEA-Annex 14. Condensation and energy: Source Book. http://onlinelibrary.wiley.com/doi/10.1002/cbdv.200490137/abstract.

Incropera, DeWitt, Bergman, L. (2015). Fundamentals of Heat and Mass Transfer. In Fluid Mechanics and its Applications (Sixth, Vol. 112). https://doi.org/10.1007/978-3-319-15793-1_19.

Infrastructure Canada. (2006). Adapting infrastructure to climate change in Canada’s cities and communities. Ottawa: Government of Canada.

International Organization for Standardization. (2009). ISO 15927-3 Hygrothermal performance of buildings - Calculation and presentation of climatic data. Switzerland: International Organization for Standardization.

IPCC. (2014). Climate Change 2014: Synthesis Report. Contribution of Working Groups I, II and III to the Fifth Assessment Report of the Intergovernmental Panel on Climate Change [Core Writing Team, R.K. Pachauri and L.A. Meyer (eds.)]. IPCC, Geneva, Switzerland, 151 pp.

IPCC, 2021: Summary for Policymakers. In: Climate Change 2021: The Physical Science Basis. Contribution of Working Group I to the Sixth Assessment Report of the Intergovernmental Panel on Climate Change [Masson-Delmotte, V., P. Zhai, A. Pirani, S. L. Connors, C. Péan, S. Berger, N. Caud, Y. Chen, L. Goldfarb, M. I. Gomis, M. Huang, K. Leitzell, E. Lonnoy, J.B.R. Matthews, T. K. Maycock, T. Waterfield, O. Yelekçi, R. Yu and B. Zhou (eds.)]. Cambridge University Press.

Janssen, H., Blocken, B., & Carmeliet, J. (2007). Conservative modelling of moisture and heat transfer in building components under atmospheric excitation. International Journal of Heat and Mass Transfer, 50(5-6), 1128-1140.

Javed, Haniya, Arianna Brambilla, and Marcus Strang. 2022. “An Australian Climate-Based Characterization of Hygrothermal Risks for Buildings.” Energy and Buildings 265: 112086. https://doi.org/10.1016/j.enbuild.2022.112086.

Johansson, S., Wadsö, L. and Sandin, K. (2010). Estimation of mould growth levels on rendered façades based on surface relative humidity and surface temperature measurements. Building and Environment, 45(5), pp.1153-1160.

K. Salminen et al., “Mould growth in building materials in laboratory and field experiments,” 9th Nord. Symp. Build. Phys. NSB 2011, vol. 2, pp. 859–866, 2011.

Kalagasidis, A. S. (2004). HAM-tools: An integrated simulation tool for heat, air and moisture transfer analysis in building physics. (Ph.D. Thesis). Chalmers University of Technology, Gothenburg, Sweden.

Kalamees, T., & Vinha, J. (2004). Estonian Climate Analysis for Selecting Moisture Reference Years for Hygrothermal Calculations. Journal of Building Physics, 27(3), 199–220. https://doi.org/10.1177/1097196304038839.

Kalamees, T., & Vinha, J. (2003). Hygrothermal calculations and laboratory tests on timber-framed wall structures. Building and Environment, 38(5), 689–697. https://doi.org/10.1016/S0360-1323(02)00207-X.

Karagiozis, A.N. 2002. WeatherFile Analyzer Software, Oak Ridge National Laboratory.

Kesik, T., Rose, D. De, & Melnichuk, S. (2006). hygrothermal performance classification methodology for wood-frame wall assemblies faculty of Architecture , Landscape and Design , University of Toronto Halsall Associates Limited , Toronto , Ontario , Canada Department of Civil Engineering , University. 73–80.

Kočí, J., Maděra, J., Keppert, M., & Černý, R. (2017). Damage functions for the cold regions and their applications in hygrothermal simulations of different types of building structures. Cold Regions Science and Technology, 135, 1–7. https://doi.org/10.1016/j.coldregions.2016.12.004.

Kunzel, H. M. (1995). Simultaneous heat and moisture transport in building components (Ph.D. Thesis). Fraunhofer Institute of Building Physics. Stuttgart, Germany.

Kunzel, H. M. (1998). The smart vapor retarder: An innovation inspired by computer simulation. ASHRAE Transactions, 104(2), 903-907.

L. Van Gelder, P. Das, H. Janssen, S. Roels, Comparative study of metamodelling techniques in building energy simulation: Guidelines for practitioners, Simulation Modelling Practice and Theory. 49 (2014) 245–257. doi:10.1016/j.simpat.2014.10.004.

Lacasse, M.A. (2019). An overview of durability and climate change of building components. Canadian Journal of Civil Engineering, 46(11), pp.v-viii.

Lacasse, M. A., Gaur, A., & Moore, T. V. (2020). Durability and climate change-implications for service life prediction and the maintainability of buildings. Buildings, 10(3). https://doi.org/10.3390/buildings10030053.

Lacasse, M. A., Ge, H., Hegel, M., Jutras, R., Laouadi, A., Sturgeon, G., & Wells, J. (2018). Guideline on design for durability of building envelopes. https://nrc-publications.canada.ca/eng/view/fulltext/?id=45b6a70c-e5a7-419a-bb1a-4687435c7895.

Langmans, J., & Roels, S. (2015). Experimental analysis of cavity ventilation behind rainscreen cladding systems: A comparison of four measuring techniques. Building and Environment, 87, 177–192. https://doi.org/10.1016/j.buildenv.2015.01.030L. Garverick, Corrosion in the Petrochemical Industry, ASM international, 1994.

Li, Q. (2008). Development of a hygrothermal simulation tool (HAM-BE) for building envelope study. (Ph.D. Thesis). Concordia University, Montreal, Canada.

Maref, W., Kumaran, K., Lacasse, M. A., Swinton, M. C., & van Reenen, D. (2002). Laboratory measurements and benchmarking of an advanced Hygrothermal model. Proceeding of International Heat Transfer Conference 12. https://doi.org/10.1615/ihtc12.720.

Mehmood T, Sæbø S, Liland K. Comparison of variable selection methods in PartialLeast Squares Regression. Journal of Chemometrics. 2020;34:e3226. https://doi.org/10.1002/cem.3226.

Moon, H. J., & Augenbroe, G. (2005). Assessing mold risks in buildings under uncertainty. College of Architecture, Doctor of(August), 245.

Mukhopadhyaya, P. (2003c). “MEWS project produces long-term moisture response indicator”, Construction Innovation. Volume 8, No. 1, pp. 6-7.

Mundt-Petersen, S. O., & Harderup, L. E. (2013). Validation of a one-dimensional transient heat and moisture calculation tool under real condition. Thermal Performance of the Exterior Envelopes of Whole Buildings XII. Florida, USA.

M. Vohland, M. Ludwig, S. Thiele-Bruhn, and B. Ludwig, “Determination of soil properties with visible to near- and mid-infrared spectroscopy: Effects of spectral variable selection,” Geoderma, vol. 223–225, no. 1, pp. 88–96, 2014, doi: 10.1016/j.geoderma.2014.01.013.

Natural Resources Canada. (2007). From impacts to adaptation: Canada in a changing climate. Ottawa: Government of Canada.

Ngah Abdul Wahab, S., Khamidi, M. F., & Jamaludin, N. (2014). Assessment of mould growth for library buildings in tropical climates. MATEC Web of Conferences, 15, 1–7. https://doi.org/10.1051/matecconf/20141501028.

Nielsen A, Möller EB, Rasmussen TV, et al. (2012) Use of sensitivity analysis to evaluate hygrothermal conditions in solid brick walls with interior insulation. In: Proceedings of the 5th international building physics conference (IBPC)—NSB 2011, Kyoto, Japan, 28– 31 May, vol. 1, pp. 377–384. Japan: Department of Architecture and Architectural Engineering of Kyoto University.

Nijland, T. G., Adan, O. C. G., Van Hees, R. P. J., & Van Etten, B. D. (2009). Evaluation of the effects of expected climate change on the durability of building materials with suggestions for adaptation. Heron, 54(1), 37–48.

Nik, & Moussavi, V. (2012). Hygrothermal Simulations of Buildings Concerning Uncertainties of the Future Climate (Issue May 2012).

Nik, V., & Kalagasidis, A. S. (2010). Influence of the uncertainties in future climate scenarios on the hygro-thermal simulation of an attic. December 2015.

Nik, V. M., Mundt-Petersen, S. O., Kalagasidis, A. S., & De Wilde, P. (2015). Future moisture loads for building facades in Sweden: Climate change and wind-driven rain. Building and Environment, 93(P2), 362–375. https://doi.org/10.1016/j.buildenv.2015.07.012.

Nik, V. M., Sasic Kalagasidis, A., & Kjellström, E. (2012). Assessment of hygrothermal performance and mould growth risk in ventilated attics in respect to possible climate changes in Sweden. Building and Environment, 55, 96–109. https://doi.org/10.1016/j.buildenv.2012.01.024.

Ojanen Tuomo, Viitanen Hannu, Peuhkuri Ruut, Lähdesmäki Kimmo, Vinha Juha, S. K. (2010). Mold Growth Modeling of Building Structures Using Sensitivity Classes of Materials.

OSHA Field Safety and Health Manual (2011).

Rahiminejad, M., & Khovalyg, D. (2021). Review on ventilation rates in the ventilated airspaces behind common wall assemblies with external cladding. Building and Environment, 190, 107538. https://doi.org/10.1016/j.buildenv.2020.107538.

Ritschkoff A., Viitanen H.,Koskela K. The Response of Building Materials to the Mould Exposure at Different Humidity and Temperature Conditions. Proceedings of Healthy Building. 2000, Vol. 3, pp. 317-322.

Rode, C. (1990). Combined heat and moisture transfer in building constructions. (Ph.D. Thesis). Technical University of Denmark, Copenhagen, Denmark.

Rode C. Reference years for moisture calculations. Denmark. Report T2-DK-93/02, International Energy Agency, Energy Conservation in Buildings and Community Systems Program, Annex 24 Heat, Air, and Moisture Transfer in Insulated Building Parts (HAMTIE).

Rowan, N. J., Johnstone, C. M., McLean, R. C., Anderson, J. G., & Clarke, J. A. (1999). Prediction of toxigenic fungal growth in buildings by using a novel modelling system. Applied and Environmental Microbiology, 65(11), 4814–4821. https://doi.org/10.1128/aem.65.11.4814-4821.1999.

Sahyoun, S., Ge, H., Aggarwal, C., Defo, M., & Moore, T. (2020). Effect of Selected Moisture Reference Year on the Durability Assessment of Wall Assemblies under Future Climates. 0–8. https://doi.org/10.23967/dbmc.2020.056.

Salonvaara, M. (2004). Development of heat, air, moisture and pollutant transport model, BEESL/EQS quality assurance and project plan for CHAMPS development. Syracuse, NY: Syracuse University.

Salonvaara, M., Sedlbauer, K., Holm, A., & Pazera, M. (2010). Effect of selected weather year for hygrothermal analyses. Thermal Performance of the Exterior Envelopes of Whole Buildings - 11th International Conference.

Sedlbauer, K. (2001). Prediction of mould fungus formation on the surface of/and inside building components.247.http://www.ibp.fraunhofer.de/content/dam/ibp/en/documents/ks_dissertation_et cm1021-30729.pdf.

Sedlbauer, K. (2002). Prediction of mould growth by hygrothermal calculation. Journal of Thermal Envelope and Building Science, 25(4), pp.321-336.

Service, F. (2005). Wood Handbook 1999. 1–486. papers2://publication/uuid/3258D7CF-6851-4BF4-BBCB-CD58D90BEAE1.

Simpson, T. W., Peplinski, J. D., Koch, P. N., & Allen, J. K. (2001). Metamodels for computer-based engineering design: Survey and recommendations. Engineering with Computers, 17(2), 129–150. https://doi.org/10.1007/PL00007198.

Straube, J., & Burnett, E. (2001). Overview of hygrothermal (HAM) analysis methods. Moisture analysis and condensation control in building envelopes, 81-89.

Straube, J. F., & Schumacher, C. J. (2003). Hygrothermal Enclosure Models: Comparison with Field Data. Research in Building Physics - Proceedings of the 2nd CIB Co-Sponsored International Conference on Building Physics, September 2003. http://www.irbnet.de/daten/iconda/CIB2377.pdf.

Tian, W., & De Wilde, P. (2011). Uncertainty and sensitivity analysis of building performance using probabilistic climate projections: A UK case study. Automation in Construction, 20(8), 1096–1109. https://doi.org/10.1016/j.autcon.2011.04.011.

Tijskens, A., Roels, S., & Janssen, H. (2019). Neural networks for metamodelling the hygrothermal behaviour of building components. Building and Environment, 162(May), 106282. https://doi.org/10.1016/j.buildenv.2019.106282.

Tijskens, Astrid, Staf Roels, and Hans Janssen. 2021. "Hygrothermal Assessment of Timber Frame Walls Using a Convolutional Neural Network." Building and Environment 193(November 2020): 107652. https://doi.org/10.1016/j.buildenv.2021.107652.

V. Marincioni, G. Marra, H. Altamirano-medina, Development of predictive models for the probabilistic moisture risk assessment of internal wall insulation, Building and Environment. 137 (2018) 257–267. doi:10.1016/j.buildenv.2018.04.001.

Vandemeulebroucke, I., Defo, M., Lacasse, M. A., Caluwaerts, S., & Van Den Bossche, N. (2020). Canadian initial-condition climate ensemble: Hygrothermal simulation on wood-stud and retrofitted historical masonry. Building and Environment, 107318. https://doi.org/10.1016/j.buildenv.2020.107318.

Vandemeulebroucke, Isabeau, Steven Caluwaerts, and Nathan Van Den Bossche. 2022. "Decision Framework to Select Moisture Reference Years for Hygrothermal Simulations." Building and Environment 218(March): 109080. https://doi.org/10.1016/j.buildenv.2022.109080.

Vanpachtenbeke, M., Langmans, J., Van den Bulcke, J., Van Acker, J., & Roels, S. (2020). Modelling moisture conditions behind brick veneer cladding: Verification of common approaches by field measurements. Journal of Building Physics, 44(2), 95–120. https://doi.org/10.1177/1744259120908283.

VanStraaten, R. & Straube, J (2004). Field study of airflow behind brick veneers. Report for Task 6 of ASHRAE RP 1091. ASHRAE: Atlanta, USA.

Vereecken, E., & Roels, S. (2012). Review of mould prediction models and their influence on mould risk evaluation. Building and Environment, 51, 296–310. https://doi.org/10.1016/j.buildenv.2011.11.003.

Viitanen, H.A. (1997). Modelling the time factor in the development of mould fungi-The effect of critical humidity and temperature conditions on pine and spruce sapwood. Holzforschung-International Journal of the Biology, Chemistry, Physics and Technology of Wood, 51(1), pp.6-14.

Viitanen, H., Hanhijärvi, A., Hukka, A. and Koskela, K. (2000). Modelling mould growth and decay damages. In Healthy Buildings 2000 (pp. 341-346).

Viitanen, H., & Ojanen, T. (2007). Improved Model to Predict Mold Growth in Building Materials. Buildings X, 1–8.

Viitanen, H., & Ritschkoff, A. (1991). Mould growth in pine and spruce sapwood in relation to air humidity and temperature. Report no 221. Department of Forest Products, The Swedish University of Agricultural Sciences, Uppsala.

Viitanen, H., Vinha, J., Salminen, K., Ojanen, T., Peuhkuri, R., Paajanen, L. and Lähdesmäki, K. (2011). Moisture and bio-deterioration risk of building materials and structures. INTECH Open Access Publisher.

Wang, G. G., & Shan, S. (2007). Review of metamodeling techniques in support of engineering design optimization. Journal of Mechanical Design, Transactions of the ASME, 129(4), 370–380. https://doi.org/10.1115/1.2429697.

Wang, L., & Ge, H. (2018). Stochastic modelling of hygrothermal performance of highly insulated wood framed walls. Building and Environment, 146(September), 12–28. https://doi.org/10.1016/j.buildenv.2018.09.032.

X. Fan, Y. Liu, J. Tao, and Y. Weng, “Soil salinity retrieval from advanced multi-spectral sensor with partial least square regression,” Remote Sens., vol. 7, no. 1, pp. 488–511, 2015, doi: 10.3390/rs70100488.

Xie, Yuquan et al. 2022. “Artificial Neural Network Modeling for Predicting and Evaluating the Mean Radiant Temperature around Buildings on Hot Summer Days.” Buildings 12(5).

X. Zhang and B. Huang, “Prediction of soil salinity with soil-reflected spectra: A comparison of two regression methods,” Sci. Rep., vol. 9, no. 1, pp. 1–9, 2019, doi: 10.1038/s41598-019-41470-0.

Y. Qu, S. Jiao, and X. Lin, “A partial least square regression method to quantitatively retrieve soil salinity using hyper-spectral reflectance data,” Geoinformatics 2008 Jt. Conf. GIS Built Environ. Classif. Remote Sens. Images, vol. 7147, no. May, p. 71471H, 2008, doi: 10.1117/12.813254.

Zhou, X., Carmeliet, J., & Derome, D. (2020). Assessment of risk of freeze-thaw damage in internally insulated masonry in a changing climate. Building and Environment, 175(September 2019), 106773. https://doi.org/10.1016/j.buildenv.2020.106773.

Zhou, X., Derome, D., & Carmeliet, J. (2016). Robust moisture reference year methodology for hygrothermal simulations. Building and Environment, 110, 23–35. https://doi.org/10.1016/j.buildenv.2016.09.021.

Zhou, X., Derome, D., & Carmeliet, J. (2017). Hygrothermal modeling and evaluation of freeze-thaw damage risk of masonry walls retrofitted with internal insulation. Building and Environment, 125, 285–298. https://doi.org/10.1016/j.buildenv.2017.08.

Appendices

Appendix 1. Boundary conditions in DELPHIN

Outdoor boundary conditions include heat conduction, vapor diffusion, wind-driven rain, short wave radiation, and longwave radiation. There are multiple ways to assign a particular boundary condition in DELPHIN according to the type of input parameter. The types of boundary conditions along with the equations describing them are explained in detail below:

Heat transfer

Heat transfer is one of the most important boundary conditions. DELPHIN allows different methods to assign this boundary condition namely, surface value, imposed flux, exchange coefficient, boundary layer, and heat pipe in wall method. Details of each method are provided below:

In the Surface value method, the value at the surface of the boundary element is kept fixed. It is further described as follows:

$$j_{diff}^{Q} = 1000\left(T_{elem} - T_{surf}\right) \tag{A-1}$$

where, j_{diff}^{Q} is heat flux in W/m^2, T_{elem} is the temperature of the boundary element in K and T_{surf} is given surface temperature in K.

In the Imposed flux method, heat flux through the selected boundary is defined and it can be set as a climate condition.

$$j_{diff}^{Q} = j_{imp}^{Q} \tag{A-2}$$

where, j_{imp}^{Q} is Imposed heat flux in W/m^2.

For the Exchange coefficient method, parameters such as temperature and heat exchange coefficient are defined as climate conditions.

$$j_{diff}^{Q} = h(T_{elem} - T_{ambient}) \tag{A-3}$$

Where, h is the heat exchange coefficient in W/m^{2}K and $T_{ambient}$ is the temperature of ambient air in K.

a) Heat exchange coefficients depending on the heat flow scenarios

Flow scenario	Exchange coefficient (W/m²K)	Convective exchange coefficient (W/m²K)	Radiative exchange coefficient (W/m²K)
Inside, heat flow upwards	10.0	5.0	5.0
Inside, heat flow horizontal	7.6	2.5	5.1
Inside, heat flow vertical	5.8	0.7	5.1
Outside	25.0	20.0	5.0

The heat exchange coefficient can be set according to the current surroundings. The values are taken from EN ISO 6946. The heat exchange coefficient includes both convective as well as radiative parts. Table (a) shows the typical values for varying conditions.

The boundary layer method involves the dependency of the heat exchange coefficient on the speed of air. In this method, temperature and wind speed are set as climate conditions and heat exchange coefficient as a parameter.

$$j_{diff}^{Q} = h\,(v)(T_{elem} - T_{ambient}) \tag{A-4}$$

$$h\,(v) = h_0 + k_{slope}.\,v^{k_{exp}} \tag{A-5}$$

where, h_0 is base heat exchange coefficient i.e. at zero airspeed, k_{slope} is the slope in J/m^{3}K, k_{exp} is exponent, v is air speed from climatic condition data in m/s and $T_{ambient}$ is the temperature of ambient air in K.

Furthermore, from EN ISO 6946, convective heat exchange can be calculated using the equation given below.

$$h_{ce} = 4 + 4v \tag{A-6}$$

Finally, the Heat pipe in wall method simulates the behavior of a pipe inside other material through which a liquid flow. This liquid flow goes in the z-direction. The heat flow between the pipe and surrounding material goes in the x and y directions. The mean heat flow from the pipe to the surrounding material is used as the boundary condition. The model is assumed to be in the steady state which means equilibrium of heat flow caused by flowing liquid and heat flow from pipe to the surrounding is assumed. The heat flow can be calculated using the following formula:

$$Q_H = -m.c.(T_v - T_e).\left(1 - e^{-\frac{U_p.L}{m.c}}\right) \tag{A-7}$$

Where, m is the fluid mass flow in kg/s, c is the Heat capacity of fluid in J/kgK, T_v is the supply temperature in K, T_e is the surrounding temperature in K, U_p and L is the heat transfer coefficient of the pipe wall and pipe length in W/m.K and m respectively.

In this thesis, the boundary layer method was used for defining the heat conduction boundary condition for all the simulations.

Vapor diffusion

This boundary condition defines the diffusion of the vapor at the boundary. This can be computed using temperature and relative humidity or by providing the vapor pressure climatic condition. In DELPHIN. there are two methods to define the vapor diffusion boundary condition i.e., exchange coefficient and vapor diffusion boundary layer method.

The exchange coefficient method uses the following equations to define the vapor diffusion boundary condition.

$$j_{diff}^{m_v} = \beta_v\left(p_v^{elem} - p_v^{ambient}\right) \tag{A-8}$$

Where, $j_{diff}^{m_v}$ is mass flow density of diffusive vapor flux in kg/m^{2}s, β_v is water vapor exchange coefficient in s/m, p_v^{elem} is water vapor pressure at boundary element in Pa and $p_v^{ambient}$ is further defined as the following.

$$p_v^{ambient} = p_{v,sat}\left(T^{ambient}\right).\varphi^{ambient} \tag{A-9}$$

Where, $p_{v,sat}\left(T^{ambient}\right)$ is saturation vapor pressure for ambient air temperature in Pa, $T^{ambient}$ is the ambient air temperature in K and $\varphi^{ambient}$ is the relative humidity of ambient air.

There are two ways of defining climatic conditions. The first is setting up the air temperature and RH and the second involves setting up the vapor pressure. Also, an s_d value can be given for simulating the external coatings. This is used as additional resistance. The new vapor exchange coefficient will be calculated using the following relation:

$$\beta_{v2} = \frac{1}{\frac{1}{\beta_{v1}} + \frac{s_d . R_v . T}{D(T)}} \tag{A-10}$$

The water vapor exchange coefficient mainly depends on the convective process near the surface. Therefore, there exists an equivalent description to the convective part of the heat exchange coefficient, and it is known as Lewis's relation. For constant air pressure and low air velocity, the Lewis number is approximately 1. Hence the following relation could be written:

$$\beta_v = \frac{1}{R_v . T . \rho_{air} . c_{air}} . h_c \tag{A-11}$$

For normal pressure of 1atm and dry air conditions, the following simplified relation can be used:

$$\beta_v \approx 6.1 * 10^{-9} \frac{Kms}{W} . h_c \tag{A-12}$$

The second method called Vapor diffusion–Boundary layer takes into consideration the dependency of exchange coefficient on airspeed.

Similar to the previous method for vapor diffusion, this method also has two possibilities for defining the boundary condition. However, wind speed as climate conditions is used in this method.

$$j_{diff}^{m_v} = \beta(v)\left(p_v^{elem} - p_v^{ambient}\right) \tag{A-13}$$

$$\beta(v) = \beta_0 + k_{slope} . v^{k_{exp}} \tag{A-14}$$

Where, $\beta(v)$ is water vapor exchange coefficient in s/m, β_0 is base exchange coefficient at zero wind speed, k_{slope} is the slope in s^2/m^2, k_{exp} is exponent, v is air speed in m/s, p_v^{elem} is water vapor pressure at boundary element in Pa and $p_v^{ambient}$ is defined as follows:

$$p_v^{ambient} = p_{v,sat}\left(T^{ambient}\right) . \Phi^{ambient} \tag{A-15}$$

Where, $p_{v,sat}\left(T^{ambient}\right)$ is saturation vapor pressure for ambient air temperature in Pa, $T^{ambient}$ is the ambient air temperature in K and $\Phi^{ambient}$ is the relative humidity of ambient air.

The model for convective heat exchange coefficient from EN ISO 6946 can be used and following this, the Lewis relation can be used to calculate the above-mentioned parameter with h_{ce} and β_v.

$$\beta_v = 2.44 * 10^{-8} + 2.44 * 10^{-8}. v \tag{A-16}$$

For the present work, the Vapor diffusion – Boundary layer method was used for imposing the vapor diffusion boundary layer for all the simulation work.

Wind-driven rain (WDR)

Wind Driven Rain (WDR) is an essential boundary condition for hygrothermal simulations. Two methods are available in DELPHIN to impose wind-driven rain as a boundary condition namely, Imposed flux and standard rain model. In the Imposed flux method, the rain flux density normal to the wall surface is calculated by the user and it is then directly used to make further calculations. On the other hand, the Standard rain model involves the calculation of rain flux density normal to the wall surface using rain flux density on a horizontal plane, the wind direction, and the wind velocity using the wall parameters orientation and inclination.

Knowing the rain flux density normal to the wall surface the liquid water flux over the boundary can be calculated. The maximum liquid water flux over the boundary is determined by the multiplication of the liquid water conductivity of the material with a capillary pressure gradient calculated from the difference of the moisture content in the surface volume element to its saturation value. If the driving rain flow on the surface exceeds the maximum liquid water flux, this maximum flux will be used as liquid water flux into the boundary element. The difference in the driving rain flow can be considered as run-off.

$$j_{conv}^{m_w} = min\left(j_{imp}^{m_w}, j_{max}^{m_w}\right) \tag{A-17}$$

Where, $j_{conv}^{m_w}$ is the mass of convective liquid water flux in kg/m^{2}s, $j_{imp}^{m_w}$ is imposed water flux in kg/m^{2}s and $j_{max}^{m_w}$ i.e. maximum water flux into the element in kg/m^{2}s is defined as follows:

$$j_{max}^{m_w} = -\left(K_l\left(w_{eff}^{elem}\right) + K_l\left(w_l^{elem}\right)\right).\frac{p_l^{elem}}{x^{elem}} \tag{A-18}$$

Where, $K_l(w)$ is liquid water conductivity in s, w_{eff}^{elem} is the effective saturation water content in kg/m^3, w_l^{elem} is the current water content in kg/m^3, p_l^{elem} is current capillary pressure in element in Pa and x^{elem} is the thickness of the element in m.

The liquid water flux into the boundary element is calculated by using one of the two models. From this, an enthalpy flow can be calculated.

$$j_{conv}^{U_w} = u_w(T_w).j_{conv}^{m_w} \tag{A-19}$$

Where, $j_{conv}^{U_w}$ denotes the internal energy of liquid water flux in J/m^{2}s, $u_w(T_w)$ being the specific internal energy of liquid water in J/kg with T_w as defined below:

$$T_w = T_{dew}(T_{air}, \varphi_{ai}) \tag{A-20}$$

With T_w being the temperature of imposed flux in K and $T_{dew}(T_{air}, \varphi_{ai})$ is the dew point temperature of ambient air in K.

Further, both rain models, exposure coefficient, minimum rain temperature, and minimum rain flux should be defined. The exposure coefficient is a factor with which the rain flow density will be multiplied. It can be used to take sheltering effects or similar into account. The minimum of this value is 0 and there is no upper limit to this coefficient. The minimum rain temperature is used for distinguishing rain from snow. Below the minimum rain temperature, the model does not consider rain. Finally, the minimum rain flux is used to neglect very small rain flux densities.

For the Imposed flux method, the flux must be given by a climate condition i.e. the normal rain, air temperature, relative humidity, and wall data.

For the standard rain model method, driving rain flow density at a surface with a specified orientation depending on wind direction and wind speed is calculated. The following equations are used for the calculation:

$$j_{conv}^{m_w} = min\left(j_{nor}^{m_w}, j_{max}^{m_w}\right) \tag{A-21}$$

Where,

$$j_{rain,nor}^{m_w} = k_{wind}.\, k_{rain}.\, j_{rain,hor}^{m_w} \tag{A-22}$$

With, $j^{m_w}_{rain,nor}$ being the rain flux density normal to the wall surface in kg/m^{2}s, k_{wind} is the wind coefficient and k_{rain} denotes the rain exposure coefficient.

k_{wind} depends on wall orientation, wind direction, and wind speed and the expression used is only valid for a vertical wall with a given orientation. For a horizontal surface, the value is set to 1. It depends on an important parameter i.e. wind angle, β. It describes the angle between the wall-normal and the wind direction.

$$\beta_{wind} = |\alpha_{wall} - \alpha_{wind}| \tag{A-23}$$

$$\beta_{wind} = \begin{cases} \beta_{wind} > \pi = \beta_{wind} \\ \beta_{wind} \geq \pi = 2\pi - \beta_{wind} \end{cases} \tag{A-24}$$

Where, α_{wall} and α_{wind} represent the wall orientation and wind direction respectively in radian.

Finally, for the calculation of k_{wind} , following formula is used except for the case in which the wind angle exceeds 90° and if the wind speed is 0 m/s, wherein it is assumed 0.

$$\mathrm{k_{wind}} = \frac{\cos(\beta_{wind})}{\sqrt{1 + 1142.\frac{\sqrt{3600.j^{m_w}_{rain,hor}}}{v^4_{wind}}}} . e^{\left(-\frac{12}{5.v_{wind}.\sqrt[4]{3600.j^{m_w}_{rain,hor}}}\right)} \tag{A-25}$$

For the present study, Imposed flux method was used to compute the WDR boundary condition.

Short wave radiation

Short-wave radiation is mainly solar radiation with a wavelength between 0.2µm (sometimes 0.38µm) and 3µm. To define this boundary condition, there are two available methods in DELPHIN:

Imposed flux, in this method, the radiation flux density normal to the wall surface has been entered manually by the user. Another method i.e. Direct sun radiation model, where the radiation flux density normal to the wall surface is calculated from the daytime, the direct sun radiation, and diffuse sun radiation components and using the wall parameters such as orientation, inclination, and latitude.

For imposed flux method, the following equations are used for computation:

$$\mathrm{j}^{\mathrm{Q}}_{\mathrm{swrad}} = \alpha_{\mathrm{sw}}.\mathrm{j}^{\mathrm{Q}}_{\mathrm{imp}} \tag{A-26}$$

Where, $\mathrm{j}^{\mathrm{Q}}_{\mathrm{swrad}}$ is short wave radiation flux in W/m^2, α_{sw} is absorption coefficient for short-wave radiation and $\mathrm{j}^{\mathrm{Q}}_{\mathrm{imp}}$ is the imposed radiation flux in W/m^2.

The absorption coefficient for short-wave radiation mainly depends on the color of the surface finish. **Error! Reference source not found.** shows the typical values from the German standard DIN 18599.

b) Absorption coefficient for different colored materials

Name	Absorption coefficient
Light colored paint	0.4
Muted paint	0.6
Dark paint	0.8
Clinker brickwork	0.8
Light-colored exposed brickwork	0.4
Roof: brick color	0.6
Roof: dark surface	0.8
Roof: bare metal	0.2
Roof: bitumen (sanded)	0.6

For the Direct sun radiation model, the following equations are solved to compute the short-wave radiation:

$$j^{Q}_{swrad} = \alpha_{sw}.\left(j^{Q}_{dir,n} + j^{Q}_{diff,n}\right) \tag{A-27}$$

Where,

$$j^{Q}_{dir,n} = j^{Q}_{dir,h}.f_{dir}\left(\alpha_{wall}, \beta_{wall}, l_{geo}, t\right) \tag{A-28}$$

$$j^{Q}_{diff,n} = j^{Q}_{diff,h}.cos^2\left(\frac{\beta_{wall}}{2}\right) + r_{albedo}.j^{Q}_{glob,h}.sin^2\left(\frac{\beta_{wall}}{2}\right) \quad \text{(A-29)}$$

$$j^{Q}_{glob,h} = j^{Q}_{diff,h} + j^{Q}_{dir,h} \quad \text{(A-30)}$$

Where, $j^{Q}_{dir,n}$ denotes the direct radiation flux normal to the surface in W/m^2, $j^{Q}_{diff,n}$ is the diffuse radiation flux normal to the surface in W/m^2, $j^{Q}_{glob,h}$ is the global radiation flux on a horizontal surface in W/m^2, $j^{Q}_{diff,h}$ is diffuse radiation flux on a horizontal surface in W/m^2, $j^{Q}_{dir,h}$ is direct radiation flux on a horizontal surface, $f_{dir}(\alpha_{wall}, \beta_{wall}, l_{geo}, t)$ is the direct radiation factor, α_{wall} being wall orientation in degree, β_{wall} being wall inclination in degree, l_{geo} being geographic latitude of location in degree, t being time in seconds and r_{albedo} being the ground reflection coefficient.

For this study, the direct sun radiation model was used with direct sun radiation, diffuse sun radiation, and wall data being the input parameters.

Longwave radiation

Long-wave radiation is infrared radiation with the wavelength between 4µm and 40µm. There are three methods available for defining this boundary condition.

Imposed flux, wherein the radiation flux density normal to the wall surface is calculated by the user. Long wave components, in which the radiation flux density normal to the wall surface is calculated from the heat emission of the building and the atmospheric counter radiation using the wall parameter Inclination. And finally, Boltzmann calculation, where the radiation flux is calculated based on Boltzmann's law. The surface temperature is used for the long wave emission and the air temperature is used instead of the sky temperature for calculating the atmospheric counter radiation. Except for imposed flux, the emission coefficient of the surrounding ground is taken into account.

For imposed flux method, the following equation is solved to get the long wave radiation flux:

$$j^{Q}_{lwrad} = \varepsilon_{sw}.j^{Q}_{imp} \quad \text{(A-31)}$$

Where, j^Q_{lwrad} is long-wave radiation flux in W/m^2, ε_{sw} is emission coefficient for long-wave radiation and j^Q_{imp} is the imposed radiation flux in W/m^2.

For the long wave components method, the radiation flux density normal to the wall surface is calculated from the heat emission of the building and the atmospheric counter radiation using the wall parameter Inclination.

For considering the radiation exchange between construction and surrounding ground, the ground emission radiation flux can be added as a climate condition and a ground emission coefficient as the parameter.

$$j^Q_{lwrad} = f_{sky}.\left(j^Q_{sky} - \sigma.T^4_{surf}\right) + f_{grd}.\left(j^Q_{grd} - \sigma.T^4_{surf}\right) \tag{A-32}$$

Where, j^Q_{lwrad} is long-wave radiation flux in W/m^2, $j^Q_{sky}$is atmospheric counter radiation in W/m^2, j^Q_{grd} is ground emission radiation flux in W/m^2, σ being the Stefan Boltzmann constant, T_{surf} being the surface temperature in K and f_{sky} & f_{grd} are given as follows:

$$f_{sky} = cos^2\left(\frac{\beta_{wall}}{2}\right).\varepsilon_{lw,surf} \tag{A-33}$$

$$f_{grd} = sin^2\left(\frac{\beta_{wall}}{2}\right).\frac{1}{\frac{1}{\varepsilon_{lw,surf}} + \frac{1}{\varepsilon_{lw,grd}} - 1} \tag{A-34}$$

Where, f_{sky} is sky radiation factor, f_{grd} is ground radiation factor, β_{wall} is wall inclination, $\varepsilon_{lw,surf}$ is long wave emission coefficient of surface and $\varepsilon_{lw,grd}$is the long wave emission coefficient of ground.

Finally, for the Boltzmann calculation model, the long-wave radiation from the construction is calculated by the Stefan Boltzmann equation with the current surface temperature of the construction. The long-wave radiation from the sky is calculated using sky temperature and sky emissivity or a model based on cloud covering. The radiation exchange with the surrounding ground can be calculated in the same way as the Long Wave Components model.

$$j^Q_{lwrad} = f_{sky}.\sigma.\left(T^4_{sky} - T^4_{surf}\right) + f_{grd}.\sigma.\left(T^4_{grd} - T^4_{surf}\right) \tag{A-35}$$

$$T_{sky} = T^{air}.\sqrt[4]{f_{RH}.f_{CC}} \tag{A-36}$$

Where, j_{lwrad}^{Q} is long-wave radiation flux in W/m^2, T_{sky} is sky temperature in K, T_{grd} is the ground temperature in K and is equal to T^{air}, T_{surf} is surface temperature in K and is equal to the T^{elem} and f_{RH} (relative humidity factor) & f_{CC} (cloud covering factor) are defined as below:

$$f_{RH} = 0.82 - 0.25 * 10^{-0.00075006.p_v^{air}} \tag{A-37}$$

$$f_{CC} = 1 + 0.2B^2 \tag{A-38}$$

Where, p_v^{air} is water vapor pressure in the air in Pa and B is cloud cover.

For sky temperature, two different models can be used. The sky temperature is directly given as climate condition. Alternatively, it is possible to calculate the sky temperature from air temperature, air relative humidity, and cloud covering.

The Boltzmann calculation method was used for long-wave radiation boundary conditions in this thesis.

Appendix 2. WDR Distribution for 11 cities across different orientations

1. North Orientation

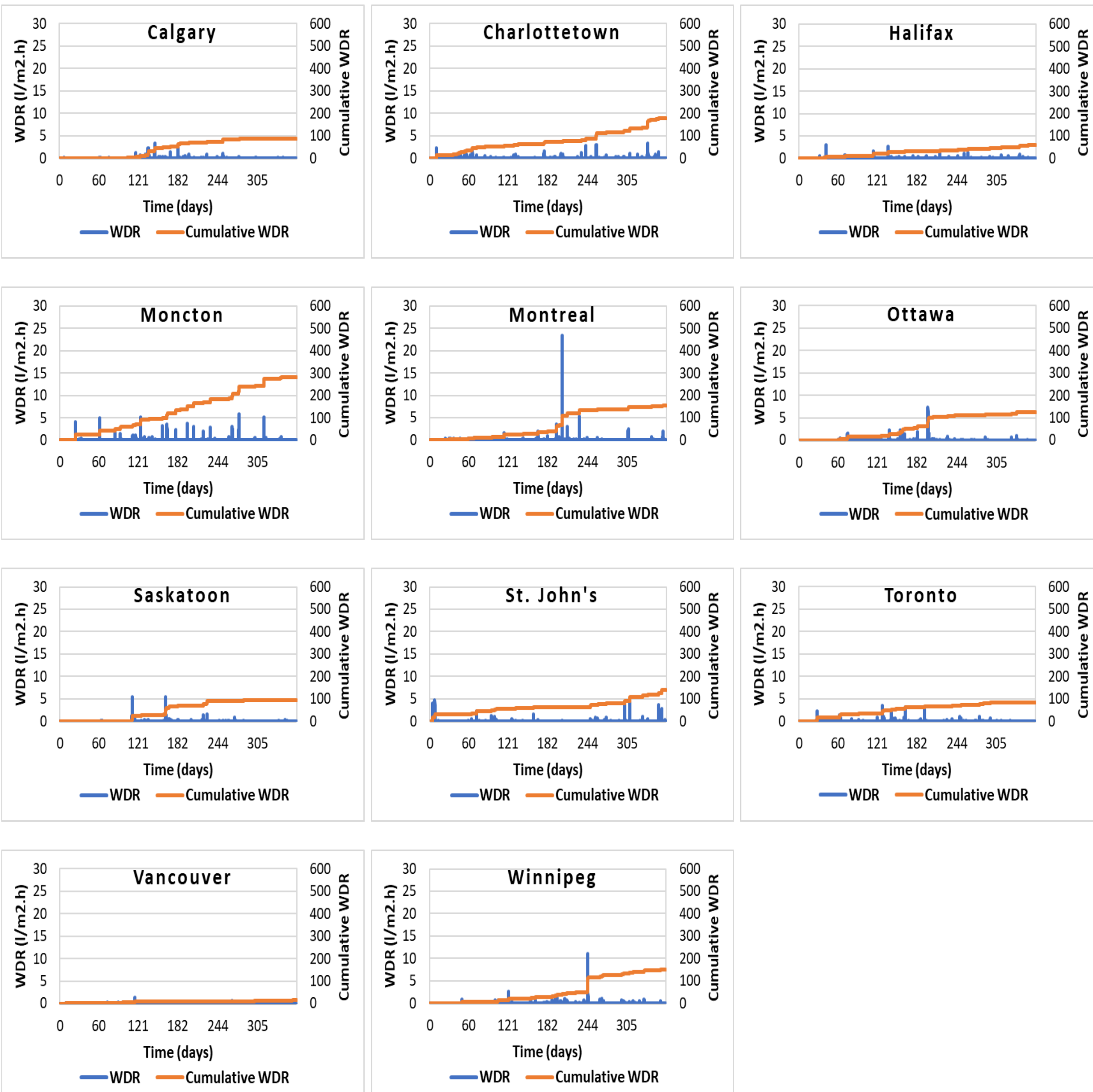

b) Hourly and cumulative values of WDR for all cities for the North orientation

2. East Orientation

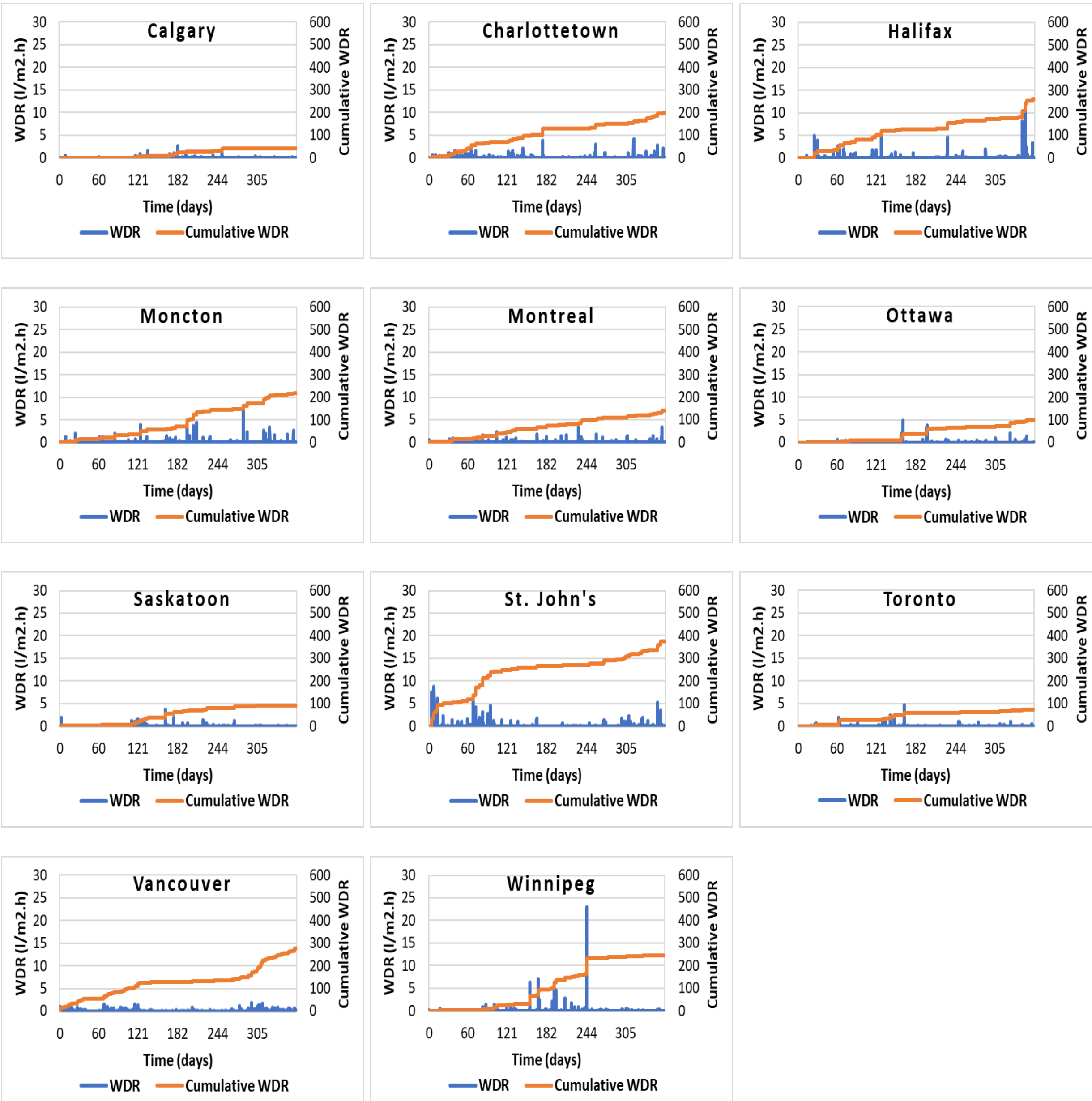

c) Hourly and cumulative values of WDR for all cities for the East orientation

3. South Orientation

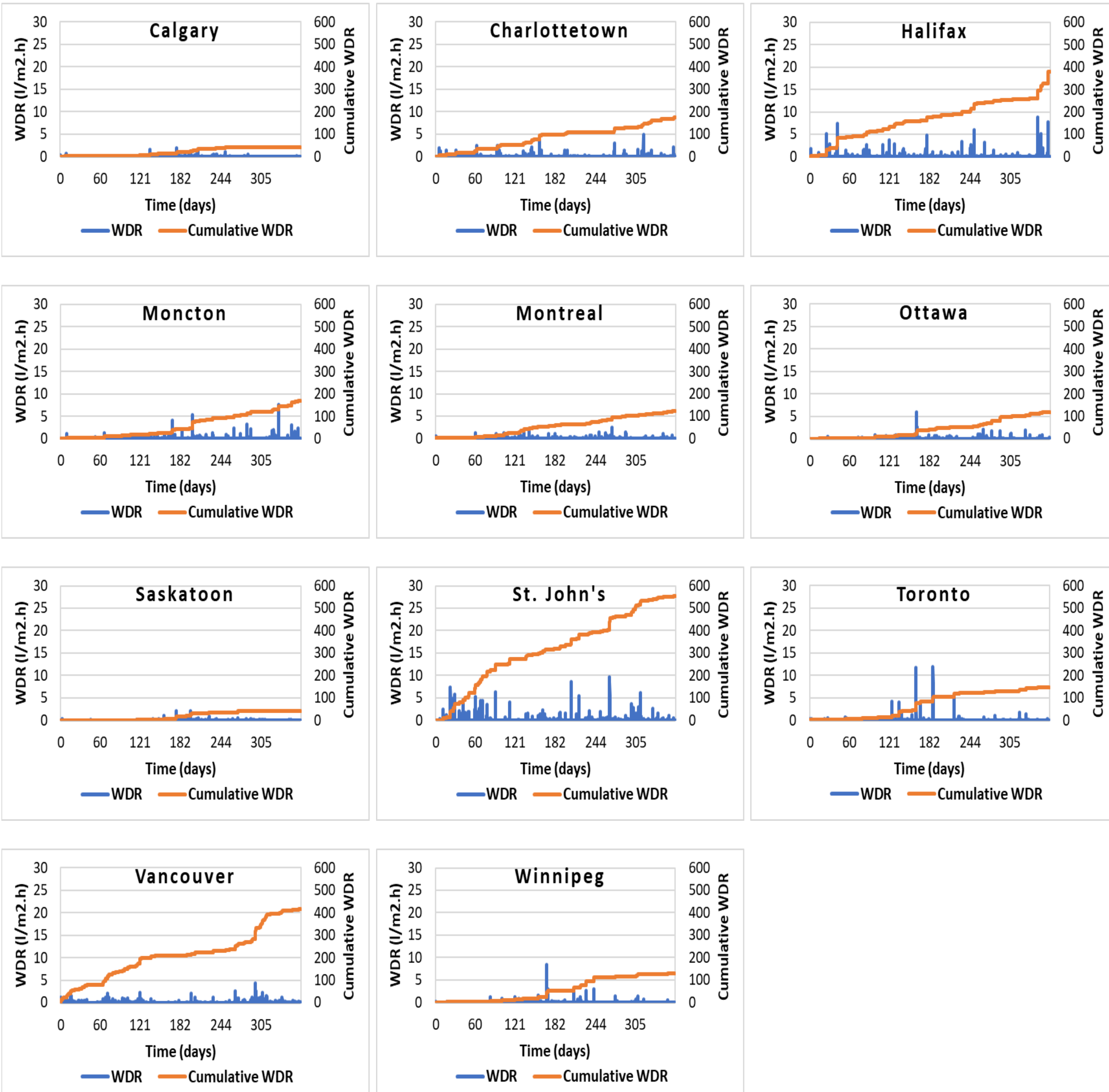

d) Hourly and cumulative values of WDR for all cities for the South orientation

4. West Orientation

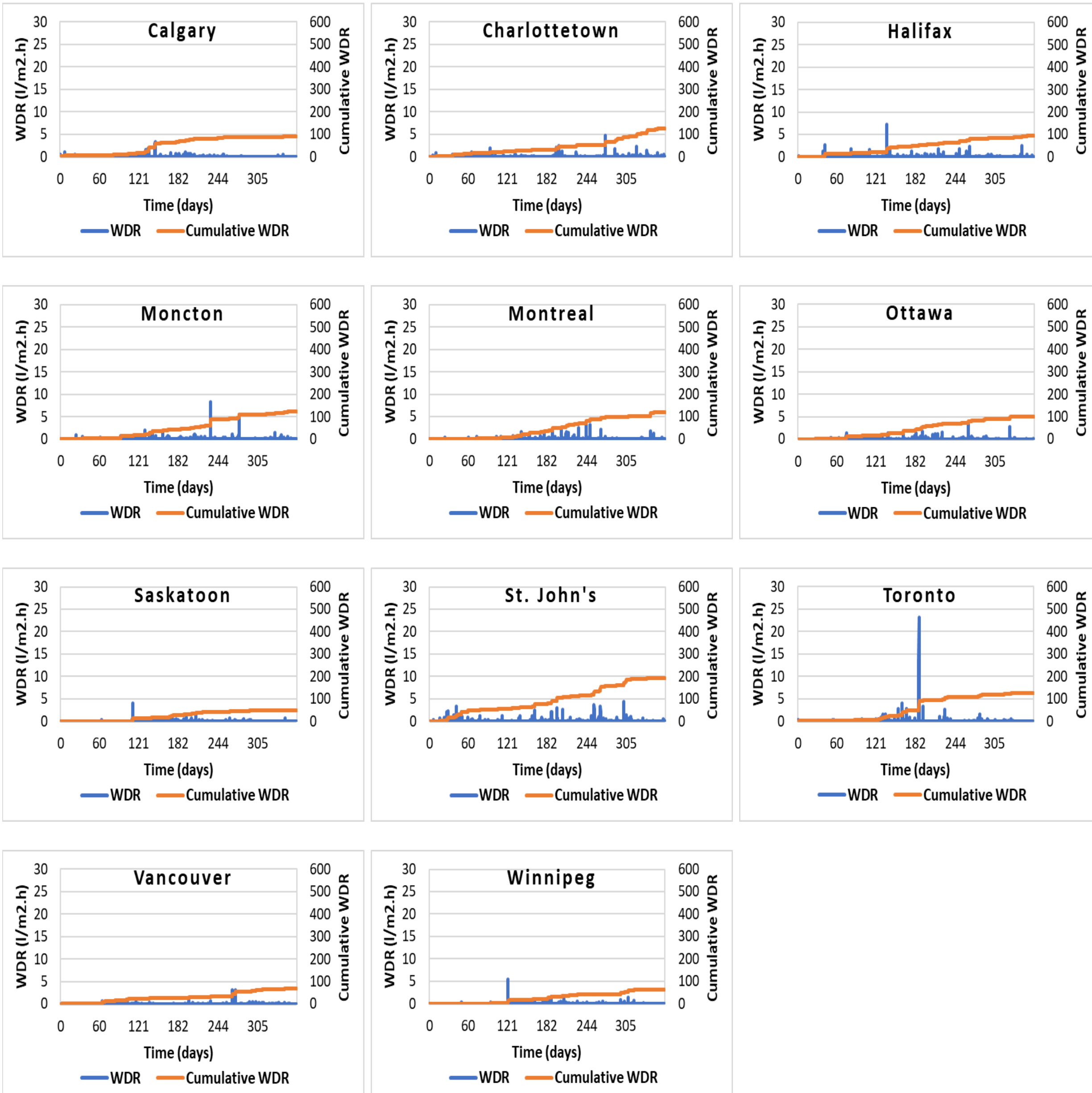

e) Hourly and cumulative values of WDR for all cities for the West orientation

5. Default Orientation

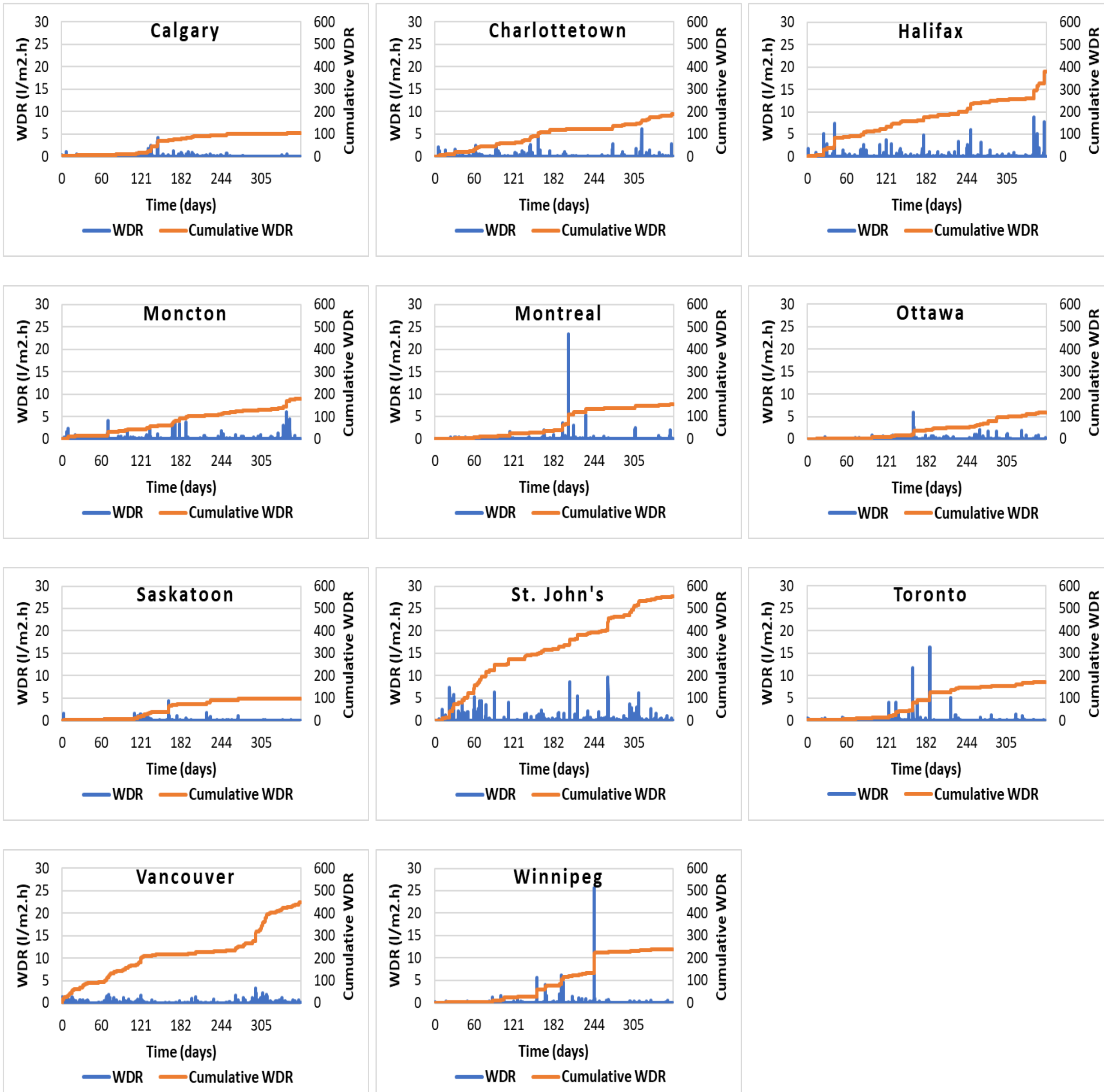

f) Hourly and cumulative values of WDR for all cities for the Default orientation

A3. Results obtained with the Maximum Moisture Content (MC)

1. Cases with no WDR and no water source

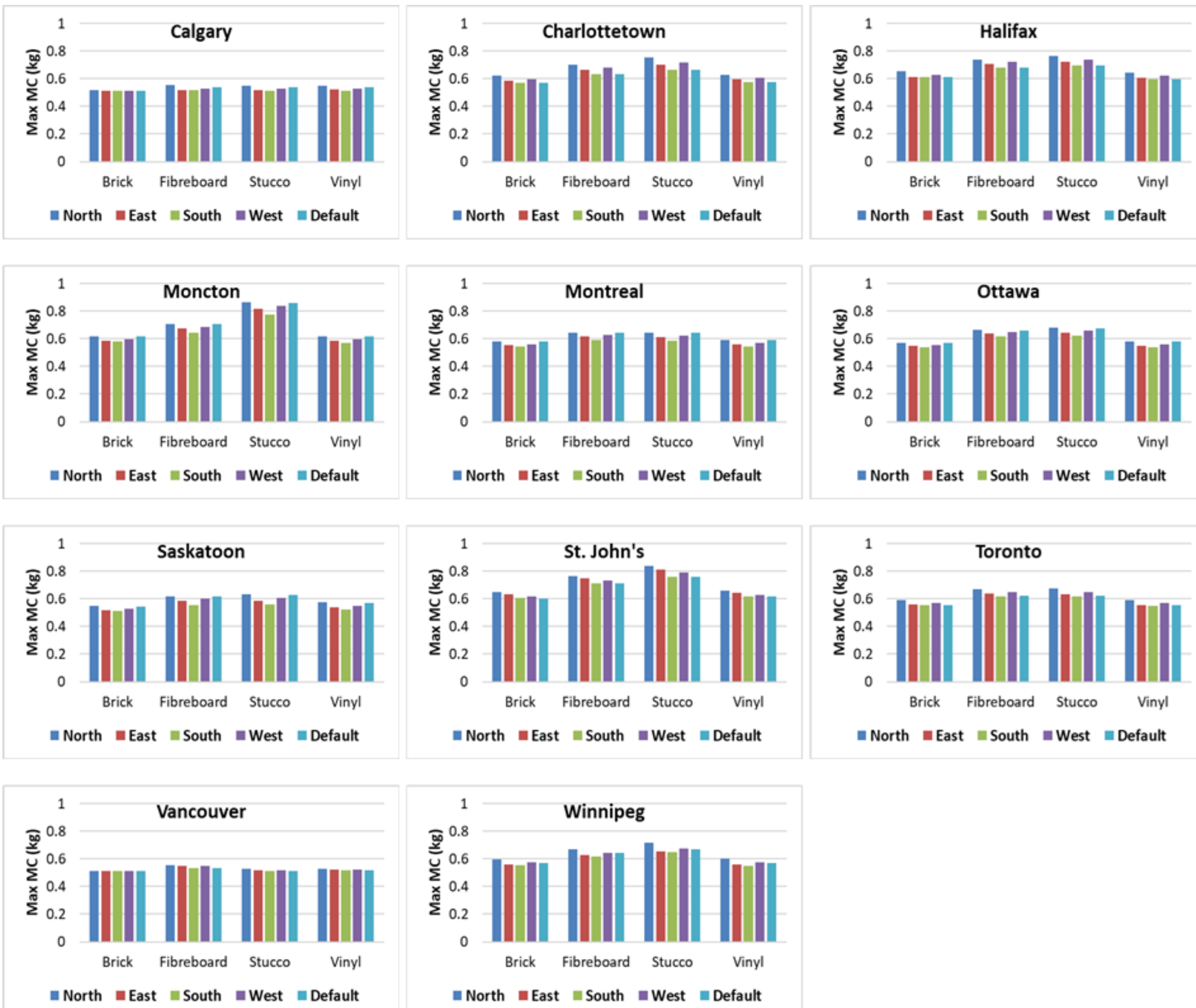

a) Maximum Moisture content of OSB layer for all selected cities with no WDR and no water source

2. Cases with WDR and no water source

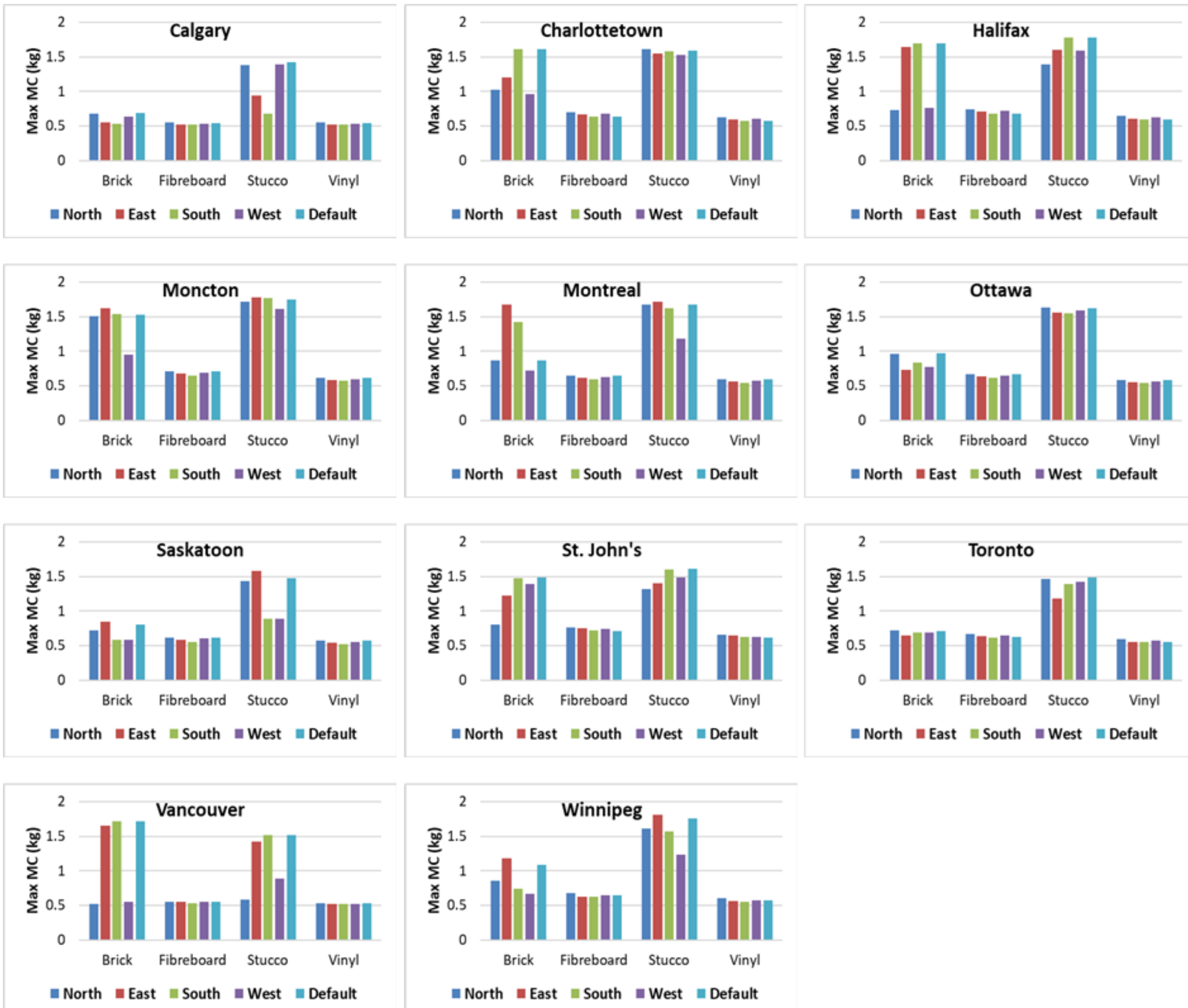

b) Maximum Moisture content of OSB layer for all selected cities with WDR and no water source

3. Cases with WDR and water source

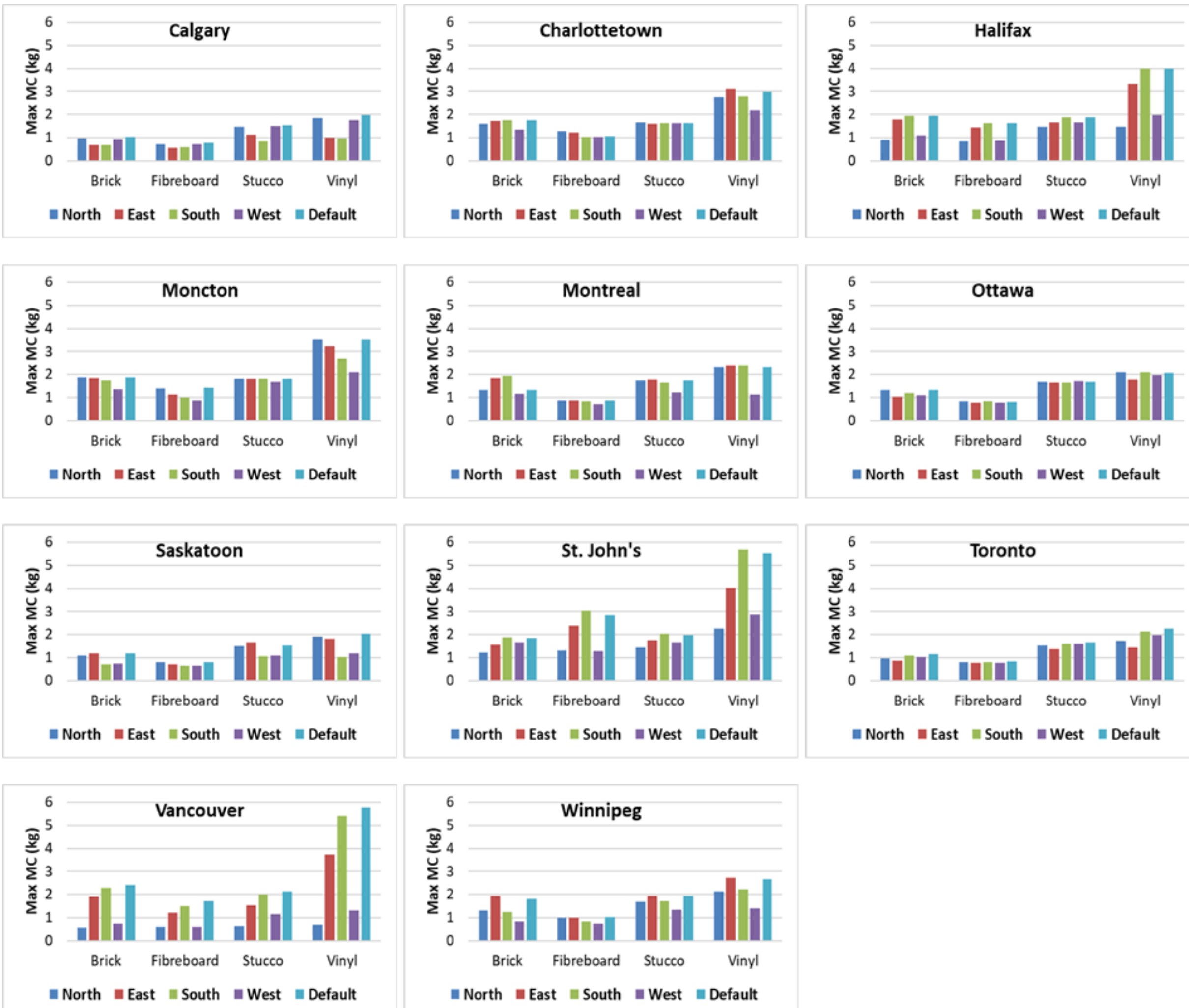

c) Maximum Moisture content of OSB layer for all selected cities with WDR and water source

A4. Results obtained with the Mean Moisture Content (MC)

1. Cases with no WDR and no water source

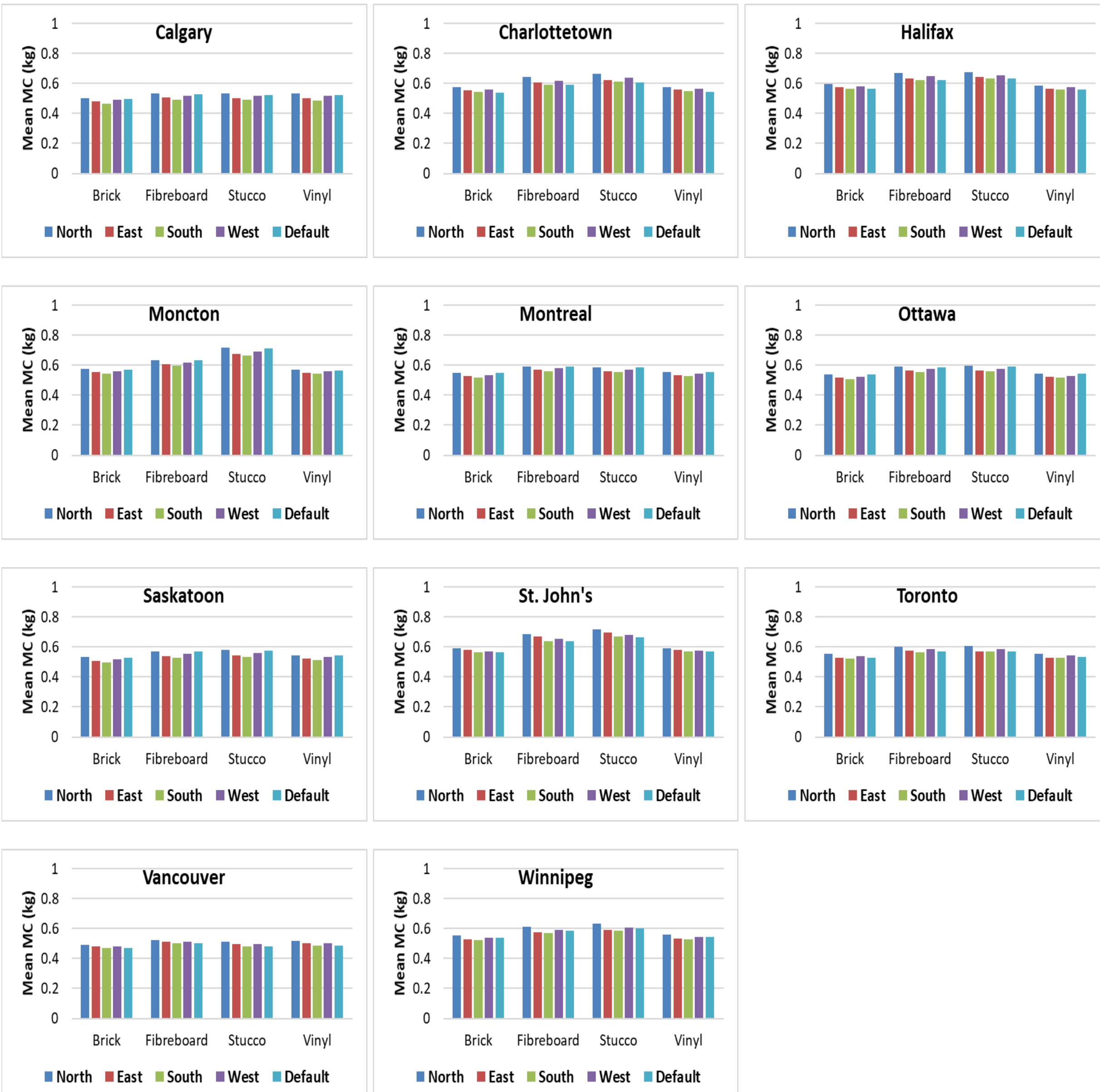

a) Mean Moisture content of OSB layer for all selected cities with no WDR and no water source

2. Cases with WDR and no water source

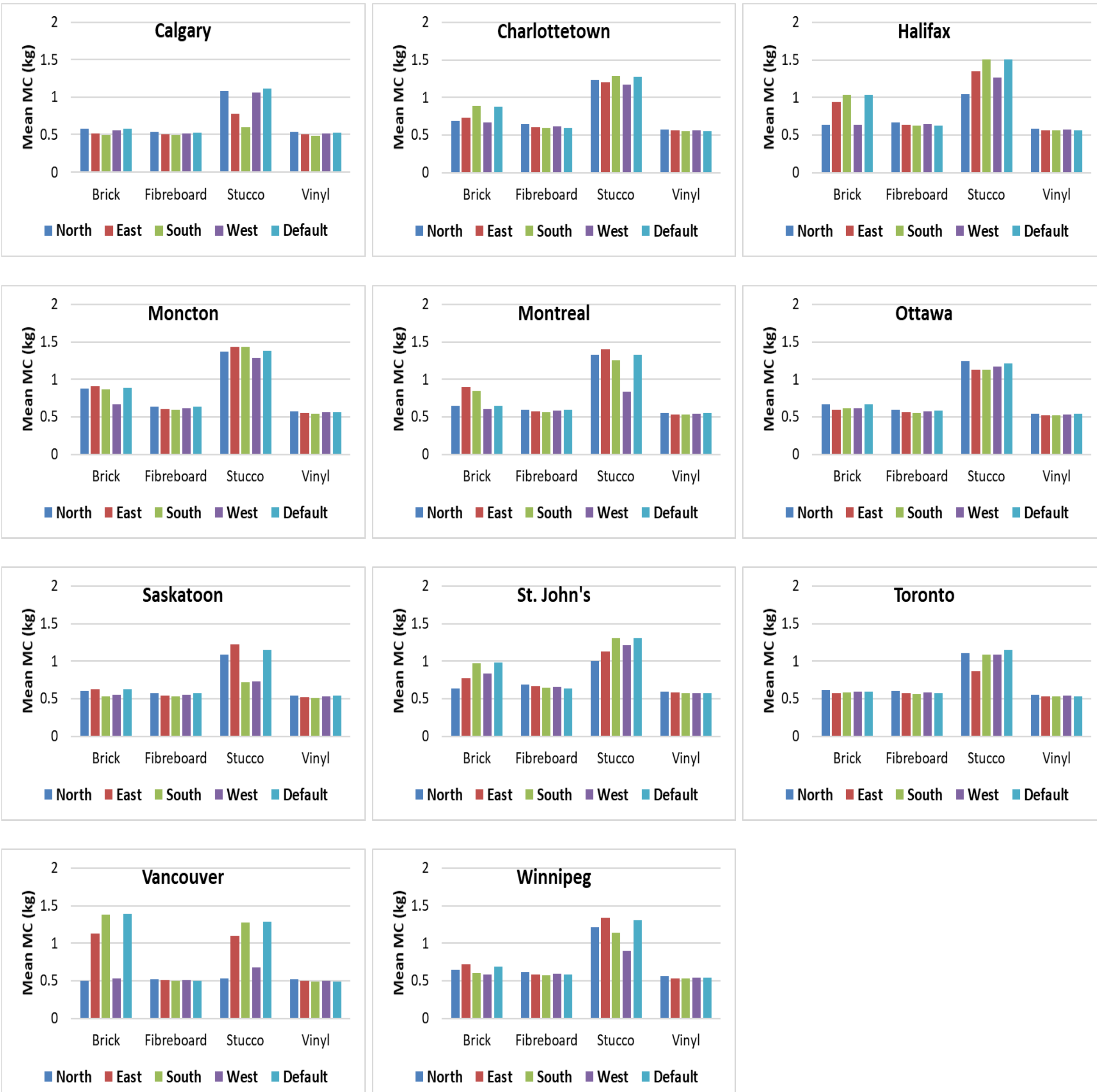

b) Mean Moisture content of OSB layer for all selected cities with WDR and no water source

3. Cases with WDR and water source

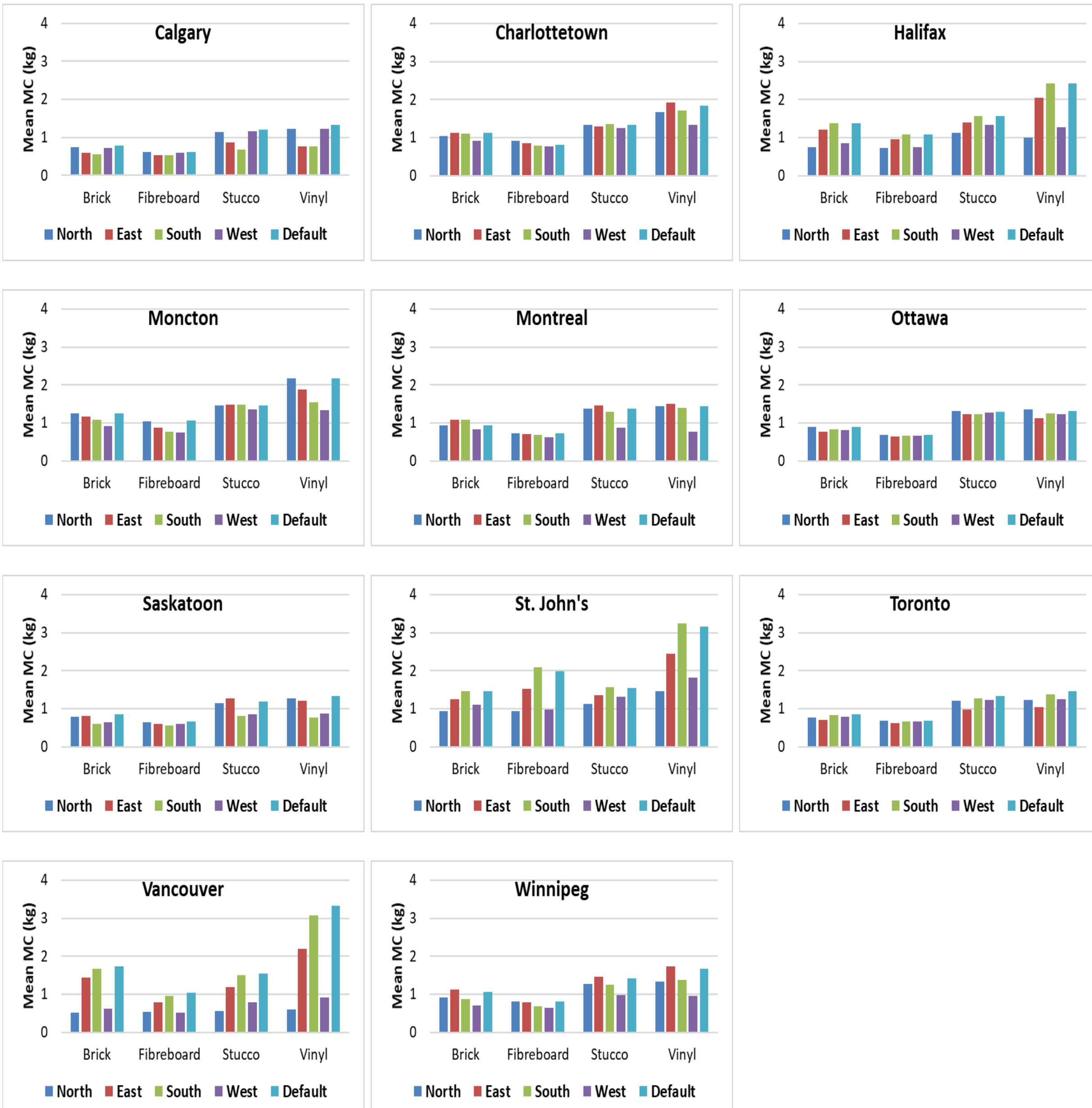

c) Mean Moisture content of OSB layer for all selected cities with WDR and water source

A5. Results obtained with the Mould Index (MoI)

1. Results with maximum MoI as performance indicator

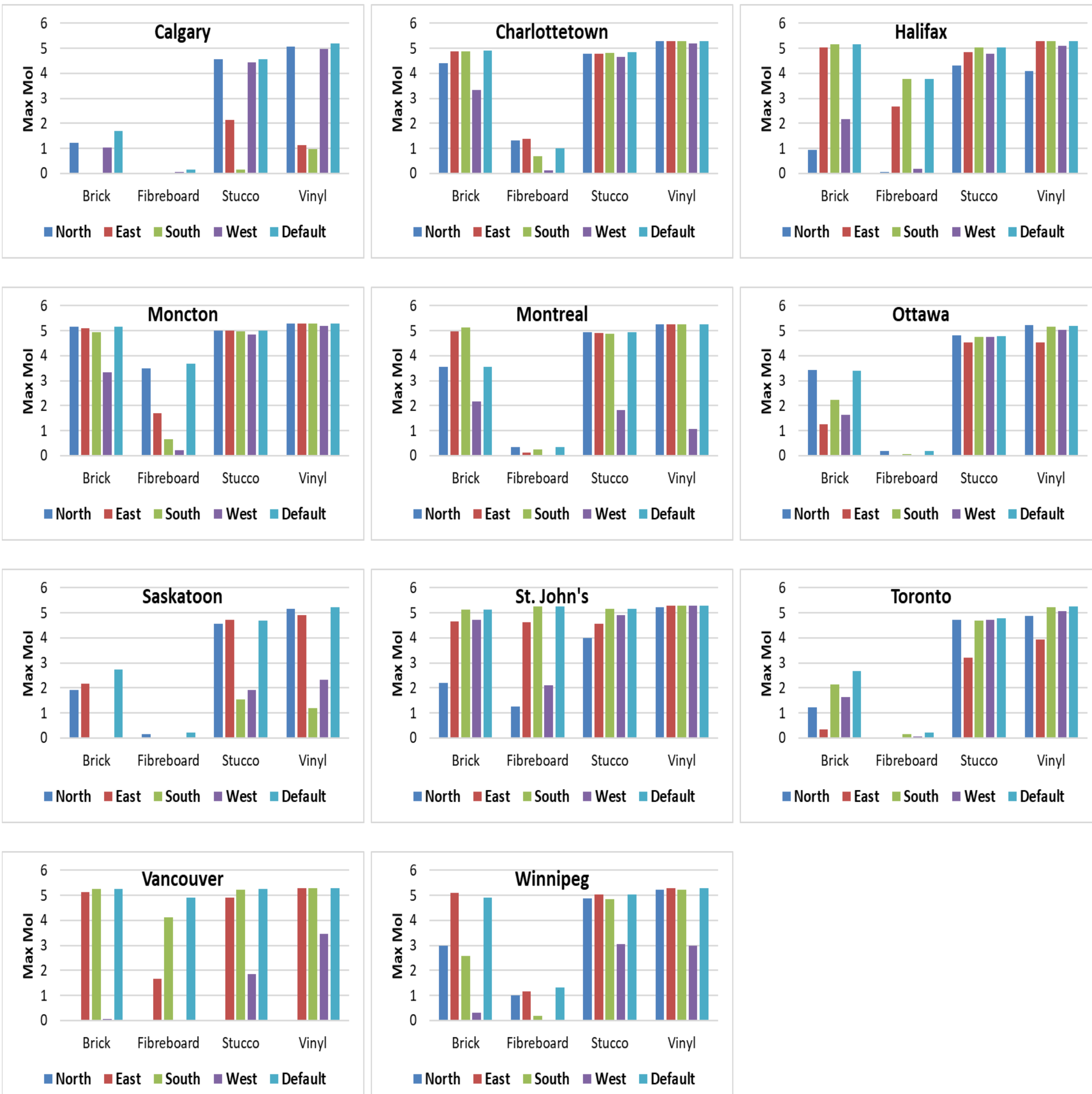

a) Maximum Mould Index at the exterior layer of OSB for all selected cities with WDR and water source

2. Results with mean MoI as performance indicator

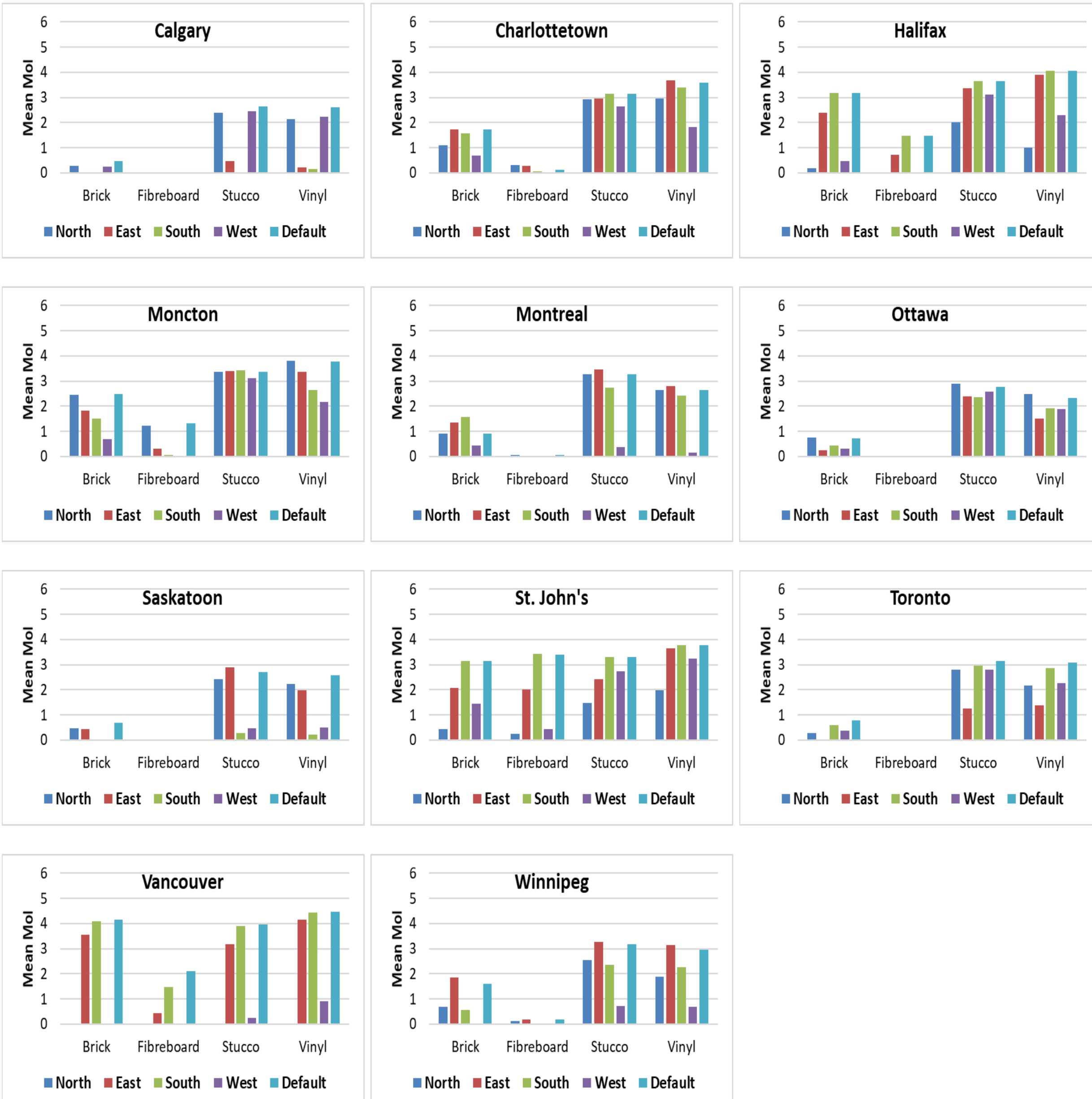

b) Mean Mould Index at the exterior layer of OSB for all selected cities with WDR and water source